ISSN 2355-3286

ULTIMA Computing

Jurnal Sistem Komputer

INDRA APRIYANI, INDRI YANTI, DARSANTO
Implementation of the Fuzzy Logic Mamdani Method in the KUB Chicken Egg Incubator

NICHOLAS PRANATA, MUHAMMAD SALEHUDDIN
Field Assessment for Initial Preparation of Net Zero Building Certification for The Universitas Multimedia Nusantara (UMN) Building: A Case Study On Visual Comfort in C and D Tower

TESYA PERMADI, SILMI ATH THAHIRAH AL AZHIMA, MARIYA AL QIBTYA, NURUL FAHMI ARIEF HAKIM
Modeling and Simulation of Manipulator Robot Using MATLAB

MOCHAMAD RIZAL FAUZAN, SAIQA FATUR KHAIRI, NENENG PUSPITA KANIARUDI, SILMI ATH THAHIRAH AL AZHIMA, NURUL FAHMI ARIEF HAKIM, IWAN KUSTIAWAN, MARIYA AL QIBTIYA, SISCKA ELVYANTI
One-Phase Smart Switch using OpenCV Hand Gesture Recognition

IRVAN BUDIAWAN, DANU FEBRI WIGIANTO, BAGUS WICAKSONO, ARIF ROHMAN HAKIM
Air Quality Monitoring System Design Based on Wireless Sensor Network Integrated with the Internet of Things

ABDUL HAMID, EKO MURSITO BUDI, ESTIYANTI EKAWATI
Gross Error Detection and Data Correction in IIoT-Based Data Center Cooling System

Engineering | Vol. 16 | No. 1 | Page 1 - 45 | June 2024 | ISSN 2355-3286

UMN

UNIVERSITAS
MULTIMEDIA
NUSANTARA

ISSN 2355-3286

EDITORIAL BOARD

EDITORIAL ADDRESS

Universitas Multimedia Nusantara (UMN)
Jl. Scientia Boulevard
Gading Serpong
Tangerang, Banten - 15811
Indonesia
Phone. (021) 5422 0808
Fax. (021) 5422 0800
Email : ultimacomputing@umn.ac.id

Ultima Computing : Jurnal Sistem Komputer is a Journal of Computer Engineering Study Program, Universitas Multimedia Nusantara which presents scientific research articles in the field of Computer Engineering and Electrical Engineering as well as current theoretical and practical issues, including Edge Computing, Internet-of-Things, Embedded Systems, Robotics, Control System, Network and Communication, System Integration, as well as other topics in the field of Computer Engineering and Electrical Engineering. The Ultima Computing : Jurnal Sistem Komputer is published regularly twice a year (June and December) and is jointly managed by the Computer Engineering and Electrical Engineering Study Program at Universitas Multimedia Nusantara.

Call for Papers

International Journal of New Media Technology (IJNMT) is a scholarly open access, peer-reviewed, and interdisciplinary journal focusing on theories, methods and implementations of new media technology. Topics include, but not limited to digital technology for creative industry, infrastructure technology, computing communication and networking, signal and image processing, intelligent system, control and embedded system, mobile and web based system, and robotics. IJNMT is published twice a year by Faculty of Engineering and Informatics of Universitas Multimedia Nusantara in cooperation with UMN Press.

Ultimatics : Jurnal Teknik Informatika is the Journal of the Informatics Study Program at Universitas Multimedia Nusantara which presents scientific research articles in the fields of Analysis and Design of Algorithm, Software Engineering, System and Network security, as well as the latest theoretical and practical issues, including Ubiquitous and Mobile Computing, Artificial Intelligence and Machine Learning, Algorithm Theory, World Wide Web, Cryptography, as well as other topics in the field of Informatics.

Ultima Computing : Jurnal Sistem Komputer is a Journal of Computer Engineering Study Program, Universitas Multimedia Nusantara which presents scientific research articles in the field of Computer Engineering and Electrical Engineering as well as current theoretical and practical issues, including Edge Computing, Internet-of-Things, Embedded Systems, Robotics, Control System, Network and Communication, System Integration, as well as other topics in the field of Computer Engineering and Electrical Engineering.

Ultima InfoSys : Jurnal Ilmu Sistem Informasi is a Journal of Information Systems Study Program at Universitas Multimedia Nusantara which presents scientific research articles in the field of Information Systems, as well as the latest theoretical and practical issues, including database systems, management information systems, system analysis and development, system project management information, programming, mobile information system, and other topics related to Information Systems.

ISSN 2355-3286

FOREWORD

ULTIMA Greetings!

Ultima Computing : Jurnal Sistem Komputer is a Journal of Computer Engineering and Electrical Engineering at Multimedia Nusantara University which presents scientific research articles in the field of Computer Systems as well as the latest theoretical and practical issues, including Edge Computing, Internet-of-Things, Embedded Systems, Robotics, Control Systems, Network and Communication, System Integration, and other topics in the field of Computer Engineering and Electrical Engineering.

In this June 2024 edition, Ultima Computing enters the 1st Edition of Volume 16. In this edition there are six scientific papers from researchers, academics and practitioners in the fields of Computer Engineering and Electrical Engineering. Some of the topics raised in this journal are: Implementation of the Fuzzy Logic Mamdani Method in the KUB Chicken Egg Incubator, Field Assessment for Initial Preparation of Net Zero Building Certification for The Universitas Multimedia Nusantara (UMN) Building: A Case Study On Visual Comfort in C and D Tower, Modeling and Simulation of Manipulator Robot Using MATLAB, One-Phase Smart Switch using OpenCV Hand Gesture Recognition, Air Quality Monitoring System Design Based on Wireless Sensor Network Integrated with the Internet of Things, and Gross Error Detection and Data Correction in IIoT-Based Data Center Cooling System.

On this occasion we would also like to invite the participation of our dear readers, researchers, academics, and practitioners, in the field of Engineering and Informatics, to submit quality scientific papers to: International Journal of New Media Technology (IJNMT), Ultimatics : Jurnal Teknik Informatics, Ultima Infosys: Journal of Information Systems and Ultima Computing: Journal of Computer Systems. Information regarding writing guidelines and templates, as well as other related information can be obtained through the email address ultimacomputing@umn.ac.id and the web page of our Journal here.

Finally, we would like to thank all contributors to this June 2024 Edition of Ultima Computing. We hope that scientific articles from research in this journal can be useful and contribute to the development of research and science in Indonesia.

June 2024,

M.B.Nugraha, S.T., M.T.
Editor-in-Chief

ISSN 2355-3286

TABLE OF CONTENT

Implementation of the Fuzzy Logic Mamdani Method in the KUB Chicken Egg Incubator
Indra Apriyani, Indri Yanti, Darsanto 1-8

Field Assessment for Initial Preparation of Net Zero Building Certification for The Universitas Multimedia Nusantara (UMN) Building: A Case Study On Visual Comfort in C and D Tower
Nicholas Pranata, Muhammad Salehuddin 9-19

Modeling and Simulation of Manipulator Robot Using MATLAB
Tesya Permadi, Silmi Ath Thahirah Al Azhima, Mariya Al Qibtya, Nurul Fahmi Arief Hakim 20-25

One-Phase Smart Switch using OpenCV Hand Gesture Recognition
Mochamad Rizal Fauzan, Saiqa Fatur Khairi, Neneng Puspita Kaniarudi, Silmi Ath Thahirah Al Azhima, Nurul Fahmi Arief Hakim, Iwan Kustiawan, Mariya Al Qibtiya, Siscka Elvyanti 26-32

Air Quality Monitoring System Design Based on Wireless Sensor Network Integrated with the Internet of Things
Irvan Budiawan, Danu Febri Wigianto, Bagus Wicaksono, Arif Rohman Hakim 33-38

Gross Error Detection and Data Correction in IIoT-Based Data Center Cooling System
Abdul Hamid, Eko Mursito Budi, Estiyanti Ekawati 39-45

ISSN 2355-3286

Implementation of the Fuzzy Logic Mamdani Method in the KUB Chicken Egg Incubator

Indra Apriyani[1], Indri Yanti[2*], Darsanto[3]
[1,2,3] Department of Computer Engineering, Faculty of Engineering, Universitas Wiralodra, Indramayu, Indonesia
[1]indraapriyani04@gmail.com, [2]indriyanti.ft@unwir.ac.id, [3]shantost.ft@unwir.ac.id

Accepted on 27 April 2024
Approved on 28 May 2024

***Abstract*— Poultry farming plays an important role in rural Indonesia's economy, with increasing demand for poultry meat and protein-rich eggs. One of the main challenges for farmers is the limited production of chicken seeds and suboptimal egg incubation methods. Modern egg incubators offer a solution with higher ease and efficiency compared to traditional methods. However, existing machines on the market have weaknesses, such as less accurate temperature and humidity control, and less optimal power source switching. The use of fuzzy logic methods in egg incubators has proven to be more efficient than manual methods, with a hatching success rate of 100% for 10 eggs. Fuzzy logic-based egg incubators start hatching earlier and more on days 18 and 19, while manual methods begin on days 19 and 20. The automatic egg-turning process in fuzzy logic machines saves labor and reduces the risk of error. This research highlights the importance of using accurate sensors and optimal temperature and humidity control systems to improve the success rate of chicken egg hatching.**

***Index Terms*— egg hatching; fuzzy logic; humidity; poultry farming; temperature.**

I. INTRODUCTION

The livestock business is a business that is quite popular in society, especially poultry farming. Poultry farming is one of the driving forces for economic development in Indonesia, especially in rural areas. Not only that, very rapid population growth will also have an impact on increasing food, especially the need for poultry meat or eggs which are rich sources of protein. This needs to be balanced with an adequate supply of food, so that the need for food that has a large source of protein remains met[1].

The main problem experienced by farmers is the limited production of chicken seeds so they are unable to serve all the buyers who order[2]. One aspect of the cause is that hatching of eggs is not optimal. The demand for poultry is increasing quite significantly every month, one of which is the proliferation of food stalls and restaurants that provide menus made from poultry. To meet this demand, breeders will not have enough time if they only rely on traditional methods because they cannot mass produce them, therefore technology is needed that can improve and make it easier to hatch eggs, namely egg incubators[3].

Hatching eggs using an egg incubator has many advantages and conveniences compared to traditional methods[4]. One of them is that eggs can be hatched in large quantities, but apart from that, certain intensity and precision is required in hatching eggs using an incubator, starting from selecting eggs, egg storage methods (position or location of eggs), temperature and humidity which we must pay attention to.

Currently, egg incubator machines have been widely discussed in previous research and are also widely sold on the market, but the automatic egg incubator machines on the market are less efficient to use because the light bulb that functions as a room heater is only controlled to turn on and off. This often causes the bulb to quickly become damaged (no longer functioning), and a non-functioning bulb will affect the success of the hatching process. For this reason, there is a need for a more efficient and smart egg incubator.

The problem that is often faced in the process of hatching chicken eggs is that the temperature and humidity in the incubator must be in accordance with the needs of the hatching eggs, so a temperature and humidity control system is needed that can be adjusted to the needs of the hatching eggs. There are five main things that need to be paid attention to in the egg hatching room, namely temperature, humidity, ventilation, turning the eggs and cleanliness of the hatching room [5]. According to the Banten Agricultural Technology Research Center (BPTP), the incubation temperature occurs at 38ºC to 39.5ºC and air humidity is around 60% RH to 70% RH [6]. The incubation temperature is between 36ºC – 42ºC with air humidity of 55% - 60% RH[7]. Embryos will develop if the air temperature around the egg is at least 21.11ºC and the best temperature is between 38ºC-40ºC[8].

Research on egg incubators was carried out by [9] using an LM35 temperature sensor and a heating element in the form of a 5W/220VAC light bulb. The result is that the temperature generated by the heating element in the egg incubator room can be measured and controlled by a temperature sensor from 37.5ºC to 39ºC. The drawback of this research is that the humidity factor was not involved and temperature control was still manual by pressing a push button.

Other research on egg hatching machines has also been carried out by [10]using a DHT11 sensor which

functions to measure temperature and humidity and a heating element in the form of a 5W/220VAC incandescent lamp. The temperature generated by the heating element is 37ºC to 40ºC and the stepper motor functions as a machine for turning the eggs back and forth automatically. The shortcomings of this research are that when the lights go out the egg incubator does not function and there is no tool that can even out the air temperature in the egg incubator.

Furthermore, research conducted by[11] measured temperature and humidity combined with fuzzy logic using DHT11. The object used was free-range chicken eggs, and the success percentage reached 88.89%, but the drawback was that when the electricity went out, the egg incubator could not function.

Based on previous research, there are still several shortcomings, therefore this research makes an egg incubator using the Mamdani fuzzy logic method. The research chooses the fuzzy logic and Mamdani method for the KUB chicken egg incubator due to their ability to handle the non-linear and complex interactions of temperature and humidity control. Fuzzy logic effectively manages uncertainty and imprecise data, while Mamdani rules are intuitive and resemble human decision-making, making them easy to implement and understand. This method provides precise, adaptive control essential for maintaining optimal conditions in the incubator, enhancing reliability and efficiency compared to conventional control methods, ultimately improving hatching success rates and egg quality.

The components used are Arduino Nano light bulb, DHT11 sensor, DS18B20 sensor 5W/220VAC light, 12V adapter, 16 x 2 I2C LCD, ACCU, 9VDC fan, AC dimmer module, 220VAC relay, push button, dynamo motor and 500W inverter. The DS18B20 sensor is used to measure temperature, while the DHT11 sensor is used to measure humidity which will be processed by fuzzy logic using the Mamdani method. The light bulb is used as a heater in this incubator, while the fan is used to regulate the humidity of the incubator.

This research uses the Mamdani method of fuzzy logic to regulate the temperature and humidity of the egg incubator so that it matches the ideal temperature and humidity. The ideal incubation temperature is between 36ºC – 39ºC and air humidity of around 60% RH - 70% RH. One of the advantages of the tool made is that when the power goes out the egg incubator will continue to operate by utilizing an Uninterruptible Power Supply (UPS).

II. METHODOLOGY

The method used in this research is experimental research which will produce a prototype of an egg incubator machine used to incubate Balitbangtan superior village chicken (KUB) eggs.

CFD simulation is used to analyze the total force and pressure difference between horizontal dive, vertical dive, and diagonal dive. The CFD simulation were run on 1:1 scale, 3-Dimension ROV model as shown in Figure 1 and main dimensions of mini-ROV model shown in Table 1.

A. *Research Design*

This research aims to design and make an egg incubator using fuzzy logic, so it requires several stages, the research flow stages carried out can be seen in Figure 1.

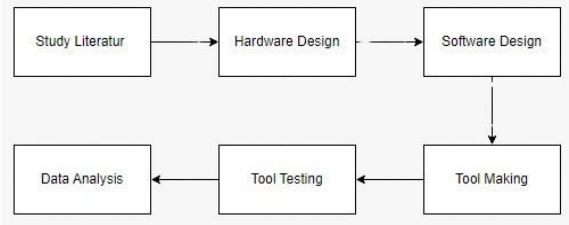

Fig. 1. Research flow diagram

The first stage is determining the title and accompanied by a search for a problem formulation related to the problem to be researched. After that, carry out tool design by preparing tools and materials, designing a series of tools. The next stage is designing the software, by creating a fuzzy logic design in Matlab. The next stage is testing the tool by testing the tool that has been made and the final step is analyzing the data.

B. *Block Diagram*

The block diagram of this research consists of 3 parts, input, process and output, as shown in Figure 2. Meanwhile, Figure 3 shows the control block diagram.

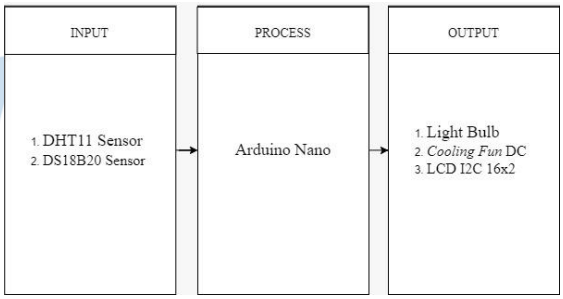

Fig. 2. The block diagram

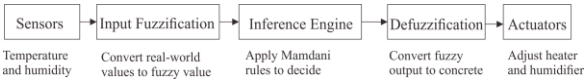

Fig. 3. The control block diagram

In the input section there is a DHT11 sensor and a DS18B20 sensor. The DHT11 (Humidity & Temperature Sensor) sensor functions to measure temperature and humidity. However, in this research, the DHT11 sensor was only used to measure humidity in the egg incubator room. Meanwhile, the DS18B20 temperature sensor (Temperature Sensor) functions to measure the temperature value in the egg incubator room. The Arduino Nano functions as a manager for the values read by the sensor and functions as a processor

for each value read from the input which will then be displayed on the LCD. In the output section there are lights, fans and a 16x2 I2C LCD. The lamp acts as a heater to warm the room inside the egg incubator. The heater will dim the light automatically if the heat in the engine room exceeds the specified limit. The I2C 16x2 LCD functions to display temperature and humidity data on the egg incubator. Meanwhile, the Cooling Fun DC fan functions to even out the temperature and control humidity in the egg incubator.

C. *Circuit Design*

The circuit design of tool plays an important role in conducting research on the creation of a fuzzy logic egg incubator using the Mamdani method. The circuit design is made to make work easier when designing and making tools. To become a tool, a schematic and footprint are needed to make the PCB, then when the PCB has been made, each component is placed on the PCB board according to the schematic. Each component has been placed on the PCB so that it is connected to each other. The schematic of the egg incubator machine circuit is shown in Figure 4.

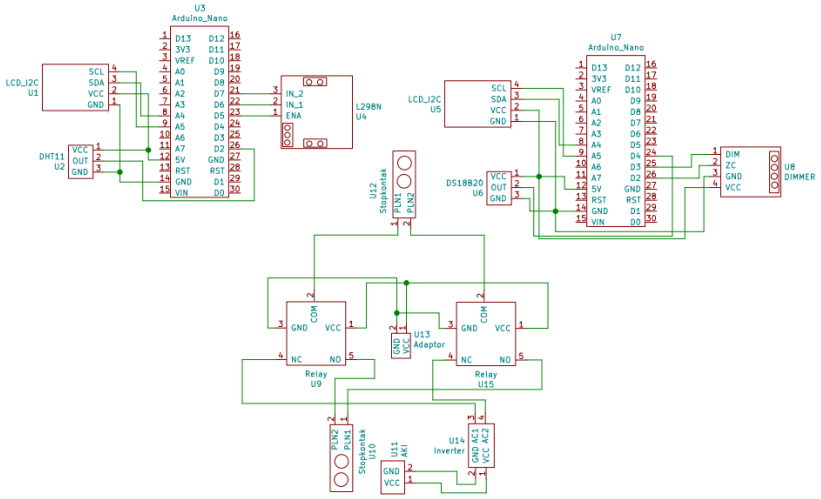

Fig. 4. The control block diagram

This incubator uses an additional UPS voltage source so that when a power outage occurs the incubator continues to function.

D. *Fuzzy Logic Design*

This research uses the Mamdani method by utilizing the MAX-MIN operation [12]. The advantage of fuzzy logic is that it can tolerate vague or inaccurate data and generally fuzzy logic is used to take an action or decision in a system [13]. Meanwhile, the advantage of the Mamdani method in fuzzy logic is that it is intuitive, covers a wide field because it uses COA (centroid of area) [14][15].

The term fuzzy is defined as a condition that is between right or wrong and is based on the degree of membership which ranges from zero to one [16]. Apart from that, fuzzy logic is also considered as an appropriate way to map input space to output space. The input space and output space in fuzzy can be linguistic variables as a substitute for using numerical calculations [17].

In this study there are two input variables, namely temperature and humidity, while the output variables in this study are light intensity and fan rotation speed. The stages in the fuzzy process include the fuzzification process, inference based on a knowledge base, and defuzzification. The inference system used in this research is the Mamdani method.

In the fuzzification stage, the fuzzy input variable consists of two membership functions, namely temperature and humidity, while the output is in the form of pulse width modulation (PWM) from the heater (light bulb) and fan. PWM settings are a way to manipulate the pulse width of a square wave with constant frequency and amplitude[18]. The temperature input memberships used are cold, warm and hot, while the humidity input memberships used are dry, humid and wet. The lights' PWM output membership includes ideal dim, bright, while the fan's PWM output membership includes slow, normal, fast.

1. Input membership function

The temperature input data is in the form of a firm value (crips) between 20 and 50. This value is obtained from the three categories of temperature values that will be used, namely temperature in the cold category when the temperature is less than 36^{o}C, temperature in the warm category when the temperature is between 36^{o}C to 40^{o}C, and the temperature is categorized as hot when the temperature conditions are above 40^{o}C. The membership degree $\mu(x)$ of temperature is expressed

by equations (1), (2), and (3). Figure 5 shows a graph of the input membership function on temperature.

$$\mu_{Cold}(x) = \begin{cases} 0, & x \geq 36 \\ \frac{36-x}{36-30}, & 30 \leq x \leq 36 \\ 1, & x \leq 30 \end{cases} \quad (1)$$

$$\mu_{Warm}(x) = \begin{cases} 0, & x \leq 30 \; or \; x \geq 45 \\ \frac{x-30}{36-30}, & 30 \leq x \leq 36 \\ 1, & 36 \leq x \leq 40 \\ \frac{45-x}{45-40}, & 40 \leq x \leq 45 \end{cases} \quad (2)$$

$$\mu_{Hot}(x) = \begin{cases} 0, & x \leq 40 \\ \frac{x-40}{45-40}, & 40 \leq x \leq 45 \\ 1, & x \geq 45 \end{cases} \quad (3)$$

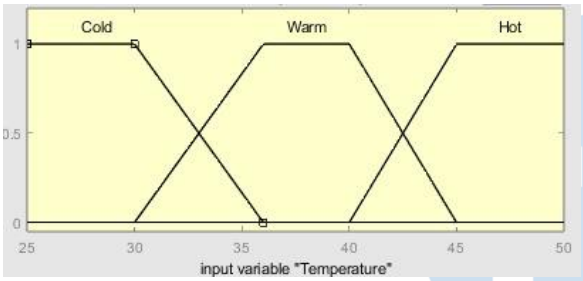

Fig. 5. Graph of input membership function on temperature

Humidity input data is also in the form of crisp values between 25 and 95. These values are obtained from the three categories of humidity values that will be used, namely humidity in the dry category when the humidity is less than 55% RH, humidity in the damp category when the room humidity is between 55 % RH 65% RH and humidity in the wet category when room humidity conditions are above 65% RH. The membership degree of humidity is expressed by equations (4), (5), and (6). Figure 6 shows a graph of the input membership function on humidity.

$$\mu_{Dry}(x) = \begin{cases} 0, & x \geq 55 \\ \frac{55-x}{55-40}, & 40 \leq x \leq 55 \\ 1, & x \leq 40 \end{cases} \quad (4)$$

$$\mu_{Damp}(x) = \begin{cases} 0, & x \leq 40 \; or \; x \geq 80 \\ \frac{x-40}{55-40}, & 40 \leq x \leq 55 \\ 1, & 55 \leq x \leq 65 \\ \frac{80-x}{80-65}, & 65 \leq x \leq 80 \end{cases} \quad (5)$$

$$\mu_{Wet}(x) = \begin{cases} 0, & x \leq 65 \\ \frac{x-65}{80-65}, & 65 \leq x \leq 80 \\ 1, & x \geq 80 \end{cases} \quad (6)$$

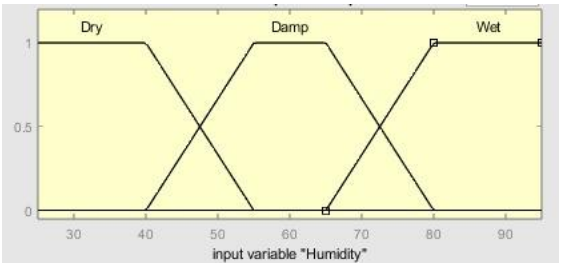

Fig. 6. Graph of input membership function on humidity

2. Output membership function

The temperature PWM output is 8bit or between 0 to 255. This value is obtained from the PWM which is sent to the microcontroller to regulate the light intensity from 0 to 255 and is converted into a fuzzy set in the form of dim, ideal, bright. The membership degree of light intensity is expressed by equations (7), (8), and (9). Figure 7 shows a graph of the light intensity output membership function.

$$\mu_{Dim}(x) = \begin{cases} 0, & x \geq 128 \\ \frac{128-x}{128-64}, & 64 \leq x \leq 128 \\ 1, & x \leq 64 \end{cases} \quad (7)$$

$$\mu_{Ideal}(x) = \begin{cases} 0, & x \leq 64 \; or \; x \geq 192 \\ \frac{x-64}{128-64}, & 64 \leq x \leq 128 \\ \frac{192-x}{192-128}, & 128 \leq x \leq 192 \end{cases} \quad (8)$$

$$\mu_{Bright}(x) = \begin{cases} 0, & x \leq 128 \\ \frac{x-128}{192-128}, & 128 \leq x \leq 192 \\ 1, & x \geq 192 \end{cases} \quad (9)$$

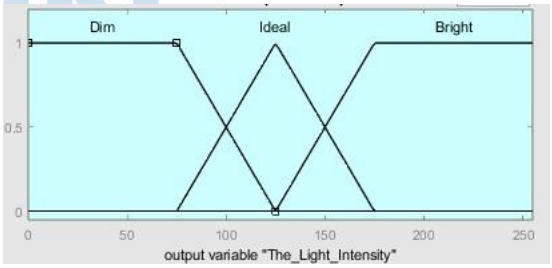

Fig. 7. Graph of output membership function at temperature

The humidity PWM output is 8bit or between 0 to 255[18]. This value is obtained from the PWM which is sent to the microcontroller to regulate the light intensity from 0 to 255 and is converted into a fuzzy set in the form of slow, normal and fast. The membership degree of fan speed is expressed by equations (10), (11), and (12). Figure 8 shows a graph of the output membership function in the form of fan speed.

$$\mu_{Slow}(x) = \begin{cases} 0, & x \geq 128 \\ \dfrac{128 - x}{128 - 64}, & 64 \leq x \leq 128 \\ 1, & x \leq 64 \end{cases} \quad (10)$$

$$\mu_{Normal}(x) = \begin{cases} 0, & x \leq 64 \; or \; x \geq 192 \\ \dfrac{x - 64}{128 - 64}, & 64 \leq x \leq 128 \\ \dfrac{192 - x}{192 - 128}, & 128 \leq x \leq 192 \end{cases} \quad (11)$$

$$\mu_{Fast}(x) = \begin{cases} 0, & x \leq 128 \\ \dfrac{x - 128}{192 - 128}, & 128 \leq x \leq 192 \\ 1, & x \geq 192 \end{cases} \quad (12)$$

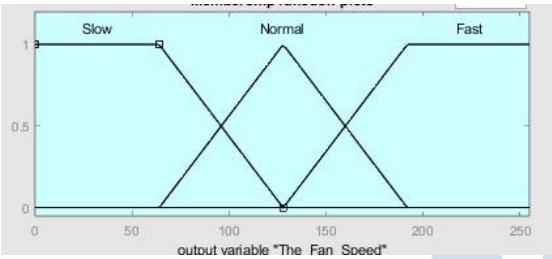

Fig. 8. Graph of output membership function on humidity

3. The rule base of fuzzy logic

After create linguistic variables, defining linguistic terms, and creating membership functions, the last step of fuzzy system design is creating a rule base. Rules describe, in words, the relationships between input and output linguistic variables based on their linguistic terms. A rule base is the set of rules for a fuzzy system. To create a rule, you must specify the antecedents, or IF portions, and consequents, or THEN portions, of the rule. Table I shows the fuzzy logic rule base used in the incubator created in this research.

TABLE I. RULE BASE

Lamp/Fan	Cold	Warm	Hot
Dry	Bright/ Fast	Ideal/ Fast	Dim/ Fast
Medium	Bright/ Normal	Ideal/ Normal	Dim/ Normal
Moist	Bright/ Slow	Ideal/ Slow	Dim/ Slow

E. Tool Working System

The working system of the egg incubator machine can be seen in the flowchart image. The following Figure 9 is a flowchart of the temperature and humidity system.

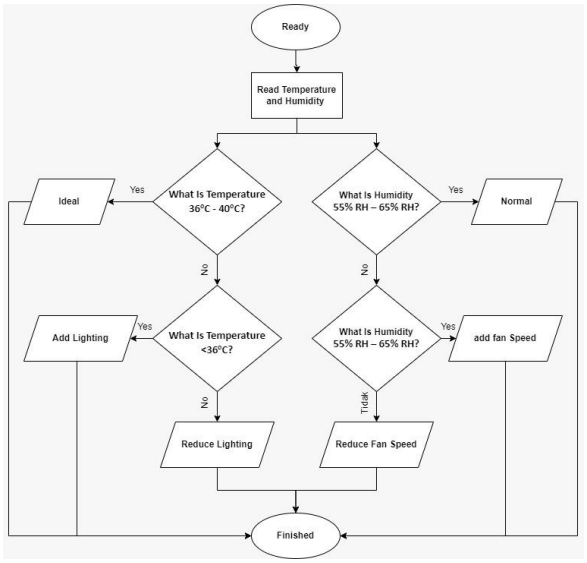

Fig. 9. Temperature and humidity system flowchart graph

The way this egg incubator works is that when the DHT11 sensor detects a room temperature of more than 40°C, the incandescent lamp will dim the lighting. If the temperature is below 36°C then the incandescent lamp will provide lighting and if the temperature is between 36-40°C then the lamp will be in ideal condition [19]. Likewise with the humidity in the egg incubator room, the ideal humidity for incubating chicken eggs is 55-65%RH [20]. To regulate the humidity in the egg incubator room, this research uses a DC cooling fan which will be controlled by fuzzy logic and the way it works is that if the DHT 11 sensor receives humidity above 65%RH, the fan will reduce the speed and if the humidity in the room is less than 55%RH then the fan will increase speed and if the humidity is between 55-65%RH then the fan speed will be normal.

To turn the egg, this research used a TYD 49-R motor dynamo. The TYD 49-R motor dynamo is controlled using a DH48S-S Timmer which will reverse the speed 4 times every day [21].

III. RESULT AND ANALYSIS

The results of this research include the results of testing the accuracy of the temperature and humidity values of the tool that has been made, testing automatic voltage transfer when a power outage occurs, testing the entire egg incubator system and discussion of hatching results.

A. Temperature and Humidity Value Testing

Accurate levels of temperature and humidity play an important role in the success of hatching eggs. In this case, it is necessary to compare the sensor from the tool that has been made with the tool that has been calibrated to determine the level of accuracy of the tool that has been made. The results of the comparison of

temperature and humidity are shown in Figure 10 and Figure 10 respectively.

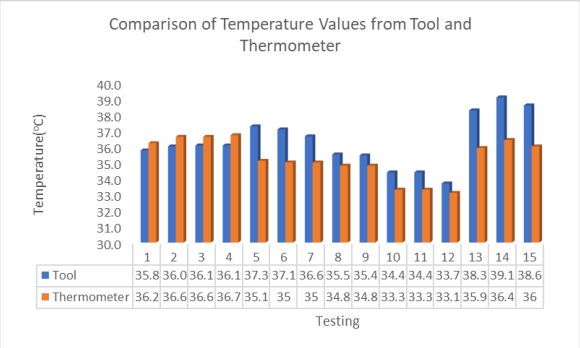

Fig. 10. The result of comparison of temperature values from tool and thermometer

Figure 10 shows the results of comparing temperature values between the tool that has been made and a calibrated thermometer. In the last three tests the difference was quite large, namely 2.4ºC, 2.7ºC, and 2.6ºC. This is due, in part, to the sensitivity of the DS18B20 temperature sensor used in the tool. Based on the datasheet from DS18B20, the error value reaches ± 2ºC.

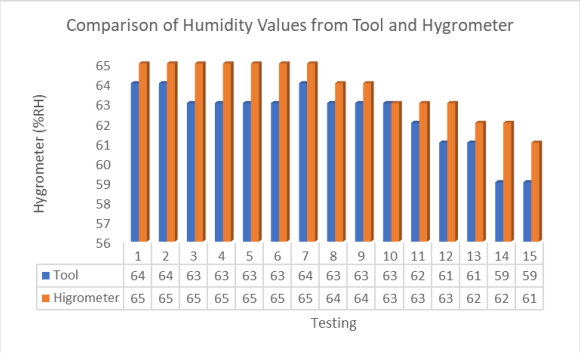

Fig. 11. The result of comparison of hygrometer values from tool and hygrometer

Figure 11 shows the results of the humidity comparison between the tool that has been made and a calibrated hygrometer. The 14th test showed the largest difference value, namely 3%RH, while the other tests only had a difference of 1-2%RH with the hygrometer. Based on the datasheet, the DHT11 humidity sensor has an error of 5% RH, so the measurement error produced by the tool is still within the error range of the DHT11 sensor. Figure 11 shows the results of comparing temperature with a thermometer and figure 12 shows the results of comparing humidity with a calibrated hygrometer.

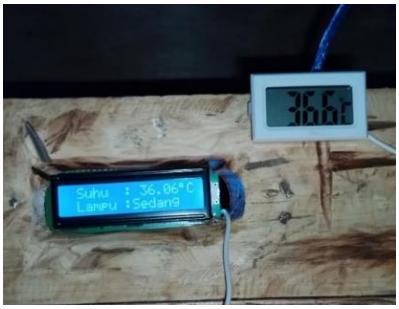

Fig. 12. Comparison results of temperature sensors with thermometer

Fig. 13. Comparison results of humidity sensors with hygrometer

B. Comparison of PWM Value Results

The PWM value is the result of fuzzy logic inference which describes the light intensity of the lamp and fan speed. Figure 14 and Figure 15 shows a comparison graph between the PWM values on the tool and MATLAB.

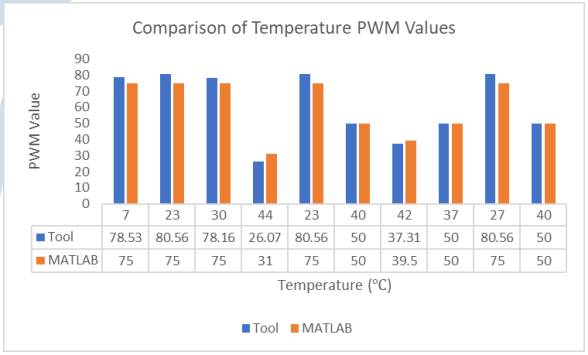

Fig. 14. Temperature PWM values comparison graph

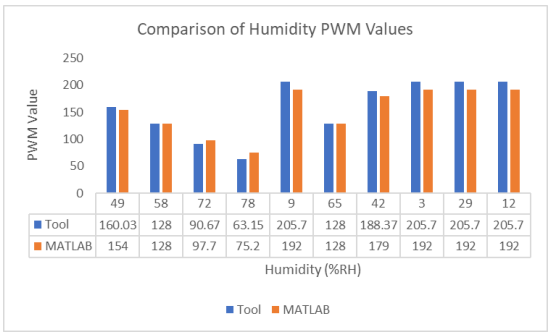

Fig. 15. Humidity PWM values comparison graph

Based on Figure 14 and 15, it can be seen that the results of comparing the PWM value of light intensity between the tool and MATLAB have the largest difference of 5.56, while the PWM of fan speed has the largest difference of 13.7.

C. Whole System Testing

Hatching eggs using the fuzzy logic method is in principle conditioned like a chicken egg being incubated by its mother. Hatching of chicken eggs takes approximately 21 days with the ideal room temperature of 36ºC-40ºC and ideal humidity of 55%RH-65%RH. This research carried out a test for hatching KUB chicken eggs using the Mamdani fuzzy logic method and using conventional methods as a comparison material for the tests carried out, each of the two methods hatched 10 KUB chicken eggs [22]. Testing of egg incubators using the Mamdani fuzzy logic method started hatching on 22 January 2024 and manual egg incubators starting on 30 January 2024. The egg rotation was carried out in different ways, for the fuzzy logic egg incubator machine it used a motor dynamo as an automatic tool for turning. turning the eggs, while manual egg incubators are done with human assistance [23]. The egg rotation time for both eggs is carried out 4 times a day with the hatching results per day shown in Figure 16.

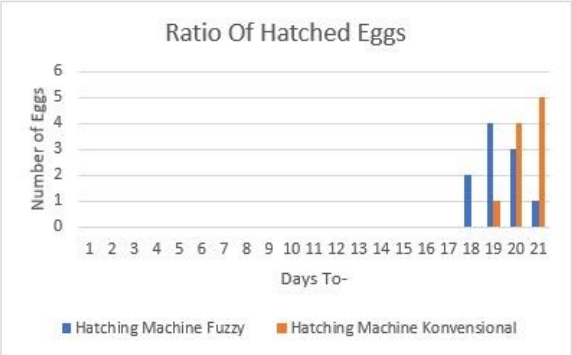

Fig. 16. PWM value comparison graph

Based on Figure 14, it can be seen that the results of the comparison between egg incubators using the fuzzy logic method and manual egg incubators, both have a percentage of 100% hatchability for 10 eggs each, however hatchability using the fuzzy logic method is better than when using manual methods. Where the testing of eggs hatched using the fuzzy logic method started to hatch on the 18th day and more hatched on the 19th day, while eggs hatched using the manual method started to hatch on the 19th day and more hatched on the 20th day. Turning the eggs in the fuzzy logic incubator is done automatically so that it can save energy and avoid forgetting to turn the eggs. The egg hatching process can be seen in Figure 17 and Figure 18.

Fig. 17. Egg hatching results using fuzzy logic

Fig. 18. Hatching eggs using conventional methods

D. Automatic Electrical Voltage Transfer Testing

Electrical voltage is one of the important things for running an egg incubator. In general, egg incubator machines are run from a PLN voltage source. To anticipate problems with the PLN voltage source, this research implemented a voltage source shift. The voltage transfer is carried out automatically by relying on a relay which will regulate the transfer of the voltage source when the PLN electricity source goes out. In this research, an Uninterruptible Power Supply (UPS) is used as a backup voltage source. The UPS used has a power rating of 360VA, power consumption of 360W, output voltage of 230V and input and output frequencies of 50/60 Hz. The test was carried out by connecting the UPS and the PLN voltage source to the relay, then connecting the relay to the egg incubator. Figure 19 shows a device that gets voltage from the UPS.

Fig. 19. UPS is used in incubator

The test of switching the voltage source from PLN to the UPS of the egg incubator machine was successfully carried out, but with a full battery condition, the UPS could only replace the PLN function for less than 1 hour with a stable voltage output of 220 volts. Figure 18 shows the voltage source transfer test from PLN to UPS.

IV. Conclusion

Based on the research that has been carried out, it can be concluded that temperature and humidity settings using a fuzzy logic system are able to maintain temperature and humidity in accordance with the given set points, namely 36 – 40ºC and 55–65%RH. In this research, calibration results were obtained from testing the DS18B20 sensor and the DHT11 sensor with a hygro-thermostat which had a difference in values of 0.5 – 2.7ºC and 1-3% RH. Egg hatching testing using fuzzy logic has a success rate of 100% for the 10 eggs hatched, each of the two methods hatches 10 eggs. Where the results of the hatching test on the egg incubator machine used fuzzy logic by rotating the egg rack 4 times a day and managed to hatch early, precisely on the 18th to the 20th day, while the results of the hatching test on the manual egg incubator machine by rotating the egg rack 4 times a day has a percentage of egg hatching success rate of 100% and they start to hatch on the 19th to the 21st day. In this research, the application of the voltage source switching system from PLN to UPS was successful but only lasted less than 1 hour. This can be concluded that the use of UPS is not yet efficient when applied to egg incubators.

References

[1] H. Hafid, A. Indi, D. Sutopo, D. M. Daoed, A. Pratiwi, and L. Sahaba, "BIMBINGAN TEKNIS BUDIDAYA AYAM KAMPUNG SUPER UNTUK PEMBERDAYAAN POTENSI MASYARAKAT DI KELURAHAN MATABUBU KECAMATAN POASIA KOTA KENDARI," *Anoa J. Pengabdi. Masy. Sos. Polit. Budaya, Hukum, Ekon.*, vol. 2, no. 3, 2021, doi: 10.52423/anoa.v2i3.22550.

[2] R. Rozalina, B. R. Juanda, K. M. Z. Basriwijaya, and L. A. Krista, "Pemberdayaan Kelompok Wanita Tani Melalui Keterampilan Beternak Ayam Ras Petelur di Desa Bate Puteh Kecamaatan Langsa Lama Kota Langsa," *J. Masy. Madani Indones.*, vol. 2, no. 4, 2023, doi: 10.59025/js.v2i4.165.

[3] Z. Alfath, F. Basuki, and R. A. Nugroho, "PENGARUH TINGKAT KEPADATAN TELUR YANG BERBEDA TERHADAP EMBRIOGENESIS, LAMA WAKTU PENETASAN DAN DERAJAT PENETASAN TELUR IKAN TAWES (Barbonymus gonionotus)," *Sains Akuakultur Trop.*, vol. 4, no. 2, 2020, doi: 10.14710/sat.v4i2.4643.

[4] R. P. Dewi and W. Arnandi, "Peningkatan Produktivitas Peternak Itik Melalui Penerapan Mesin Penetas Telur," *JPPM (Jurnal Pengabdi. dan Pemberdaya. Masyarakat)*, vol. 3, no. 2, 2019, doi: 10.30595/jppm.v3i2.4460.

[5] R. Kartasudjana, "Penetasan Telur," *Modul Progr. Keahlian Budid. Ternak*, pp. 1–43, 2001.

[6] M. Fajri, H. Amnur, and A. Erianda, "Alat Pengatur Suhu pada Mesin Penetas Telur Ayam menggunakan Mikrokontroler, Android dan Server AWS (Amazon Web Service)," *JITSI J. Ilm. Teknol. Sist. Inf.*, vol. 1, no. 3, 2020, doi: 10.30630/jitsi.1.3.16.

[7] A. A. R. Sentono, "Rancang Bangun Inkubator Penetas Telur Berbasis Internet Of Things," pp. 1–29, 2020.

[8] A. R. Mahmud, "Pembuatan Mesin Penetas Telur Otomatis Berbasis Mikrokontroler," pp. 1–96, 2021.

[9] E. Fadhila and H. H. Rachmat, "Pengendalian Suhu Berbasis Mikrokontroler Pada Ruang Penetas Telur," *J. Reka Elkomika ©Teknik Elektro | Itenas |*, vol. 2, no. 4, pp. 2337–439, 2014.

[10] S. Ridho, *ALAT PENETAS TELUR OTOMATIS BERBASIS MIKROKONTROLER*, vol. 561, no. 3. 2019.

[11] P. Simbolon, "Rancang Bangun Mesin Penetas Telur Otomatis." 2016.

[12] A. Wanto, "Analisis Penerapan Fuzzy Inference System (FIS) dengan Metode Mamdani pada Sistem Prediksi Mahasiswa Non Aktif (Studi Kasus: AMIK Tunas Bangsa Pematangsiantar)," *Pros. Semin. Nas. Inov. dan Teknol. Inf.*, no. November 2016, 2016, [Online]. Available: http://j-ptiik.ub.ac.id

[13] M. Rivai, Rendyansyah, and D. Purwanto, "Implementation of fuzzy logic control in robot arm for searching location of gas leak," *2015 Int. Semin. Intell. Technol. Its Appl. ISITIA 2015 - Proceeding*, no. December 2016, pp. 69–74, 2015, doi: 10.1109/ISITIA.2015.7219955.

[14] C. L. Haura, I. Yanti, and M. Pauzan, "Alat Pendeteksi Formalin Menggunakan Deret Sensor HCHO dan MQ-7 dengan Logika Fuzzy," *J. Nas. Tek. Elektro dan Teknol. Inf.*, vol. 12, no. 2, pp. 117–123, 2023, doi: 10.22146/jnteti.v12i2.7097.

[15] L. Qothrunnada, I. Yanti, M. Pauzan, U. Wiralodra, P. Korespondensi, and L. Fuzzy, "IMPLEMENTASI LOGIKA FUZZY PADA ALAT PENDETEKSI KUALITAS MINYAK GORENG BERDASARKAN pH DAN TINGKAT KEJERNIHAN IMPLEMENTATION OF FUZZY LOGIC IN COOKING OIL QUALITY DETECTION DEVICE BASED ON pH AND CLARITY LEVEL," *J. Teknol. Inf. dan ilmu Komput.*, vol. 11, no. 1, 2024, doi: 10.25126/jtiik.20241118289.

[16] A. Patel, S. K. Gupta, Q. Rehman, and M. K. Verma, "Application of Fuzzy Logic in Biomedical Informatics," *J. Emerg. Trends Comput. Inf. Sci.*, vol. 4, no. 1, pp. 57–62, 2013, [Online]. Available: http://citeseerx.ist.psu.edu/viewdoc/download?doi=10.1.1.644.2777&rep=rep1&type=pdf

[17] A. Fathoni, M. Mustain, and R. Wardhani, "Sistem Pendukung Keputusan Penjurusan Siswa Pada Sma Pancamarga 1 Lamongan Menggunakan Metode Fuzzy," *Joutica*, vol. 3, no. 1, p. 151, 2018, doi: 10.30736/jti.v3i1.202.

[18] N. Iksan *et al.*, "Sistem Kendali Suhu dan Kelembapan pada Alat Penetas Telur Berbasis Fuzzy Logic Controller," *JEPIN (Jurnal Edukasi dan Penelit. Inform.*, vol. 8, no. 2, pp. 245–254, 2022.

[19] S. Darmo, I. . Alit, I. . B. Susana, I. . Joniarta, and S. Sultan, "Penetas Telur Sistem Rak Putar Dengan Kontrol Suhu RTD," *J. KARYA Pengabdi.*, vol. 2, no. 1, 2020, doi: 10.29303/jkp.v2i1.37.

[20] F. Rahman, S. Sriwati, N. Nurhayati, and L. Suryani, "RANCANG BANGUN SISTEM MONITORING DAN KONTROL SUHU PADA MESIN PENETAS TELUR OTOMATIS BERBASIS MIKROKONTROLER ESP8266," *ILTEK J. Teknol.*, vol. 15, no. 01, 2020, doi: 10.47398/iltek.v15i01.499.

[21] F. B. Paimin, *Membuat dan Mengelola Mesin Tetas*. 2011.

[22] R. Hidayah, I. Ambarsari, and S. Subiharta, "Kajian Sifat Nutrisi, Fisik dan Sensori Daging Ayam KUB di Jawa Tengah," *J. Peternak. Indones. (Indonesian J. Anim. Sci.*, vol. 21, no. 2, p. 93, 2019, doi: 10.25077/jpi.21.2.93-101.2019.

[23] S. Rahadi, "Buku Manajemen Peternakan Ayam Petelur." pp. 33–34, 2012.

ISSN 2355-3286

Field Assessment for Initial Preparation of Net Zero Building Certification for The Universitas Multimedia Nusantara (UMN) Building: A Case Study On Visual Comfort in C and D Tower

Nicholas Pranata, Muhammad Salehuddin
Engineering Physics, Universitas Multimedia Nusantara, Tangerang, Indonesia
nicholas.pranata@student.umn.ac.id, muh.salehuddin@umn.ac.id

Accepted on 17 May 2024
Approved on 13 June 2024

***Abstract*— Ensuring optimal physical comfort, the need for a comprehensive evaluation of the performance of building systems was established. This investigation endeavors to meticulously scrutinize illuminance and light power density metrics across distinct temporal segments (morning, noon, afternoon, and night), as well as the dynamism of daylighting and artificial lighting presence within Tower C and D of Universitas Multimedia Nusantara (UMN). Noteworthy for their incorporation of double skin facades, these edifices serve as focal points of inquiry. The empirical findings reveal that illuminance levels within classrooms and offices, irrespective of natural or artificial lighting, consistently fall short of the prescribed 350 lux threshold based on SNI across most floor levels. The efficacy of the double skin facade manifests in a discernible attenuation, diminishing illuminance ingress to the building by approximately 50%, and precipitously by up to 90% about window fixtures. Furthermore, the analysis of light power density underscores an energy efficiency quotient hovering around 60%. These empirical insights are intended to serve as a foundational resource for guiding the initiation of Net Zero Healthy Greenship certification endeavors.**

***Index Terms*— double skin facade SNI; illuminance; light power density; lighting systems; Net Zero Healthy.**

I. INTRODUCTION

The lighting system is one of the factors in the Net Zero Healthy program. The significance of lighting systems in a building design is correlated with health in many ways. Fundamentally, physical comfort based on thermal, humidity, and lighting as well as other aspects play an important role in ensuring the well-being of building occupants [1], [2], [3], [4]. For instance, the temperature designed based on the standard comfort methodologies does not comply with the preference of hospital patients based on the clothing insulation and activities inside the room [1]. For humidity, an imbalance of relative humidity greatly impacts the spread of viruses and bacteria indoors, causing health risks [2], [3]. Lighting systems show a similar concept in which the use of proper lighting will prevent sicknesses such as headache, blurred vision, and even stress, etc. [4].

With the current behavior of humans, which is spending time mostly in indoor environments, exposure to outdoor daylight is reduced and in contrast, light is exposed to occupants even in the hours of natural darkness [5]. Concerning comfort levels, there is a significant correlation with the phenomenon known as sick building syndrome (SBS), which refers to symptoms potentially induced by indoor environmental quality and the duration of time spent within a building [6], [7], [8], [9]. Symptoms of sick-building syndrome (SBS) appear in occupants such as nausea, eye irritation, olfactory disturbances, dry skin, sore throat, difficulty in concentrating, flu, and many others that greatly towards their performance [7], [10]. Hence, making the best designs, especially in lighting systems, will help in improving performance on visual tasks and avoid negative health impacts [11], [12], [13]. As an example, it is shown that symptoms of affective disorder and depression can be reduced by lighting therapy [14].

The Net Zero Healthy program delineates rigorous criteria for the integration of standardized lighting systems within building design. As stipulated by GBC Indonesia, the foundational requisites for ensuring the health and comfort of occupants encompass comprehensive considerations, encompassing not only air circulatory dynamics and thermal equilibrium but also the critical dimension of visual amenity. Specifically, adherence to the latest edition of SNI 03-6197 is mandated for illuminance levels by the Indoor Health and Comfort or IHC 5 New Building 2.0 framework [15].

In addition to illuminance standards, stringent compliance with prescribed light power density regulations, as outlined in the latest iteration of SNI 03-

6197, is imperative. These regulatory mandates are informed by a compendium of reference documents, including but not limited to SNI 03-2396 for natural lighting provisions, ISO 50015:2014 for the meticulous management of energy systems and the verification of organizational energy performance, as well as ANSI/ASHRAE/IES Standards 90.1-2019 delineating the Energy Standard for Buildings Except Low-Rise Residential Buildings [16]. The value of the standard for both variables is strongly adherent with room function, one such example like classroom criteria with 350 lux and 7.53 Watt/m^2 for illuminance and light power density respectively. Hence specific and careful measurements procedure for both cases must be well executed to get the expected result.

Following the measurement strategy, for lighting systems, another standard can be used, namely SNI 7062-2019 for the measurement of illuminance in the working environment. Whilst for light power density, technical data such as the room area, number of lamps, and the power consumed for the lighting is needed. With the measurement method provided, a determination of how good a lighting system in a building design can be made. Moreover, to the necessity for Indonesia's buildings to reach Net Zero Healthy, this research is conducted to contribute to support and reach a healthy environment in a building as well as become the basis and findings, especially in visual comfort, to promote energy efficiency and renewable energy implementation further. This research is conducted from February to May 2024 in UMN's C and D Tower by collecting pre-requisite data, location survey, administrative processing, measuring visual comfort based on illuminance and light power density, analyzing, and finally concluding and resulting in recommendations.

Currently, UMN's D Tower is categorized as Net Zero Ready with the condition of as long as energy efficient measures are applied, and renewable energy is used at a minimum threshold [15]. Accordingly, this tower along with New Media Tower (C) had applied a unique design based on a double skin facade to help in building energy efficiency. In this case, the double skin facade has optimally helped in allowing natural lighting into the building while controlling overexposure to light and heat through its design filtering method. Double Skin facade (DSF) in general, is a three-layer design consisting of internal skin, intermediate area, and external skin that covers buildings [17]. The uniqueness of this design signifies the transparency with which daylight penetrates with a glare-free characteristic. The benefits of DSF include environmental benefits (reduced energy consumption, ventilation, airflow regulation, thermal comfort enhancement, control of daylighting and glare, noise reduction) and economic benefits (decreasing cost in long term perspectives due to energy efficiency aspect and sustainability) [17], [18]. However, the disadvantages of DSF including investment cost and the risk of overheating on sunny days (needing to install a cooling system) must also not be overlooked [17]. The key components of a Double Skin Facade (DSF) primarily include the cavity gap, intermediate space, outer and inner glass layers, along with shading devices [18], [19]. In the case of UMN, as seen in Fig. 1., the inner skin is made from m-system panels, concrete and plaster with 13 cm thickness for walls and clear glass up to 80% of the wall with 8 mm thickness [20], [21]. While the outer skin consists of hollow aluminum frames that are integrated by perforated aluminum plates. The intermediate spaces have various sizes yet can be accessed as a pathway.

a) b) c)

Fig. 1. Double Skin Facade View of UMN's a) C, b) D Tower from Inside and c) Outside of Clasrooms

Thus, this helps in giving controlled natural lighting which will reduce the usage of artificial lighting that consumes energy, supporting energy efficiency. In addition, it also helps in regulating air flow and heat transfer between the outside and inside parts of the tower, giving sufficient fresh air and preferable temperature for occupants without having to avoid overdependence on mechanical air conditioning systems.

The effect of double skin facades in an office on daylight performance shows values for double skin facades decrease by 25-30% compared to single skin, however, it slightly raises the illuminance near the rear wall to support uniformity [22]. Another study examines the performance of the double skin facade in the Henricus Constant building of Soegijapranata Catholic University along with the level of natural lighting in buildings. Results show that the secondary skins create shade in the building's interior, however causing natural lighting to be 30 lux, far less than 350 lux for classroom standard (SNI) [23]. Thus, daylight parameters are a vital aspect to be considered by architects and designers to let optimum penetration of daylight, such as using double skin facade [24].

Hence, this research is intended as a media for field assessment towards the readiness of UMN's building specifically in C and D towers that integrated double skin facade since the facilities fulfill the criteria for Net Zero Building are presented such as natural ventilation on the class corridor, natural lighting systems and so forth. The findings of this research are expected to contribute significantly to enhancing preparedness and serve as valuable scientific contributions. It is hoped that these insights will inspire further research in similar domains, thus fostering the advancement of Net Zero initiatives in Indonesia.

II. METHODS

In this study, quantitative descriptive methods are employed, encompassing data collection, processing, analysis, evaluation, and the formulation of recommendations regarding illuminance and light power density across various room types within UMN's C and D Towers. The research methodology's flow is delineated comprehensively through the following procedure in Fig. 2.

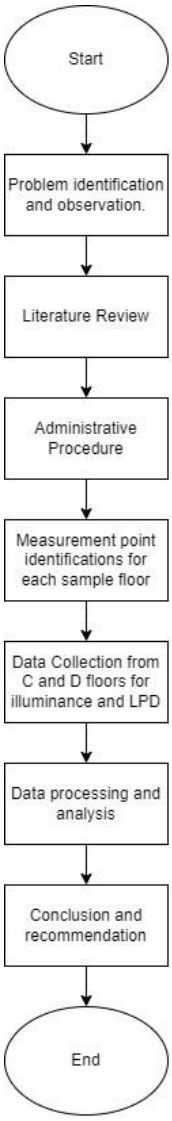

Fig. 2. Research Method Flow Chart

To provide a clearer understanding of data collection and data analysis, each variable for illuminance and light power density can be elaborated as follows:

A. Data Collections

a. Illuminance Data Collection

Illuminance measurements are done using DT-8820 Environment Meter which has been calibrated by comparing to other similar device such as lux meter to show the same result when positioned in the same spot. The measurements are made for both C and D tower which consist of classrooms, offices, storage, panel rooms, toilets, halls, and canteen as well as a parking area. Rooms within the C (New Media) and D (PK Ojong) Towers are appropriately categorized based on their designated functions and taken as sample as seen in Table I. Every floor will undergo comprehensive measures determined based on its area, classified in namely SNI 7062-2019 with the following method shown in Fig 3. This standard provides the methodology for illuminance measurement in working environments.

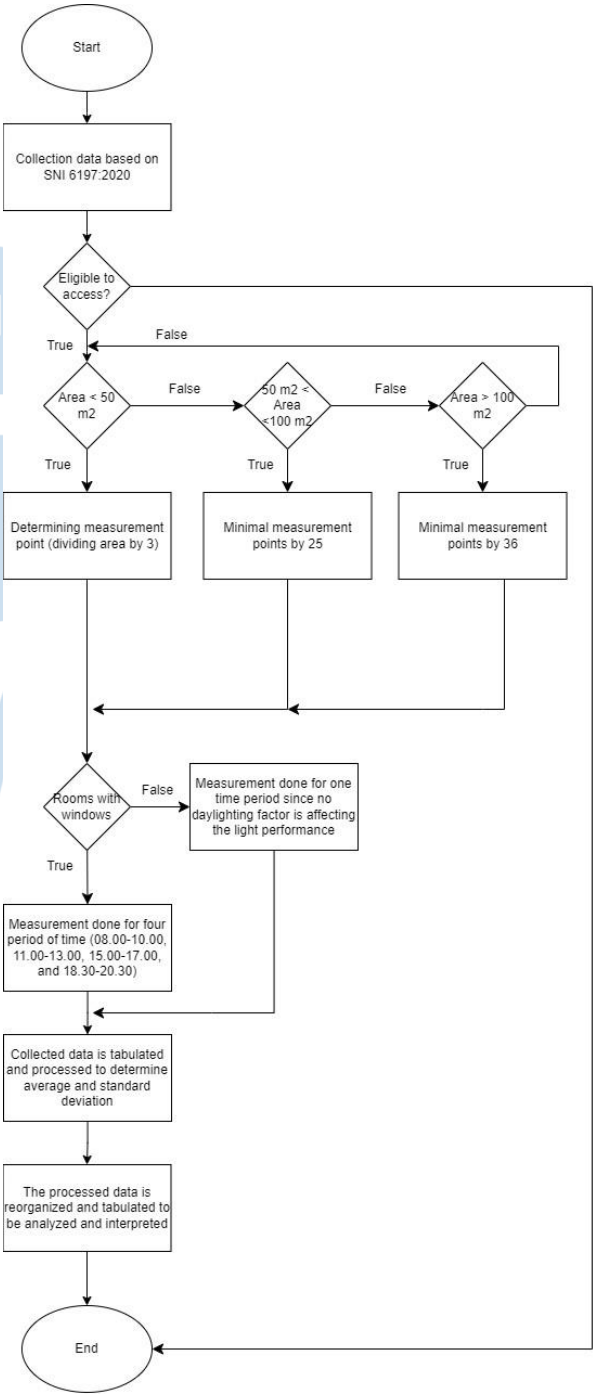

Fig. 3. Measurement Method Flow Chart

TABLE I. RULE BASE

Lamp/Fan	Cold	Warm	Hot
Dry	Bright/ Fast	Ideal/ Fast	Dim/ Fast
Medium	Bright/ Normal	Ideal/ Normal	Dim/ Normal
Moist	Bright/ Slow	Ideal/ Slow	Dim/ Slow

For clarity, as an example, the selected rooms are determined for their distributed measurement points, shown in Fig. 4. and 5.

Fig. 4. Tower C Seventh Floor for Laboratories Measurement Points

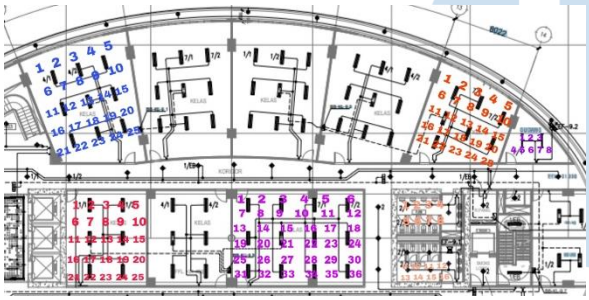

Fig. 5. Tower D's Classes, Laboratories, Architecture Studios, Toilets, and Storage Measurement Points

Fig 4. and 5. Shows C and D Tower in which the numbers in colors (black, blue, red, orange, and purple) shows the measurement points. Moreover, several factors must be considered such as repetition of 3 times for measurement with the height of 0.8 m from floor and the sensor being adjacent to the measured surface. Researchers must also position themselves to avoid light obstruction and should not wear reflective clothes. Further, this research uses the equation of illuminance from SNI 6197-2020 for comparison purpose which is shown in equation (1).

$$N = \frac{E\ average\ \times A}{F_i \times K_p \times K_d} \quad (1)$$

which can be reorganized to form equations (2) :

$$\frac{N}{A}(F_i \times UF \times MF) = E_{average} \quad (2)$$

To show the estimated E (illuminance) in each selected room by collecting the specification data of the lamp used such as the luminous flux or Fi (lumen), utilization factor UF or Kp by 0.5, maintenance factor MF or Kd by 0.6, area or A (m^2) and number of lamps or N. Both values of UF and MF will be utilized for all rooms illuminance calculation with the sense as an anticipation for the least optimum conditions for the current lighting system in both towers. In detail, as an example, with the given lamp specification of lamp specifications which are FL TL5 2700 lumen 28 W Philips for C Tower and LED tubes T8 1600 lumen 16 W for D Tower, the illuminance can be calculated by multiplying the number of lamps with its luminous flux along with the UF and MF value which then divided by the area for each floor. The lamps vary in which for C Tower, ranging from 10-24 while for D Tower by 12-18 for most of the typical rooms although several larger and/or smaller rooms have different numbers of lamps. While the areas vary from 50-110 m^2 and 60-100 m^2 for C and D Towers respectively.

The data processing is facilitated by Microsoft Excel in which tables of number of measurement points with 5 repetitions each are made to find the average and standard deviation. The illuminance obtained (E), both from manual measurements (average value as mentioned) and calculations, are compared to SNI 6197-2020 standards based on room function for visualization.

b. Light Power Density (LPD) Data Collection

The measurement method for light power density involves the need for technical data which is the lamp specification mention priorly. Then another data that must be obtained includes details such as the quantity of lamps used for illumination during activities as well as areas for each room that have also been explained. Thus, the given data can produce the calculation for LPD by multiplying the number of lamps by its power and then dividing by the room area. This data was gathered based on the specific conditions of each room, organized into tables, and then compared against the standards outlined in SNI 6197-2020. Finally, efficiency for this variable can be made by subtracting maximum values in SNI to the obtained LPD and then divided again by the SNI value to obtain the efficiency or saving percentages.

B. Data Analysis Technique

The collected and organized data undergoes analysis. This process involves comparing the measured results with the standards specified in SNI 6197-2020 for illuminance and light power density, as detailed in Table II. This standard, namely Energy Conservation for Lighting System, provides the values and specifications for the minimum and maximum values for illuminance, LPD, as well as other parameters including luminance, etc. that acts as a baseline to limits the utilization of lighting systems for energy conservation purposes.

TABLE II. ILLUMINANCE AND LIGHT POWER DENSITY STANDARD ACCORDING TO SNI 6197:2020 [16]

Type of Room	Illuminance (Lux)	Light Power Density (W/m^2)
Office		
Working Room	350	7.53
Meeting Room	300	7.53
Drawing Room	750	7.53
Parking Lot	100	7.53
Archive Storage	150	7.53
Education Institute		
Classroom	350	7.53
Laboratory	500	7.53
Computer Laboratory	500	7.53
Exhibition	300	7.53
Canteen	200	7.53
Parking Lot	100	1.4
Restaurant		
Fine Dining Room	30	8.61
Lounge	100	8.61
Cleaning Room	100	8.61
Toilet	200	8.61
Hotel		
Receptionist Room	200	6.03
Kitchen	300	6.03
Eating Room (Restaurant)	250	6.03
Multipurpose Room	250	6.03

The results of this research are derived from the analysis of three sets of measurement data encompassing illuminance, measured through both instrumentation and manual calculation, across four distinct periods (morning, noon, afternoon, and night), with and without daylight presence, alongside light power density. Certain conditions were established throughout the measurement process as follows:

1. Measurements are conducted in accessible rooms.
2. Measurements are conducted in four distinct periods: morning, noon, and afternoon. During each of these periods, measurements are taken twice under conditions with (C1) and without (C2) artificial lighting. For nighttime measurements, conditions without daylighting (C3) are used. Special considerations are made for areas such as the parking lot, where artificial lighting remains active at all times, and the canteen, where artificial lighting is adjusted based on situational requirements across all periods.
3. Illuminance measurements are conducted once in rooms without windows due to the absence of daylighting factors. Measurements are limited to accessible rooms only.

III. RESULT AND ANALYSIS

A. *Illuminance Measurement Result*

Measurements conducted during time periods—morning, noon, and afternoon—reveal a decrease in illuminance values in the absence of artificial lighting, predominantly ranging from 300-400 lux, which then drops to 150-250 lux for classrooms and laboratories, and 140-240 lux to 30-60 lux for offices. These variations are observed distinctly by floor level, indicating the unsuccessfulness to fulfill with the standards. Other types of rooms such as meeting rooms remain under 300 lux except for morning cases. While basement, storage and toilets do not comply with the requirements of 100 lux, 150 lux, and 200 lux. In the case of night period, all rooms show illuminance that are not reaching the standard.

Based on the preceding results, pertinent information can be extracted to serve as a reference for informing recommendations in preparation for Greenship Net Zero & Healthy Building Certification at Tower C as shown in Fig. 6. Specific to this scenario, the term “Not Appropriate” or NA and OK are used to represent the appropriateness percentage towards the standard (SNI 6197 2020). The data processing involves comparison for all measurement types C1, C2, and C3 at all periods to the standards and then counting the total that lies on the NA and OK categories. The results for each room are summed up and averaged to show the percentage per floor. The method of determining the percentage is based on the calculation for all illuminance measurement condition C1, C2, and C3 that do not adhere to the standard for each rooms in each floors. As an example, the second floor of D Tower, consisting of 9 rooms, each has 7 conditions (each C1 and C2 for morning, noon, and afternoon with addition of one C3 condition for nighttime). The illuminance results for those 7 conditions when compared to values from Table II do not reach the minimum of 350 lux for classrooms, confirming as NA. Therefore, the percentage of fulfillment can be shown by comparing the numbers of conditions that lie in NA aspect with the total of conditions which in the previous case resulting by 0%. Further analysis for floors with certain fulfillment can be made by adding each C1 and C2 conditions separately for each period to show the percentage between the NA or the non-fulfillment with the OK or the fulfillment.

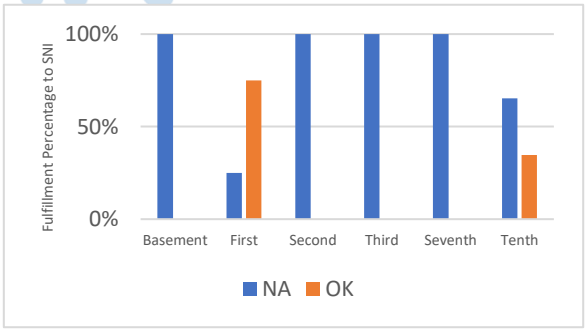

Fig. 6. Illuminance Satisfaction (%) of C Tower to SNI 6197 2020

Fig. 6. shows that all sampled floor results are not complying with the standards, except for first and tenth floor with 75% and 35% compliance respectively. For the Tenth floor especially, it can be further detailed, shown in Fig. 7. below.

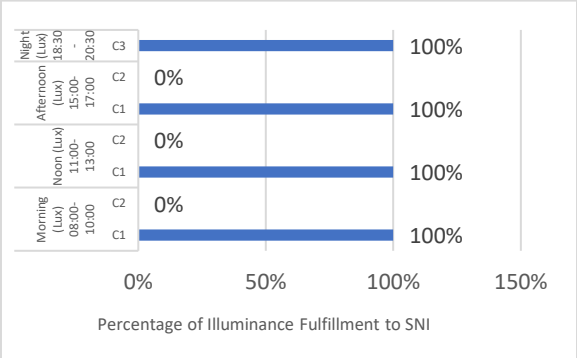

a)

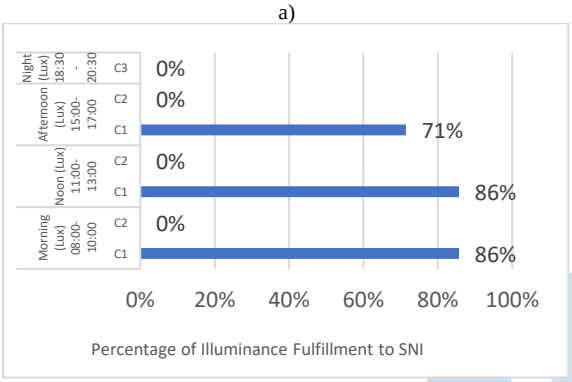

b)

Fig. 7. Condition of Illuminance at a) First Floor and b) Tenth Floor for Classes

From Fig. 6. and 7. can be seen that all rooms should immediately be adjusted to meet the standards. Cases in C2 show that the absence of artificial lighting can greatly affect the illuminance measurements since none complies with the standards, concluding that the rooms are always conditioned with artificial lighting all the time. Whilst in C3 cases where none complies with the standards, significant action must be taken such as changing the lamp type by having higher lumens up to 6500 lumens if assessed based on the calculations explained in illuminance calculation section. This includes the assumption for UF and MF by 0.5 and 0.6 along with the number of lamps, their luminous flux as well as the areas. By changing the luminous flux up to 6500 lumens, all rooms should reach the standard such as for classrooms by minimum of 350 lux for all period. This value itself is obtained by computing the current existing calculation in the illuminance calculation table with trial and error to see the maximum luminous flux than is applicable for all rooms for both C and Towers. It should be noted that for laboratories, additional lamps must be added with the recommended lumens from 22 to 27 and 24 to 30 lamps to reach around 500 lux based on the calculation method. This is recommended to counter the scenarios in which occupants use rooms without a daylighting presence at all.

Based on C1 measurements for all floors, the change of lamps mentioned priorly can help in fulfilling the gap between the existing illuminance and the required standard although the tenth floor has fulfilled to a certain extent which shows the correlation with time and height since daylighting and artificial lighting are presented as well as more amounts of light that reach the area for it being nearer to the sun. This is also supported by the fact that less shading and other factors occurred.

For Tower D data, across all types of rooms also indicate a decrease in illuminance values in the absence of artificial lighting, primarily ranging from 300-500 lux decreases to 120-300 lux for classrooms and laboratories, 170-210 lux to 30 lux for studios, and 150-390 to 15-250 lux for hotel faculty rooms. Moreover, the meeting rooms in the first and fifteenth floor do not adhere with the standard by 300 lux. Basement, storage and toilets in this tower are also not fulfilling the requirements of 100 lux, 150 lux, and 200 lux. Similarly, within C Tower, the case of night period for all rooms show inadequate result of illuminance. Significant information can be selected from the preceding results to provide highlights for recommendations in preparation for Greenship Net Zero & Healthy Building Certification at Tower D as shown in Fig. 8. below.

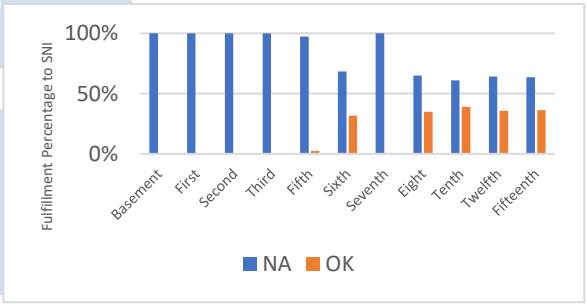

Fig. 8. Illuminance Satisfaction (%) of D Tower to SNI 6197 2020

Fig. 8. shows that all sampled floor results do not reach standards with lower levels to the third floor, and the seventh floor having 100% inappropriateness. These several floors starting from the fifth to the fifteenth can be further detailed in Fig. 9. below.

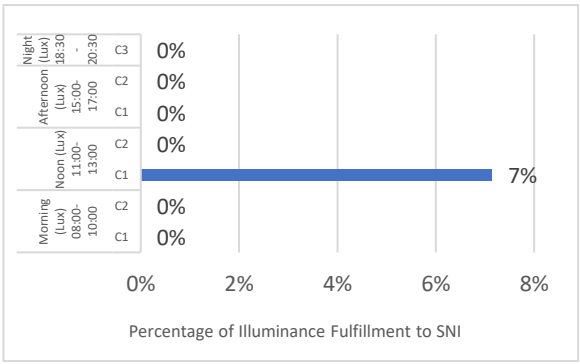

a)

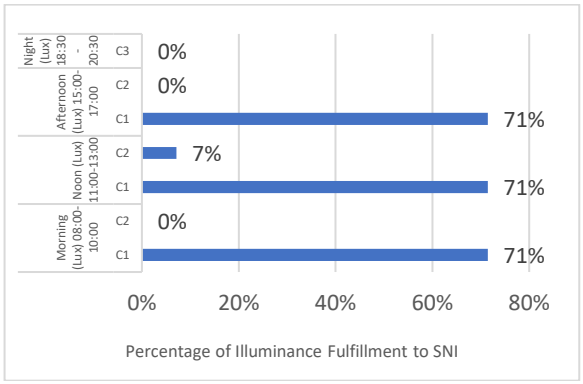

b)

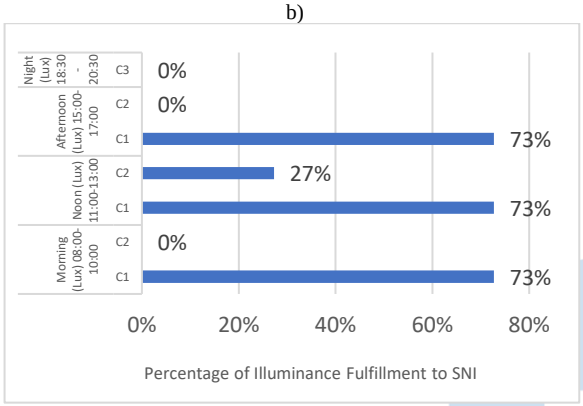

c)

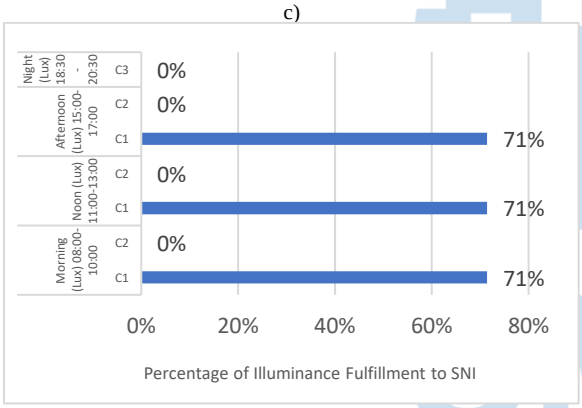

d)

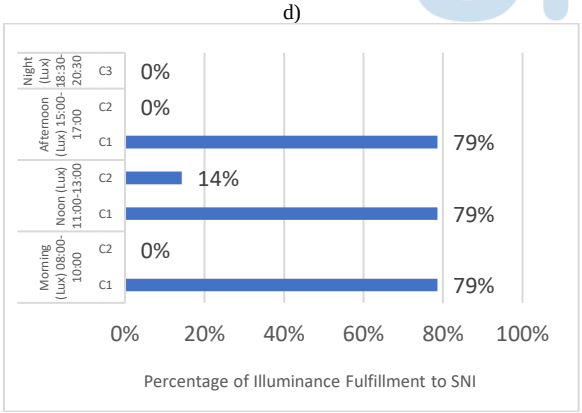

e)

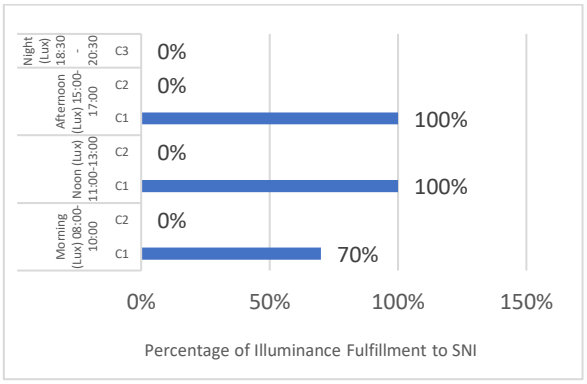

f)

Fig. 9. Illuminance Condition in Classes for a) Fifth b) Sixth c) Eight d) Tenth e) Twelfth f) Fifteenth

From Fig. 9., it is highlighted that all rooms should also immediately be adjusted to meet the standards. Comparably with C Tower results, C2 measurements had shown rooms are not encouraged to be conditioned without artificial lighting to reach the standards. C3 cases also show that significant action must be taken, i.e. changing the lamp type by having higher lumens of up to 6500 lumens if assessed based on the assumptions in calculations (discussed in the next section) with laboratories on fifth floors must be added up to 25 lamps except for smaller areas should be added up to 17 lamps for the same lumens. C1 measurements for all floors also show the need to change the lamps mentioned previously in helping to reach the gap between the standards. Fig. 9. points out that C1 measurements for the fifth to fifteenth floors (except the seventh's) do satisfy the standard of 70% above which shows that height and time also correspond to the illuminance results. The same reasoning to C Tower's tenth floor, daylighting on the higher floor gives more amounts of light to the rooms which complies with the measurements results with the standards.

It should be noted that based on the findings, highlighted information can be given to show illuminance variation factors as follows:

- Orientation = The UMN building is oriented towards the northeast, strategically positioned to leverage sunlight from the east during sunrise, illuminating the southeast portion of UMN Tower C and D, primarily comprising corridors and lower-level classrooms. Conversely, during sunset in the west, direct sunlight bathes the northwest part of the building, reaching several upper-level rooms. This solar trajectory and its effects on illuminance are illustrated in Fig. 10. As sunlight angles change throughout the day, various rooms experience fluctuations in illuminance, contingent upon the building's design features facilitating light penetration. This trend is evident in Tower C, where higher floor levels exhibit higher illuminance levels, as exemplified by the tenth-floor surpassing 350 lux, while lower levels often

remain below 300 lux. Similarly, Tower D showcases a notable disparity between higher (tenth to fifteenth) and lower floor levels, with illuminance levels hovering around 400-500 lux or higher on upper floors, particularly noticeable during the noon period. This difference can be attributed to the angle of direct sunlight reaching each area, emphasizing the influence of floor level height on illuminance results.

Fig. 10. Sunlight Direction Towards UMN

- Height = The variation in floor level height contributes significant differences. The variation in floor level height contributes significantly to the differences observed in illuminance values. Typically, higher floor levels experience increased illuminance due to reduced shading obstruction and a higher influx of sunlight.
- Shading = Shading, in this context, refers to the exterior elements of the building that cast shadows on lower floor levels, including Tower C and D up to the second floor. These shadows are caused by surrounding objects such as vegetation, other buildings, or adjacent UMN Towers, as well as internal factors like computer installations that obstruct natural light in computer laboratories.
- Reflection = Reflection is caused by external buildings.
- Weather Condition, Daylight Cycle, as well as Presence of Daylighting and/or Artificial Lighting.

B. Illuminance Calculation Result

For all the rooms, the area, number of lamps, and the specification of the lamp data are collected. Using the assumption for utilization factor as 0.5 and maintenance factor as 0.6, the result of the minimum E (illuminance) is based on the standard shown in Fig. 11 for Tower C and Fig. 12 for Tower D.

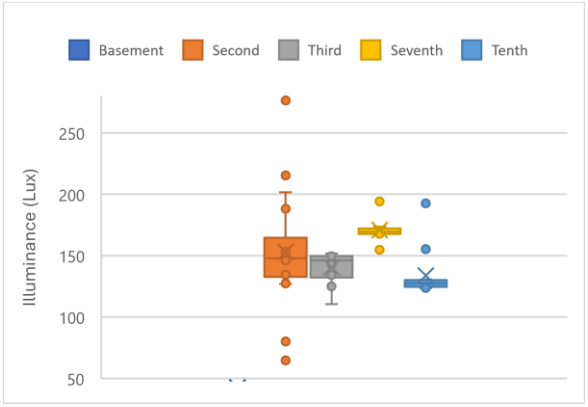

Fig. 11. Box Whisker Plot for C Tower Illuminance Calculation Results

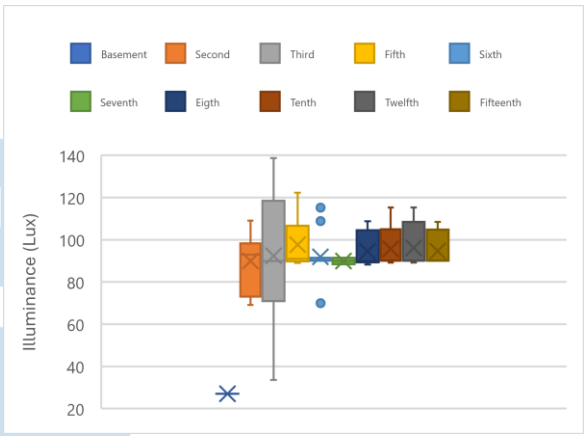

Fig. 12. Box Whisker Plot for D Tower Illuminance Calculation Results

The illuminance calculation data indicates that in Tower C, all types of rooms with known lamp data (number and luminous flux) and room area did not meet the minimum standard. This is evident in the parking lot, which measures only 42.7 lux instead of the required 100 lux. Similarly, offices mostly range around 40-150 lux while classes on the third and tenth floor lie about 120-150 lux. Laboratories on the seventh floor are also shown to be 150-190 lux. The same goes for toilets, storage, and meeting rooms. Whereas the illuminance calculation data for Tower D depicts the same trend by not meeting the minimum standard. Thus, it is recommended, as mentioned in the previous section, to change lamps to 6500 lumen types for each to reach the corresponding values in the standard also with additional lamps for laboratories according to Tower C and D existing lamps.

C. Light Power Density Measurement Result

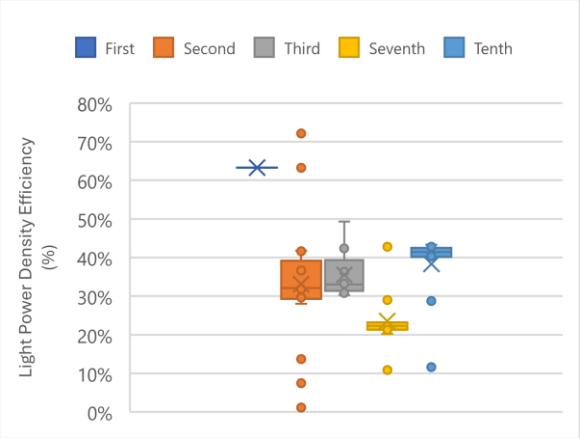

Fig. 13. Box and Whisker Plot for Light Power Density Efficiency Ranges of C Tower

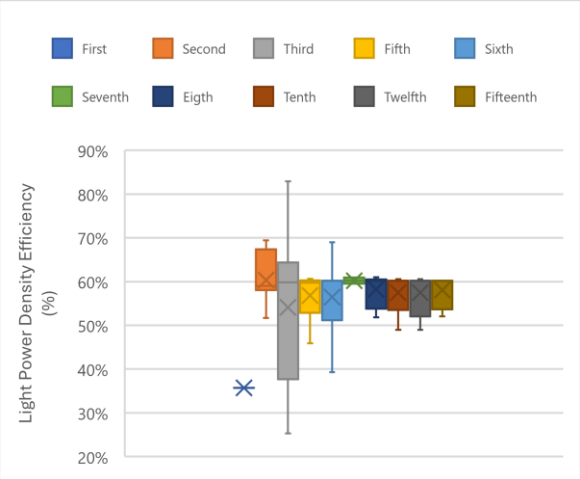

Fig. 14. Box and Whisker Plot for Light Power Density Efficiency Ranges of D Tower

Based on Fig. 13, the light power density (LPD) results for Tower C generally remain within 7.53 W/m², below the maximum standard. This indicates the energy efficiency applied throughout the tower, with the exception of the parking lot, which records an LPD of 1.47 W/m², slightly exceeding the standard of 1.4 W/m². LPD values for offices, classrooms, laboratories, and meeting rooms range from 4-5 W/m². Canteen's LPD reaches 2.77 W/m², factoring in the lamp type and wattage specified in the technical data. Efficiency calculations relative to the standard LPD (7.53 W/m²) indicate a 63.27% efficiency rate. For Tower D, the LPD results can be seen in Fig. 13.

Then based on Fig. 14., the light power density (LPD) results for Tower D generally align with or fall below the maximum standard of 7.53 W/m², as well as the educational institute standard and other standards for Hotel and Restaurant, serving as references. This indicates that energy efficiency measures have been effectively implemented across the tower. Specifically, the LPD for the parking lot, which measures 0.9 W/m² (compared to the standard of 1.4 W/m²), achieves an efficiency of 35.7%. LPD values for classes, laboratories, offices, and meeting rooms range from 2-4 W/m².

D. Double Skin Facade Impact

Tower C and Tower D, characterized by a distinctive continuous pattern on each floor level, comprehensive measurements of the Double Skin Facade's (DSF) aperture area, number of apertures, and window-to-wall ratio (WWR) per floor are imperative. This is further discussed as follows.

a) b)

Fig. 15. Double Skin Facade Tower C a) Pane Design and b) Measurement Result

Depicted in Fig. 15. for Tower C, each pane typically contains around 29 to 13 holes, totaling approximately 377 holes, each with a diameter of 2 cm. On the third floor, with a WWR of roughly 0.588 and 1.5 panes occupying the windows, the illuminance measurements reveal 9700 lux without the facade, 600 lux with the facade, and 388 lux with both windows and facade. The facade effectively filters about 94% of direct sunlight, with additional windows further reducing direct sunlight by 96%. However, these variations may also stem from factors such as sunlight angle and surrounding object shading.

Similarly, on the seventh floor with a WWR of about 0.61 and 2 panes vertically occupying the windows, illuminance measurements show up to 12550 lux without the facade, 5210 lux with the facade, and 730 lux with both facade and windows. This indicates a filtration of about 58.4% by the facade alone, with an additional decrease of 94.1% due to the presence of windows. On the tenth floor, with a WWR of approximately 0.48 and 1.5 panes vertically occupying the windows, illuminance readings are 5890 lux without the facade, 3240 lux with the facade, and 1031 lux with additional windows. This translates to a reduction of 44.9% with the facade and 82% with additional windows. These findings can be extrapolated to other orientations on the same floor based on concise measurement tests. The results indicate that the facade significantly reduces daylight illuminance in Tower C, with a decrease of more than 40%, while the inclusion of windows leads to a reduction of around 80-90%.

For Tower D, the facade design, as illustrated in Fig. 16., features circular apertures of varying sizes, with the smaller ones measuring approximately 2.5 cm and the larger ones around 25 cm. Across all floors, the window-to-wall ratio ranges from 16.5% to 24%, contributing to the filtration of light entering the rooms by the windows. Under optimal conditions, with 120 small circular holes and 45 large circular holes per room, the penetration of daylight is reduced by 31% with the facade alone and by 67% with the addition of windows.

a) b)

Fig. 16. Double Skin Facade for Tower D a) Design and b) Measurement Results

An example of this reduction is observed in the east corridor measurement during maximum direct sunlight (afternoon) on the fifteenth floor under favorable weather conditions, with illuminance levels decreasing from 16270 lux without a facade to 11230 lux with a facade and 5360 lux with additional windows. Similar reductions are seen across other floors, including the third, fifth, sixth, eighth, tenth, and twelfth levels, with reductions ranging from 30% to 40% with the facade and 70% to 90% with additional windows, under similar conditions.

Regarding the impact of the double skin facade on illuminance reduction, measurements conducted in the corridor corner reveal a significant decrease in direct daylight reaching the rooms, with a maximum reduction of 90%. While this reduction is beneficial for upper-level areas, lower-floor levels may experience insufficient daylighting, resulting in illuminance levels that do not meet the standard requirements. As an example, the third floor in C Tower suffers by lower illuminance in the noon, around 320 lux with daylighting and artificial lighting presented in which compared to the tenth floor with higher values by approximately 420 lux although shading factors also presented around the lower floors. The same goes for D Tower in which the fifth floors measurement results show illuminance value by around 300 lux whereas the twelfth floors reach above 420 lux. This clearly shows that the double skin facade affects the visual comfort in the room along with the priorly mentioned factors. Not to mention that laboratories in C and D Tower are relatively positioned vertically at the middle of the tower, illuminance results tend to not reach the minimum standard of 500 lux. Therefore, careful consideration of the double skin facade design is necessary, particularly for lower floor levels, along with consideration of other factors such as shading from surrounding objects that can further diminish sunlight intensity before it reaches the rooms.

IV. Conclusion

As the preparation for Net Zero Building's Certification, this research is conducted to assess the lighting systems for Universitas Multimedia Nusantara's Tower C and D in various periods (morning, noon, afternoon, and night) as well as the presence variation for daylighting and artificial lighting. The current condition of the lighting systems mostly did not comply with the standard. Areas that do not comply with the standard for the morning until afternoon period (C1 and C2) in Tower C are the basement (85-86 lux), second floor (130-240 lux for offices), third floor (300 lux for classes and above 190 lux for meeting rooms), and seventh floor (300-350 lux for laboratories). While for Tower D which are the basement (69-70 lux), meeting room (198 lux), second floor (above 179 lux for classes), third floor (150-200 lux for classes and laboratories), and fifth floor (280-434 lux for laboratories). Toilets and storage measurements also do not comply with the standard (below 200 and 150 lux respectively). For nighttime measurements (C3), which only rely on artificial lighting, none suffice the standard for all room cases. With proper adjustment for artificial lighting, it can support visual comfort and fill the gap to the standards. In this case, a change of lamps to 6500 lumens type can enrich the illuminance results to fulfill the standards, with important notes to add several lamps to laboratories case in which for C tower from 22 to 27 and 24 to 30 as well as D tower from 14 to 17 and 18 to 25 lamps corresponding to the number of existing lamps.

Illumination levels vary significantly among rooms within Towers C and D, with several floors falling below SNI standards from morning until afternoon. Notably, specific areas, including basements, meeting rooms, storages, classes, offices and laboratories did not meet these standards, with some areas even lacking the required illuminance by up to 500 lux (for laboratories intended) compared to reference values. Moreover, nighttime measurements across all room types on each floor also fall short of minimum standards. Despite focusing solely on artificial lighting system calculations, adjustments to factors such as utilization and maintenance may marginally improve results. However, both measured and calculated values still did not meet the SNI standards. While power efficiency remains high across room types shown by light power density outcomes, it's crucial to prioritize occupant comfort by ensuring adequate illuminance levels, even if it means sacrificing some efficiency.

The passive design, which is a double skin facade for both towers, does support the visual comfort criteria satisfaction however to some extent, as discussed on the findings earlier. In this case, several areas, especially on lower floor levels, suffer from low illuminance value since daylight is filtered not only by the double skin facade and the windows but also by surrounding objects that cause shading. Specifically, for Tower C, the sunlight is filtered above 90% on the third floor, and the seventh floor, 80% on the tenth floor. Whilst for Tower D, the sunlight is filtered by about 30-40% by the facade and up to 90% with windows addition. Future research can elaborate more on the double skin facade effect such as cavity and supported by simulations analysis for recommendations implementation as well as conducting surveys to analyze the correlation between the comfort levels felt by occupants with the existing lighting systems performance to see how far the adjustments must be done.

ACKNOWLEDGMENT

We extend our sincere appreciation to Universitas Multimedia Nusantara for graciously furnishing the resources to facilitate this research pursuit.

REFERENCES

[1] B. S. Alotaibi, S. Lo, E. Southwood, and D. Coley, "Evaluating the suitability of standard thermal comfort approaches for hospital patients in air-conditioned environments in hot climates," *Build Environ*, vol. 169, p. 106561, Feb. 2020, doi: 10.1016/J.BUILDENV.2019.106561.

[2] A. Ahlawat, A. Wiedensohler, and S. K. Mishra, "An overview on the role of relative humidity in airborne transmission of sars-cov-2 in indoor environments," *Aerosol Air Qual Res*, vol. 20, no. 9, pp. 1856–1861, Sep. 2020, doi: 10.4209/aaqr.2020.06.0302.

[3] G. Guarnieri, B. Olivieri, G. Senna, and A. Vianello, "Relative Humidity and Its Impact on the Immune System and Infections," *International Journal of Molecular Sciences*, vol. 24, no. 11. Multidisciplinary Digital Publishing Institute (MDPI), Jun. 01, 2023. doi: 10.3390/ijms24119456.

[4] D. E. Bertani *et al.*, "'Shedding Light on Light': A Review on the Effects on Mental Health of Exposure to Optical Radiation," *International Journal of Environmental Research and Public Health*, vol. 18, no. 4. MDPI AG, pp. 1–16, Feb. 02, 2021. doi: 10.3390/ijerph18041670.

[5] C. Ticleanu, "Impacts of home lighting on human health," *Lighting Research and Technology*, vol. 53, no. 5, pp. 453–475, Aug. 2021, doi: 10.1177/14771535211021064.

[6] N. Muniarti, "Hubungan Suhu dan Kelembaban dengan Keluhan Sick Building Syndrome pada Petugas Administrasi Rumah Sakit Swasta X," *Jurnal Ilmu Kesehatan Masyarakat*, vol. 7, no. 3, 2018, Accessed: Nov. 06, 2023. [Online]. Available: https://journals.stikim.ac.id/index.php/jikm/article/view/123/104

[7] R. Adiningsih and M. C. Hairuddin, "The Incidence of Sick Building Syndrome and Its Causes on Employees at the Governor's Office of West Sulawesi Province," *The Indonesian Journal Of Occupational Safety and Health*, vol. 10, no. 2, p. 153, Jul. 2021, doi: 10.20473/ijosh.v10i2.2021.153-160.

[8] E. Aryadni, I. H. Santoso Poltekkes Kemenkes Banjarmasin Jurusan Kesehatan Lingkungan Jl Mistar Cokrokusumo No, and A. Banjarbaru Kalimantan Selatan, "FAKTOR FISIK DAN BIOLOGI DENGAN KELUHAN SUBYEKTIF SICK BUILDING SYNDROME," vol. 15, no. 2, 2018, [Online]. Available: https://ejournal.kesling-poltekkesbjm.com/index.php/JKL/article/view/50

[9] P. M. Karlina, R. Maharani, D. Utari, K.: Putri, and M. Karlina, "Faktor-Faktor yang Berhubungan dengan Gejala Sick Building Syndrome (SBS)," 2021. Accessed: Nov. 06, 2023. [Online]. Available: https://doi.org/10.52022/jikm.v13i1.126

[10] V. A. Ulfa, A. Asnifatima, and A. Fathimah, "Faktor-Faktor yang Berhubungan dengan Kejadian Sick Building Syndrome (SBS) pada Karyawan RSIA Pasutri Bogor Tahun 2020," vol. 5, no. 5, pp. 428–434, 2022, doi: 10.32832/pro.

[11] P. R. Boyce, H. M. Brandston, and C. Cuttle, "Indoor lighting standards and their role in lighting practice," *Lighting Research & Technology*, vol. 54, no. 7, pp. 730–744, 2022, doi: 10.1177/14771535221126413.

[12] O. Stefani and C. Cajochen, "Should We Re-think Regulations and Standards for Lighting at Workplaces? A Practice Review on Existing Lighting Recommendations," *Front Psychiatry*, vol. 12, May 2021, doi: 10.3389/fpsyt.2021.652161.

[13] I. Wojnicki, K. Komnata, and L. Kotulski, "Comparative Study of Road Lighting Efficiency in the Context of CEN/TR 13201 2004 and 2014 Lighting Standards and Dynamic Control," *Energies (Basel)*, vol. 12, no. 8, 2019, doi: 10.3390/en12081524.

[14] O. Osibona, B. D. Solomon, and D. Fecht, "Lighting in the home and health: A systematic review," *International Journal of Environmental Research and Public Health*, vol. 18, no. 2. MDPI AG, pp. 1–20, Jan. 02, 2021. doi: 10.3390/ijerph18020609.

[15] Green Building Council Indonesia, "Net Zero." Accessed: Feb. 14, 2024. [Online]. Available: https://www.gbcindonesia.org/netzero#:~:text=GREENSHIP%20Net%20Zero%20Healthy%20(NZH,offsite%2C%20and%20offset%20renewable%20energy.

[16] Badan Standarisasi Nasional, *SNI 6197 2020 tentang Konservasi Energi pada Sistem Pencahayaan*. 2020.

[17] O. Nasir and M. Arif Kamal, "An Appraisal of Double Skin Facade in Building Design: Architectural Intervention and Sustainability," *International Journal of Architecture and Urbanism*, vol. 7, no. 1, pp. 158–172, Mar. 2023, doi: 10.32734/ijau.v7i1.11760.

[18] M. Mohammad Zin, N. Ibrahim, and A. Mohad Tazilan, "Day Lighting Research on Double Skin Facade (DSF)," *Int J Eng Adv Technol*, vol. 9, pp. 881–886, Apr. 2020, doi: 10.35940/ijeat.C5362.029320.

[19] M. A. Siddiqui and S. Dua, "Double Skin Facade & Its Impact on Energy Reduction," 2022. [Online]. Available: https://www.ciir.in

[20] Universitas Multimedia Nusantara, "Sustainability Program," umn.ac.id. Accessed: Jun. 07, 2024. [Online]. Available: https://www.umn.ac.id/en/sustainability-program-en/

[21] A. Dama Gaputra, "Material and Construction Analysis of Double Skin Facade on Universitas Multimedia Nusantara's New Media Tower Building," *Indonesian Journal of Built Environment and Sustainability*, vol. 2, no. 1, 2020.

[22] M. Ergin, "Double-Skin Facade Options for Optimum Daylight Quality: An Office Case In Izmir," Izmir Institute of Technology, 2019.

[23] A. E. Manubawa, L. M. F. Purwanto, and A. Ardiyanto, "Measuring The Quality Of Natural Lighting In A Building With Double Skin Façade (DSF) 1," *International Journal Of Architecture and Urban Development*, 2020, doi: 10.30495/IJAUD.2020.15845.

[24] M. S. ÜNLÜTÜRK and T. KAZANASMAZ, "Integration of Daylight Use and Analysis in Double Skin Facades: A Literature Review," *GAZI UNIVERSITY JOURNAL OF SCIENCE*, Aug. 2023, doi: 10.35378/gujs.1243933.

ISSN 2355-3286

Modeling and Simulation of Manipulator Robot Using MATLAB

Tesya Permadi[1], Silmi Ath Thahirah Al Azhima[2], Mariya Al Qibtya[3], Nurul Fahmi Arief Hakim[4]
[1, 2, 3, 4]Industrial Automation and Robotic Engineering Education, Indonesia University of Education, Bandung, Indonesia
[1]tesya@upi.edu, [2]silmithahirah@upi.edu, [3]mariyalqibtiya@upi.edu, [4]nurulfahmi@upi.edu

Accepted on 24 May 2024
Approved on 13 June 2024

***Abstract*— In recent decades, the rapid development of robotic technology has increased the demand for efficient and affordable robots, especially in the manufacturing industry. One type of robot that is commonly used is the robotic arm, which is capable of performing complex tasks with high precision and speed. This research focuses on the modeling and simulation of a 4-DOF RRPR robot manipulator using MATLAB software, including the SimScape Multibody Toolbox and Robotic System Toolbox. This study investigates various aspects of robot performance, such as joint angles, end-effector coordinates, and robot dynamics. With an emphasis on simulation, this research aims to accelerate the development of robotic technology and minimize the risks associated with physical implementation in the field. The simulation results provide valuable insights for improving the efficiency, precision, and reliability of robot manipulators in various applications.**

***Index Terms*— MATLAB Simulation; SimScape Multibody Link; Robotic Arm; Robot Manipulator; Robotic System Toolbox.**

I. INTRODUCTION

In recent decades, the development of robotic technology has experienced rapid progress. The need for robots that can assist human work, especially in the manufacturing industry, has driven high demand for the development of efficient and affordable robots [1]. One type of robot that is widely used is the robotic arm, which is capable of performing complex tasks with high precision and speed. However, the development process of robotic arms often requires significant time and resources. Therefore, computer simulation becomes crucial to accelerate this process and save costs [2, 3].

The mathematical and kinematic modeling of robot manipulators can provide a solid foundation for understanding and evaluating the performance of robotic systems before physical implementation in the field, as done by [4].

Previous research on robot manipulators includes the work of [5], who modeled the motion of a 4DOF (degree of freedom) robot manipulator using the MATLAB Graphic User Interface (GUI). Motion control of robots has also been explored to reduce position control errors, such as using the PID method [5, 6], Fuzzy Logic [7], and combining PID and Fuzzy Logic control [8].

The simulation of robot manipulators using MATLAB software has also been explored by [9]. In this research, the SimScape Multibody toolbox was leveraged for the visualization of the robot manipulator. This approach can help accelerate the robot development process and enhance the efficiency in utilizing resources.

Furthermore, the research on Manipulator robots has been extensively investigated by [10]. This study utilized a 4-DOF RRRR Manipulator Robot model and the Robotic System Toolbox library to compute the inverse kinematics of the manipulator. The findings of this research provide valuable insights into the development and control of such robotic systems.

This research will focus on the simulation testing of the kinematics of a Manipulator. This simulation allows researchers to evaluate various scenarios and operational conditions without having to implement the physical system in the field. By using simulation software such as the SimScape Multibody Toolbox and the MATLAB Robotic System Toolbox, This research can investigate aspects such as the joint angle values, the end-effector position coordinates, and the robot dynamics. Thus, researchers can gain a deeper understanding of the system performance and identify ways to improve the efficiency, precision, and reliability of the manipulator robot in various applications, such as in the fields of industry, healthcare, agriculture, and others.

With an emphasis on simulation, this research aims to accelerate the development process of robotic technology and minimize the risks associated with physical implementation in the field.

II. METHODS

A. Forward and Inverse Kinematics of 4-DOF RRRP Manipulator

In this research, the kinematics of the robot manipulator is divided into two types, namely Inverse Kinematics and Forward Kinematics. Inverse

kinematics is used to obtain the joint angle values for each robot joint, if the desired position (x, y, z) is known. Meanwhile, forward kinematics is used to obtain the position (x, y, z) of the robot, if the values of each joint are known. The explanation regarding the kinematics in this research can be seen in the flowchart shown in Figure 1.

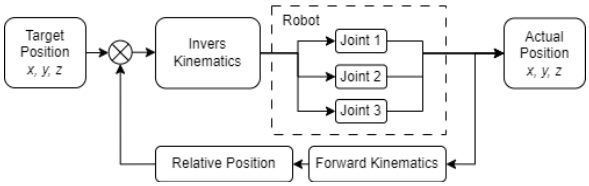

Fig. 1. Robot Kinematics

In this research, a 4-DOF RRRP manipulator was used as the model for simulation in MATLAB. The forward kinematics and inverse kinematics will be discussed in this chapter. The kinematics of the 4-DOF RRPR robot can be described in detail using the D-H parameter notation for each joint. According to [15-17], the D-H parameters are widely used in research because they are simple and easier to understand in describing the kinematics of robotic arms. Figure 2 shows the structure of the 4-DOF RRPR robot, where joints 1, 2, and 3 are revolute joints, while joint 4 is a prismatic joint. The D-H parameter values can be seen in Table 1.

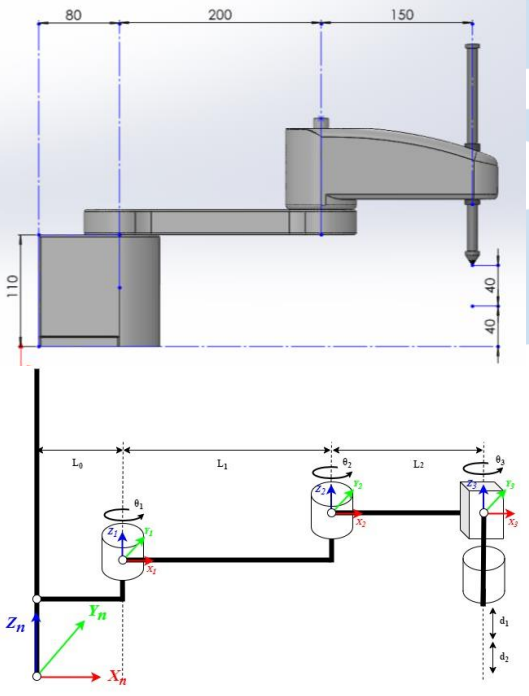

Fig. 2. Free Body Diagram of 4-DOF RRRP Manipulator

TABLE I. D-H PARAMETER OF 4-DOF RRRP MANIPULATOR

Link	a_i (m)	α_i (deg)	d_i (m)	θ_i (deg)
1	L_1	0	0	θ_1
2	L_2	π	0	θ_2
3	0	0	D_1	0
4	0	0	D_2	θ_3

From the D-H parameters shown in Table 1, the values can be transformed into a D-H matrix form as shown in Equation (1). The four values generated by each joint are combined into a single matrix, which results in an equation to find the coordinates x, y, and z. Furthermore, the lengths of the shoulder arm (L_1), elbow arm (L_2), and the length of the end-effector's rise are incorporated into that equation.

$$A_i = \begin{bmatrix} cos\theta_i & -cos\alpha_i sin\theta_i & sin\alpha_i sin\theta_i & a_i cos\theta_i \\ sin\theta_i & cos\alpha_i cos\theta_i & -sin\alpha_i cos\theta_i & a_i sin\theta_i \\ 0 & sin\alpha_i & cos\alpha_i & d_i \\ 0 & 0 & 0 & 1 \end{bmatrix} \quad (1)$$

The four values from each joint that have been transformed into matrix form are shown in Equations (2), (3), (4), and (5). These four matrices are then combined into a single matrix as shown in Equation (6). In these equations, Sin is represented by S, and Cos is represented by C.

$$A_1 = \begin{bmatrix} C_1 & -S_1 & 0 & a_1C_1 \\ S_1 & C_1 & 0 & a_1S_1 \\ 0 & 0 & 1 & 0 \\ 0 & 0 & 0 & 1 \end{bmatrix} \quad (2)$$

$$A_2 = \begin{bmatrix} C_2 & S_2 & 0 & a_2C_2 \\ S_2 & -C_2 & 0 & a_2S_2 \\ 0 & 0 & 1 & 0 \\ 0 & 0 & 0 & 1 \end{bmatrix} \quad (3)$$

$$A_3 = \begin{bmatrix} 1 & 0 & 0 & 0 \\ 0 & 1 & 0 & 0 \\ 0 & 0 & 1 & d_3 \\ 0 & 0 & 0 & 1 \end{bmatrix} \quad (4)$$

$$A_4 = \begin{bmatrix} C_4 & -S_4 & 0 & 0 \\ S_4 & C_4 & 0 & 0 \\ 0 & 0 & 1 & d_4 \\ 0 & 0 & 0 & 1 \end{bmatrix} \quad (5)$$

$$T_4^0 = A_1 \dots A_4 = \begin{bmatrix} C_{12}C_4S_{12}S_4 & -C_{12}S_4 + S_{12}C_4 & 0 & a_1C_1 + a_2C_{12} \\ S_{12}C_4 - C_{12}S_4 & -S_{12}S_4 - C_{12}C_4 & 0 & a_1S_1 + a_2C_{12} \\ 0 & 0 & -1 & -d_3 - d_4 \\ 0 & 0 & 0 & 1 \end{bmatrix} \quad (6)$$

Using Equation (6), it is possible to calculate the values of the coordinates x, y dan z. The coordinate value of x can be determined through Equation (7). The coordinate value of y can be determined through Equation (8). And the coordinate value of z can be determined through Equation (9).

$$x = a_1C_1 + a_2C_{12} \quad (7)$$

$$y = a_1S_1 + a_2S_{12} \quad (8)$$

$$z = d_3 \quad (9)$$

The inverse kinematics in this study is to find the values of θ_1, θ_2, and d_1. The solution to this inverse kinematics can be solved using the Pythagorean theorem and the cosine rule. The kinematic solution in the 4-DOF RRPRR robot is solved using a single side, namely the top view of the robotic arm structure. If we look at Figure 2, we can see that the position on the Z-

axis only depends on the translation movement of d_1, so it can be concluded that $d_1 = Z$. Figure 3 provides a representation to obtain an equation to generate the values of θ_1 and θ_2.

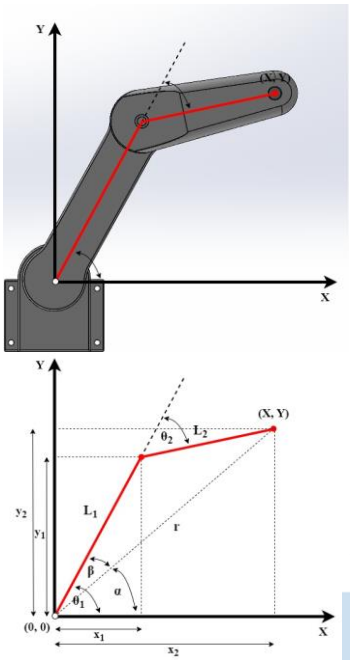

Fig. 3. Cartesian Coordinate 2-DOF Manipulator

As shown in Figure 3, L_1 represents the length of the shoulder arm and L_2 represents the length of the elbow arm. θ_1 represents the angle of the shoulder, and θ_2 represents the angle of the elbow. Using the tangent law, an equation is obtained as shown in Equation (10). To find the value of β, Equation (11) is used. Thus, the value of θ_1 will be obtained from Equation (12). The value of θ_2 is obtained using the cosine law, as shown in Equation (13).

$$\alpha = tan^{-1}\frac{y_2}{x_2} \quad (10)$$

$$\beta = tan^{-1}\frac{L_2 sin\theta_2}{L_1 + L_2 cos\theta_2} \quad (11)$$

$$\theta_1 = tan^{-1}\frac{y_2}{x_2} + tan^{-1}\frac{L_2 sin\theta_2}{L_1 + L_2 cos\theta_2} \quad (12)$$

$$\theta_2 = -cos^{-1}\frac{x_2^2 + y_2^2 - L_1^2 - L_2^2}{2L_1 L_2} \quad (13)$$

B. *Setup Experiment*

In this research, the robot manipulator is driven using MATLAB Simulink. Simulink serves as the workspace for simulating the movement of the robot manipulator. In the robot manipulator motion simulation, a task will be given to reach a predetermined position. The input provided is the coordinate point on the x, y, and z axes, which refer to the end-effector position. Subsequently, it will be observed whether the simulated motion is in accordance with the inputted trajectory.

Before conducting the simulation, the information related to the robot must be defined first using SimScape Multibody, which is a library in the MATLAB software. The defined robot dimensions include the joint positions, link lengths, and frame positions on the x, y, and z axes. The block diagram that defines the robot dimensions in Simulink can be seen in Figure 4.

To calculate the Inverse Kinematics, Forward Kinematics, joint torque, and joint force, the Robotic System Toolbox library will be used. The overall system block diagram can be seen in Figure 5.

In this research, we focused on the use of computer simulation to model the movement of the robot manipulator. However, this research has not yet considered the specifications of the robot actuators used, such as the rotational degree resolution, actuator torque, and others.

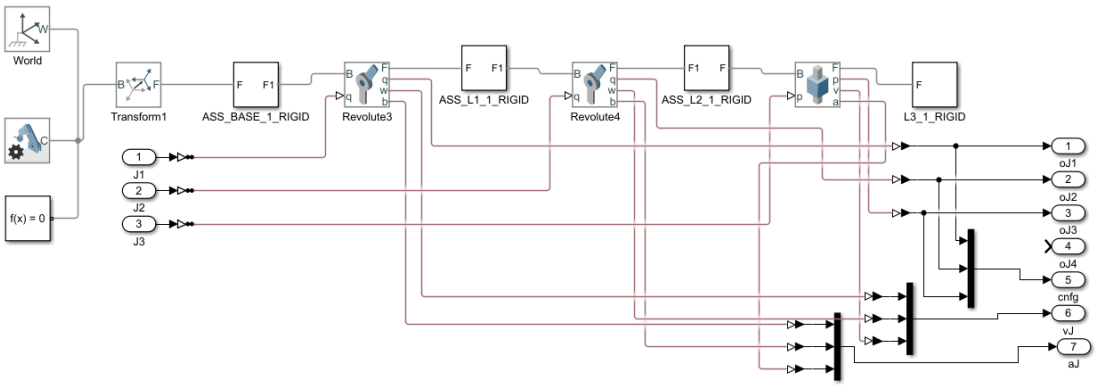

Fig. 4. Robot Block Diagram

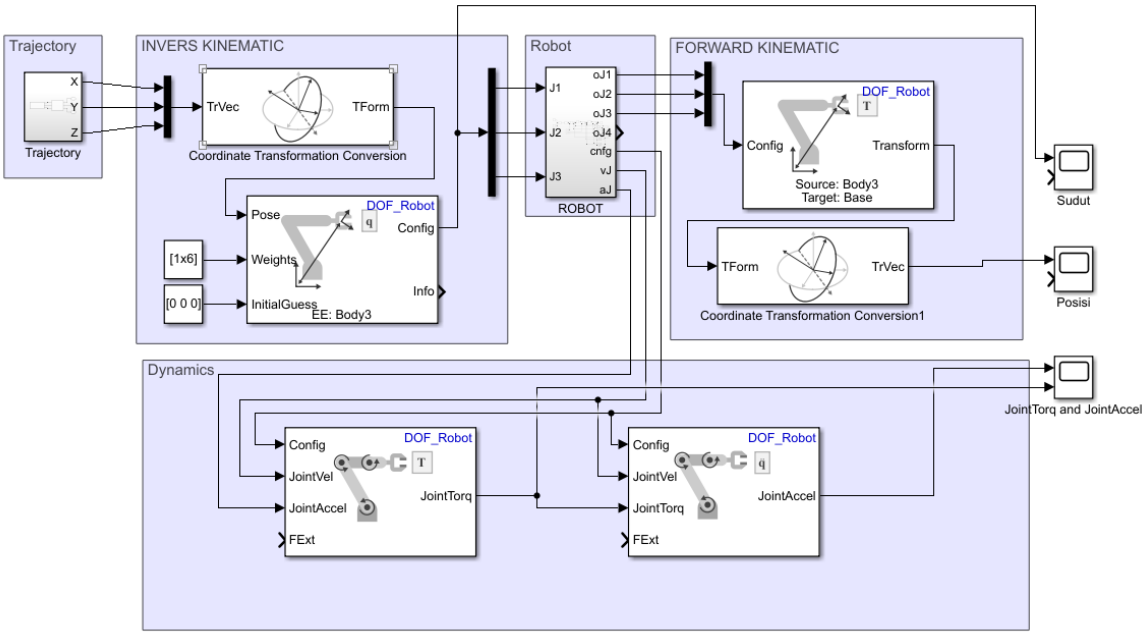

Fig. 5. System Block Diagram

III. Result and Discussions

The testing is carried out by moving the robot along a trajectory as shown in Figure 6, and the details can be seen in Table 2. This will provide the values of each joint angle obtained from the Inverse Kinematics block, as well as the End-Effector position. This research will also display the torque and acceleration values at each joint.

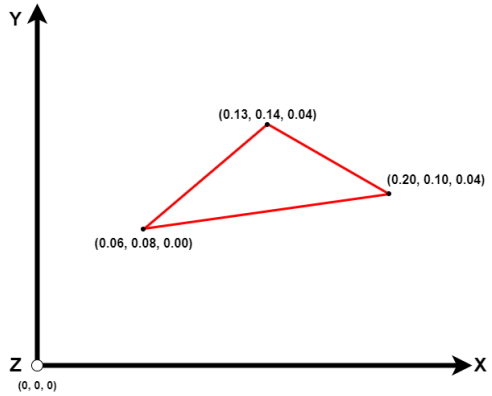

Fig. 6. Trajectory of Robot Manipulator

TABLE II. Trajectory of Robot Manipulator

Time (s)	Coordinate (m)		
	X	Y	Z
0	0.06	0.08	0.00
2	0.06	0.08	0.00
4	0.13	0.14	0.00
5	0.13	0.14	0.04
6	0.13	0.14	0.00
8	0.20	0.10	0.00
9	0.20	0.10	0.04
10	0.20	0.10	0.00
12	0.06	0.08	0.00

In this research, it is assumed that joint 3 does not rotate, so the value of $\theta_3 = 0$. After simulating the robot movement using the trajectory shown in Table 2 and Figure 6, the joint angle values were obtained as shown in Figure 7, and the End-Effector position coordinates were obtained as shown in Figure 8.

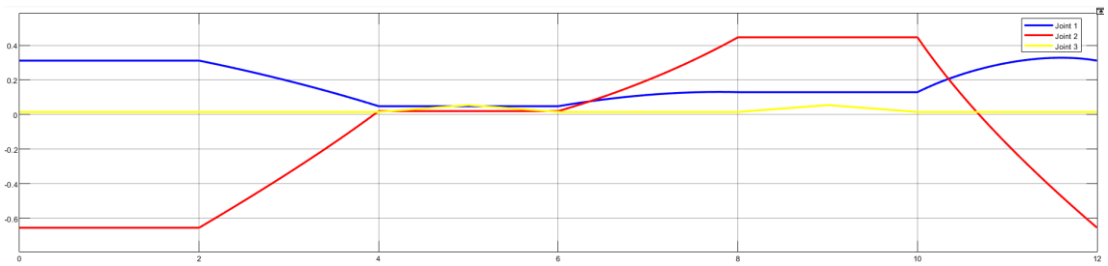

Fig. 7. Value Angle of Joint 1, joint 2 and joint 3

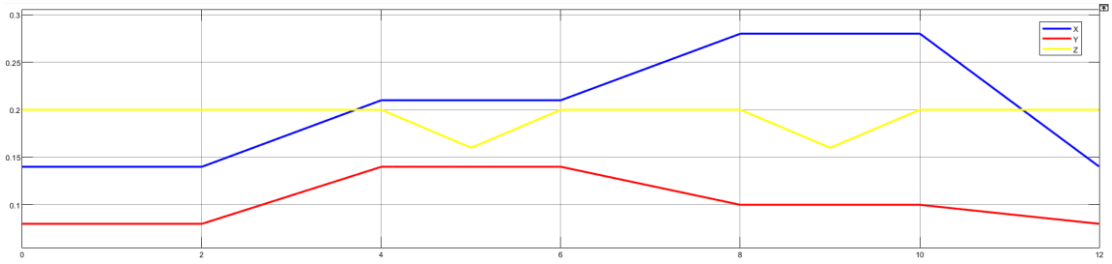

Fig. 8. Position of End-Effector

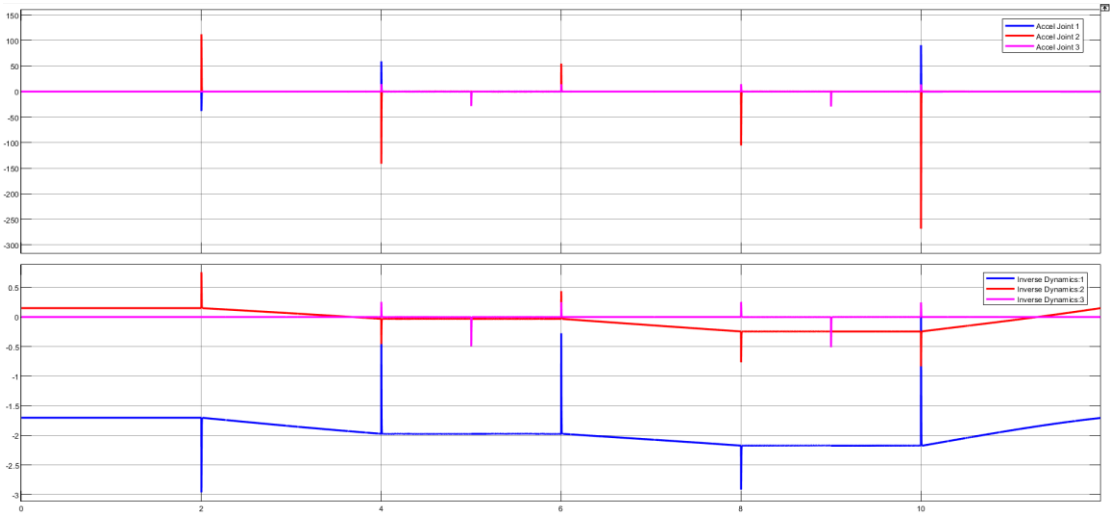

Fig. 9. Value Acceleration and Torque Robot Manipulator

From Figure 7, it can be seen that in the initial or standby position (t = 0 - 2 seconds), joint 1 is around 0.312, joint 2 is around -0.65, and joint 3 is around 0. Joint 3 only moves at (t = 4, 5, 8, 9) and when joint 3 moves, joint 1 and joint 2 do not move. Then at t = 2 - 4 seconds, joint 1 and joint 2 are around 0 - 0.05. At t = 6 - 8 seconds, joint 1 and joint 2 move up successively, approaching values of 0.13 and 0.45. When t = 10 - 12 seconds, the values of joint 1 and joint 2 return to the initial standby position.

For the End-Effector position, as shown in Figure 8, the x, y, z positions obtained from Forward Kinematics are relatively the same as the input trajectory shown in Table 2.

According to the data provided in Figure 9, the following can be observed. Joint 3 only experiences acceleration at specific time points. At t = 4, 5, 6, 8, 9, and 10 seconds, joint 3 has acceleration values of 14.7, -28.33, 14.5, 14.70, -29.22, and 14.10, respectively, along with corresponding torque values of 0.25, -0.50, 0.25, 0.25, -0.51, and 0.24.

At t = 2 seconds, joint 1 has an acceleration of -38 and a torque of -2.96, while joint 2 has an acceleration of 112.25 and a torque of 0.75. At t = 4 seconds, joint 1 accelerates at 59.25 with a torque of -0.14, and joint 2 accelerates at -141.00 with a torque of -0.45. Moving on to t = 6 seconds, joint 1 has an acceleration of 31.8 and a torque of -0.27, while joint 2 has an acceleration of 55.00 and a torque of 0.43. At t = 8 seconds, joint 1 accelerates at 4.6 with a torque of -2.91, and joint 2 accelerates at 54.88 with a torque of 0.43. Lastly, at t = 10 seconds, joint 1 has an acceleration of 90.83 and a torque of 0.01, and joint 2 has an acceleration of -268.26 and a torque of -0.83.

Overall, the data shows that the robotic system has a complex dynamic behavior with coordinated joint movements. Further analysis is required to understand the relationship between the inputs, kinematics, and dynamics of this robotic system.

IV. CONCLUSION

Based on the analysis conducted in this study, it can be concluded that the approach used provides a significant contribution to the development of robotic technology. The kinematic modeling of the robot manipulator enables the accurate identification of the joint angle values and the end-effector position coordinates. Additionally, the simulation using software such as the SimScape Multibody Toolbox and the MATLAB Robotic System Toolbox provides a deep understanding of the performance of the robot manipulator system.

The simulation accelerates the development process of robotic technology and reduces the risks associated with physical implementation in the field. The simulation results allow researchers to evaluate various scenarios and operational conditions without having to

perform physical implementation, which in turn can improve the efficiency, precision, and reliability of robot manipulators in various applications. Thus, this research provides valuable insights into the development of modern robotics and emphasizes the importance of modeling and simulation in understanding and enhancing the performance of robot manipulator systems.

For future research, researchers may consider investigating various other disturbance factors, such as electromagnetic interference, unexpected external forces, or unstable surface conditions, which can affect the performance and accuracy of the robot manipulator's movement. By identifying these sources of disturbance, the research can focus on the development of more advanced and adaptive control systems to dynamically compensate for various disturbances, thus enhancing the efficiency, precision, and reliability of robot manipulators. Additionally, exploring robot manipulators with higher degrees of freedom can also provide new insights into the development of more advanced and adaptive robotic technologies for challenging operational conditions.

REFERENCES

[1] G. Z. Yang *et al.*, "The grand challenges of Science Robotics," *Sci Robot*, vol. 3, no. 14, Jan 31 2018, doi: 10.1126/scirobotics.aar7650.

[2] W.-c. Lee and S.-a. Kuo, "Simulation and control of a robotic arm using MATLAB, simulink and TwinCAT," in *2020 International Conference on Advanced Robotics and Intelligent Systems (ARIS)*, 2020: IEEE, pp. 1-5.

[3] Z. Liqiu, A. Juan, Z. Ronghao, and M. Hairong, "Trajectory Planning and Simulation of Industrial Robot Based on MATLAB and RobotStudio," presented at the 2021 IEEE 4th International Conference on Electronics Technology (ICET), 2021.

[4] G. R. Cahyono, M. F. Setiawan, Y. Rizal, and J. Riadi, "Comparison of 4 DOF Arm Robot for Trajectory Planning with 3rd and 5th Polynomial Orders," in *2022 11th Electrical Power, Electronics, Communications, Controls and Informatics Seminar (EECCIS)*, 2022: IEEE, pp. 281-286.

[5] M. Tamre, R. Hudjakov, D. Shvarts, A. Polder, M. Hiiemaa, and M. Juurmaa, "Implementation of integrated wireless network and MatLab system to control autonomous mobile robot," *International Journal of Innovative Technology and Interdisciplinary Sciences*, vol. 1, no. 1, pp. 18-25, 2018.

[6] T. H. Noventino, M. R. Rosa, and A. Z. Fuadi, "Pid control design and kinematic modelling of 3-dof robot manipulator," in *2022 International Conference on Electrical Engineering, Computer and Information Technology (ICEECIT)*, 2022: IEEE, pp. 88-94.

[7] D. R. Ramadhan, A. R. Al Tahtawi, and K. Wijayanto, "Kendali Posisi Robot Lengan pada Misi Pick and Place dengan Metode Fuzzy Logic Control," in *Prosiding Industrial Research Workshop and National Seminar*, 2021, vol. 12, pp. 96-102.

[8] M. F. El-Khatib and S. A. Maged, "Low level position control for 4-DOF arm robot using fuzzy logic controller and 2-DOF PID controller," in *2021 International Mobile, Intelligent, and Ubiquitous Computing Conference (MIUCC)*, 2021: IEEE, pp. 258-262.

[9] B. H. Purwoto, "Pemodelan robot kinematik manipulator menggunakan matlab," *Emitor: Jurnal Teknik Elektro*, vol. 20, no. 2, pp. 141-146, 2020.

[10] M. F. Setiawan and A. Hasanah, "Pemodelan dan Implementasi Gerak Robot Manipulator dengan Menggunakan Robotics System Toolbox pada MATLAB," *JURNAL SURYA ENERGY*, vol. 8, no. 1, pp. 12-19, 2023.

[11] Tian, F., Liu, G. M., & Tao, K. (2012). Kinematics Analysis for a PRRR Manipulator. Applied Mechanics and Materials, 271-272, 1578-1581. https://doi.org/10.4028/www.scientific.net/AMM.271-272.1578

[12] "Robotics Toolbox - Peter Corke," Peter Corke. [Online]. Available: https://petercorke.com/toolboxes/robotics-toolbox/

[13] F. C. Park and K. M. Lynch, Modern Robotics: Mechanics, PlannZing and Control. 2017.

ISSN 2355-3286

Air Quality Monitoring System Design Based on Wireless Sensor Network Integrated with the Internet of Things

Mochamad Rizal Fauzan[1], Saiqa Fatur Khairi [1], Neneng Puspita Kaniarudi [1], Silmi Ath Thahirah Al Azhima[2], Nurul Fahmi Arief Hakim[2], Iwan Kustiawan[3], Mariya Al Qibtiya[2], Siscka Elvyanti[1]
[1] Pendidikan Teknik Elektro, UPI, Bandung, Indonesia
[2] Pendidikan Teknik Otomasi Industri dan Robotika, UPI, Bandung, Indonesia
[3] Teknik Elektro, UPI, Bandung, Indonesia
rizalfauzan@upi.edu, saiqafkh@upi.edu, nenengpuspita57@upi.edu, silmithahirah@upi.edu, nurulfahmi@upi.edu, iwan_kustiawan@upi.edu, marialqibtiya@upi.edu, sisckael@upi.edu

Accepted on 26 May 2024
Approved on 07 June 2024

***Abstract*— The need for simplicity in various activities encourages further technological development. One of them is a system to turn lights on and off with just a hand gesture. This hand gesture-based One-phase smart switch uses OpenCV, Arduino Nano, relays, and webcam cameras to recognize hand gestures. Static finger movements are used as buttons to turn on the lights. The results show that the algorithm used has high reliability with a precision score of 0.90, sensitivity of 0.90, accuracy of 0.96, and F1-score of 0.90. The accuracy of the system is affected by light intensity, distance, and hand tilt angle. At a light intensity of 70 LUX, the accuracy reaches 100%, while at 40 LUX the accuracy ranges from 98-99%. A distance of 30-60 cm gave the best accuracy of 100%, but decreased at longer distances. A hand tilt of 0° gives 100% accuracy, while at an angle of 60° the accuracy drops significantly, especially for the fifth finger with 64% accuracy. The average response time of the light to finger movement is 0.133 seconds. This device can recognize a variety of finger patterns well, thus meeting the desired needs.**

***Index Terms*— Arduino; computer vision; hand gesture; OpenCV.**

I. INTRODUCTION

Developing machines that can operate in the prompting of humans has been the goal of technological development since its inception. In the early years of development, people used buttons, joysticks, etc. to control circuits, fluid flows, and even mechanical transmissions to fulfill the purpose of the commands given to the machine [1]. When the modern era arrived, with further developments in the world of digital computing, HMI (*Human-Machine Interaction*) environments became even more affordable for many people. People can send information through computers with only a keyboard and mouse in their hands, and a monitor in front of their eyes [2].

In recent technological advancements, researchers have been seeking to simplify their access to HMI. The most suitable approach is a straightforward communication flow. Understandably, there are not many instruments tied to the user's body, and keeping the conversation natural. From then, the interaction system employing hand gestures was restored as a non-verbal communication flow between humans and machines [3].

In the beginning, the concept relied on a greater number of sensors and cameras to accurately record the movement of hands. z, Both static and dynamic gestures. The hand that is modeled must be equipped with a dataglove, which is capable of detecting any alterations that occur in the hand, such as finger movements or finger bent. Despite being published, this invention had a short lifespan due to its reliance on supplementary gear. Hence, employing a camera is considered to be a preferred method for the advancement of a motion tracking system.[4].

The main purpose of using hand motion tracking technology is simply to recognize and classify gestures formed by human hands. These gestures will be captured by the camera, processed by computer algorithms, and learned by the ANN concept to generate program decisions from predetermined gestures [5]. In this paper, the gesture defined is the simple gesture of "bending fingers" as if counting. Each extended finger will be captured by the camera and processed to activate the "turn on the light" program with five different levels according to the five fingers.

II. METHODS

A. Computer Vision

Computer vision is a term that broadly covers a variety of areas, including raw data retrieval, image pattern extraction, and information interpretation [6]. The field includes a blend of principles, methodologies, and ideas derived from digital image processing,

pattern recognition, artificial intelligence, and computer graphics [7].

Advances in computer vision depend on its supporting infrastructure, which includes improved image quality and image recognition capabilities. Advances in computer vision depend on the computer technology infrastructure, which includes improved image quality and image recognition capabilities [8][9].

There is a close relationship between Image Processing and basic approaches, and some researchers use the two words interchangeably. The main goal of Computer Vision is to generate models and extract data and information from images. This goal sometimes shares a common meaning and sometimes overlaps with *Human and Machine Interaction* (HMI) [10].

Computer Vision works by using optical sensors and algorithms to recreate human motion stimuli to extract valuable information automatically [11]. When compared to conventional methods, computer vision has evolved into one of the branches of AI for human motion stimulus in society [12].

B. Hand Gesture Recognition

Hand gestures are part of nonverbal communication, which can be expressed through the center area of the palm, the position of the fingers, and the shapes formed by the hands. Hand gestures are divided into two categories, which are static gestures characterized by a stable hand shape, and dynamic gestures involving hand movements such as waving. Hand gestures vary depending on the person and the situation at hand, unlike posture, which emphasizes hand shape rather than movement [13].

Convolutional Neural Network (CNN) is used by neural networks to identify hand gestures using deep learning. CNN or ConvNet, is a type of artificial neural network designed to mimic the pattern of connections found in the visual cortex of objects. CNNs exploit the spatial correlations inherent in the input data. Convolutional networks are used to train the model using a dataset of images. The model is trained using three forms of training: supervised, unsupervised, and reinforcement learning. Given that gesture recognition models rely on supervised learning and derive knowledge from labeled datasets of desired gestures, it is crucial to have high-quality data with little noise. The accuracy of the model network and the data used directly affects the accuracy of the model [14][15].

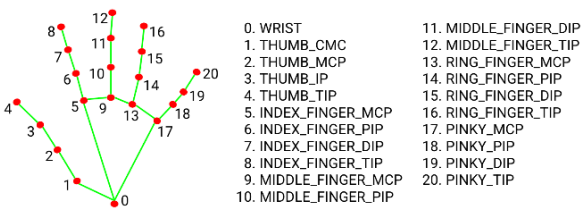

(a)

(b)

Fig. 1. 21 hand landmarks (a), Hand detection (b)

Research on hand gestures typically uses two main methodologies: sensors integrated into wearable gloves, and sensors based on camera vision. Computerized hand gesture recognition using camera-based systems involves the process of capturing and recognizing hand movements and positions through visual data. This process starts with image capturing through the camera, followed by pre-processing steps such as noise reduction and segmentation to separate the hand image from the noises [16].

C. Hand-Gesture Smart Switch

Hand gesture identification provides a very practical and modern means of non-verbal communication. Gesture recognition has significant applications in Human Computer Interactions (HCI) and sign languages [17]. The hand gesture recognition system utilizes a camera that is primarily used to capture images of gestures made by human hands. These images are then processed by the specified algorithm as input to the created system.

Hand gesture-based controls offer a variety of functions, such as acting as virtual remote controls for TVs and other home appliances, enhancing gaming experiences, and allowing interaction with public information kiosks in museums, ATMs, elevators, storefronts, and other public spaces. At the most recent Consumer Electronics Show (CES), numerous companies presented prototypes or upcoming devices featuring hand gesture-based controls. Different sensing technologies can detect hand gestures, and advancements in these technologies have enabled developers to integrate Three-Dimensional (3D) gesture control into their products. The cost of acquiring and implementing a gesture controller varies depending on the technology employed [18].

III. System Design

The system is designed with four main components: a webcam, an OpenCV program, an Arduino Nano, and a relay. The webcam, whether external or built into the laptop, is used to capture hand gesture images. Then,

OpenCV performs real-time image pre-processing to extract only the essential functions from the user's static hand gestures. The system consist on being the control for AC components through the switch function brought by the relays. The switch can be used for many components, but AC lightbulb was used to get the experimental data. These functions are transmitted via a port to the Arduino Nano, which decides which light should be turned on based on the hand gesture. The Arduino Nano then sends a signal to the relay to supply electricity to a specific light according to the captured hand gesture. The sequence of operation of this one-phase smart switch system can be seen in Figure 2.

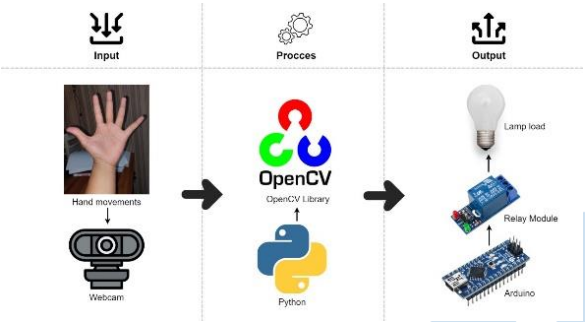

Fig. 2. System Working Stage

Figure 3 shows the classification of hand gestures to control the lighting system. Each hand gesture from 0 to 5 represents the number of fingers raised, with each finger activating one light. A no gesture turns off all relays, while a 5 gesture turns on all relays. Overall, this combination of hand gestures can result in 32 combinations of light control that can be formulated in 2^n.

Classification of Hand Gestures					
0	1	2	3	4	5
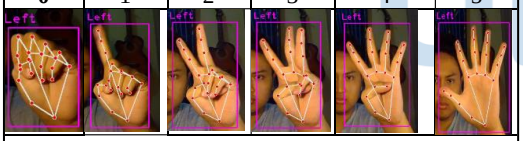					
Commands are executed on the lighting system					
All Relay Off	Relay 1 ON	Relay 1 and 2 ON	Relay 1, 2 and 3 ON	Relay 1, 2, 3 and 4 ON	All Relay ON

Fig. 3. The style of hand movements and directions used

In Figure 4 the flowchart diagram illustrates the process of controlling relays using hand gesture detection through Arduino. It starts with setting the serial port and connection between the computer and Arduino, then initializing the relay. The Arduino detects hand movements with sensors, and if movement is detected, the system will control the relays according to the finger movement. This process takes place in a master loop until the system shuts down or the command finishes executing.

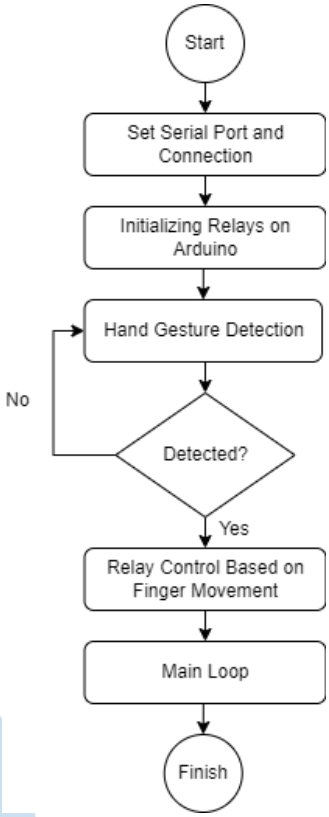

Fig. 4. System Flowchart

In the Arduino Nano system itself, as shown in Figure 5, the components needed are the Arduino Nano as a microcontroller that will turn the lights on or off, a relay that functions as a switch, and five lights as evidence of electricity flowing.

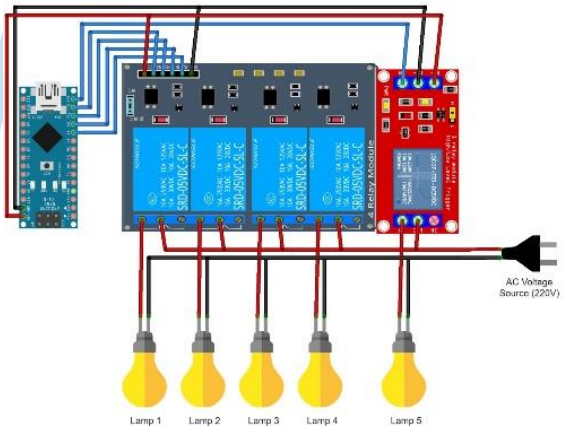

Fig. 5. System Circuits

IV. Results and Discussion

A. Hardware Design

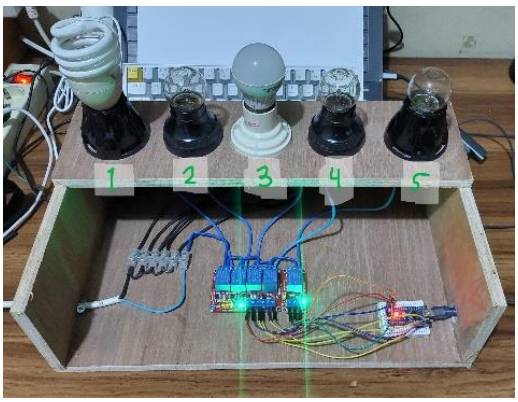

(a)

(b)

Fig. 6. Description by lamp number (a), lit condition (b)

The hardware design of the device seen in Figure 6 has a configuration where each lamp number is connected to the corresponding relay, allowing for the control of the lights' on and off states. Specific hand gestures will trigger the relevant relay, causing the bulb associated with that relay number to illuminate. As an illustration, raising a single finger will trigger relay 1 and illuminate lamp 1; raising two fingers will trigger relays 1 and 2, and illuminate lights 1 and 2, and so on. This enables convenient and effective management of the lighting system using manual movements of the hands.

B. Light Activation Logic

The specified static motion is employed to conduct device experiments, which involve the exploration of all feasible patterns. The essential motion for turning on the light, in this case, was the action of "closing and opening the fingers". This gesture serves as a benchmark due to its simplicity and minimal energy expenditure. Data collection is conducted by observing if the lights will illuminate in response to the finger being opened, either individually or in a certain order. Subsequently, the data is acquired and shown in Table 1.

TABLE I. Light Activation Data

Finger Up Combination	Lamp				
	1	2	3	4	5
0,0,0,0,0					
0,0,0,0,1					Y
0,0,0,1,0				Y	
0,0,0,1,1				Y	Y
0,0,1,0,0			Y		
0,0,1,0,1			Y		Y
0,0,1,1,0			Y	Y	
0,0,1,1,1			Y	Y	Y
0,1,0,0,0		Y			
0,1,0,0,1		Y			Y
0,1,0,1,0		Y		Y	
0,1,0,1,1		Y		Y	Y
0,1,1,0,0		Y	Y		
0,1,1,0,1		Y	Y		Y
0,1,1,1,0		Y	Y	Y	
0,1,1,1,1		Y	Y	Y	Y
1,0,0,0,0	Y				
1,0,0,0,1	Y				Y
1,0,0,1,0	Y			Y	
1,0,0,1,1	Y			Y	Y
1,0,1,0,0	Y		Y		
1,0,1,0,1	Y		Y		Y
1,0,1,1,0	Y		Y	Y	
1,0,1,1,1	Y		Y	Y	Y
1,1,0,0,0	Y	Y			
1,1,0,0,1	Y	Y			Y
1,1,0,1,0	Y	Y		Y	
1,1,0,1,1	Y	Y		Y	Y
1,1,1,0,0	Y	Y	Y		
1,1,1,0,1	Y	Y	Y		Y
1,1,1,1,0	Y	Y	Y	Y	
1,1,1,1,1	Y	Y	Y	Y	Y

Based on the data obtained, the lights can be turned on according to the number and type of fingers raised. If the thumb is raised, then lamp 5 will light up which is symbolized in variable Y. If the index finger and middle finger, then lamp 2 and lamp 3 will light up. This is following the program created.

C. Model Algorithm Accuracy

To achieve high accuracy in detecting and classifying various hand gestures. The performance evaluation of the model was performed by considering several key metrics such as accuracy, recall, precision, and F1 score. In addition, environmental settings such as a distance between the hand gesture and the camera of 40 cm and a tilt angle between the hand gesture and the camera of 0° were determined.

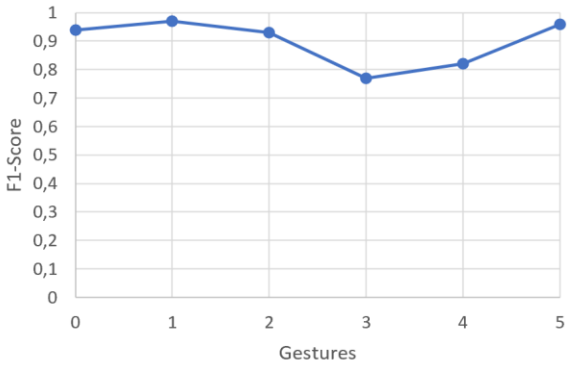

Fig. 7. F1 score results from different classes

The results from Figure 7 show the F1 scores for each class as follows: 0.94, 0.97, 0.93, 0.77, 0.82, and 0.96, with an overall average of 0.898. These scores indicate a consistent and high performance in hand gesture classification, despite variations between different classes. A high F1 score indicates a good balance between precision and recall, reinforcing the reliability of the model in detecting and classifying hand gestures accurately.

TABLE II. CLASSIFICATION REPORT

Class	Precision	Sensitivity	Accuracy	F1-Score
0	0,97	0,92	0,97	0,94
1	0,95	0,96	0,98	0,97
2	0,9	0,97	0,96	0,93
3	0,82	0,74	0,96	0,77
4	0,82	0,84	0,94	0,82
5	0,93	0,98	0,98	0,96
Mean	0,90	0,90	0,96	0,90

The results of Table 2 show that the model has high performance with an average precision of 0.90, sensitivity of 0.90, accuracy of 0.96, and F1 score of 0.90. The performance per class varied, with class 1 having the highest precision of 0.95 and F1 score of 0.97, while class 3 had the lowest F1 score of 0.77. Overall, the model showed good reliability in classifying hand gestures with high accuracy in all classes.

D. Light Activation Logic

Based on the change in lighting intensity, the accuracy of the system is calculated as the first test for the proposed system. A specialized application is used to measure the lighting intensity based on a mobile phone camera. In this study, lighting with variable intensities of 40 lux and 70 lux was used. In addition, environmental settings such as a distance between the hand gesture and the camera of 40 cm and an inclination angle between the hand gesture and the camera of 0° were also determined. The experiment was repeated 10 times for each hand gesture and light intensity.

TABLE III. ACCURACY BASED ON VARIATIONS IN LIGHT INTENSITY

Hand Gesture	Accuracy with Light Intensity (%)	
	40 LUX	70 LUX
Fingerless	98	100
One Finger	97	100
Two Fingers	98	100
Three Fingers	98	100
Four Fingers	98	100
Five Fingers	99	100

The results of Table 3 show that the accuracy of the system in detecting hand gestures is very high, with all gestures achieving 98-99% accuracy at 40 lux light intensity and 100% at 70 lux light intensity. This shows that the system functions very well under various lighting conditions.

TABLE IV. ACCURACY BASED ON DISTANCE VARIATION

Hand Gesture	Accuracy with Distance (%)				
	30 cm	60 cm	90 cm	150 cm	180 cm
Fingerless	100	100	100	93	82
One Finger	100	100	97	89	78
Two Fingers	100	100	98	88	78
Three Fingers	100	100	99	88	77
Four Fingers	100	100	99	89	78
Five Fingers	100	100	100	91	79

From the results of Table 4 of hand gesture accuracy testing at various distances, it can be concluded that hand gesture recognition has a high level of accuracy at closer distances, but decreases little by little as the distance increases. /Specifically, at a distance of 30 cm, all types of hand gestures have 100% accuracy, but the accuracy starts to decrease at a distance of 60 cm and further decreases at a distance of 90 cm and above. Nonetheless, despite the decrease, accuracy remained relatively high even at longer distances, with the lowest decrease occurring for fingerless gestures.

TABLE V. ACCURACY BASED ON TILT ANGLE VARIATION

Hand Gesture	Accuracy with Tilt Angle (%)		
	0º	30º	60º
Fingerless	100	98	95
One Finger	100	97	82
Two Fingers	100	98	84
Three Fingers	100	97	72
Four Fingers	100	97	75
Five Fingers	100	100	64

Based on Table 5 of the test results, it can be seen that the accuracy of hand gesture recognition tends to decrease as the tilt angle increases. At an angle of 0°, the accuracy is generally high, but decreases significantly at an angle of 60°. This shows that inclination affects the system's ability to recognize

hand gestures, with the lowest accuracy occurring at higher inclination angles.

E. Light Activation Logic

The time test is conducted to find out the elapsed time between the input being provided and the execution of the output. In this scenario, manual gestures serve as inputs that initiate the motion of the light arrangement. The reaction time is determined based on the instant the input is provided. The laptop does data processing and transmits instructions directly to the Arduino Nano over the COM connection. Subsequently, every hand motion is subjected to response time testing. Each manual motion underwent three rounds of testing.

TABLE VI. LAMP RESPONSE TIME TEST

Hand Gesture	Reaction Time Average (s)
Fingerless	0,023
One Finger	0,148
Two Fingers	0,137
Three Fingers	0,192
Four Fingers	0,134
Five Fingers	0,164
Total Average Reaction Time (s)	0,133

The results are shown in Table 6 for testing reaction time to hand movements. The result shows an overall average reaction time of 0.133 seconds. Fingerless hand movements have the fastest reaction time (0.023 seconds), while movements with three fingers require the longest reaction time (0.192 seconds). Movement complexity affects reaction time, with simpler movements tending to have faster responses.

V. CONCLUSION

Based on the analysis conducted in this study, it can be This paper develops a hand gesture-based *One-Phase Smart Switch* using CNN algorithm in OpenCV program library with Arduino Nano, relay, laptop webcam camera, and OpenCV program on *Python platform*. The main goal of this research is to create a device for better HMI communication, especially as a switch to a one-phase AC line. In this research, AC lightbulbs were used as the experimental components, with the main goal that the light can turn on and of based on passive hand gestures. The results show that the algorithm logic model used has high reliability in classifying hand gestures, with a precision score of 0.90, sensitivity of 0.90, accuracy of 0.96, and F1 score of 0.90. Changes in light intensity, distance, and tilt angle affected the accuracy of the system, although not significantly. At a light intensity of 70 LUX, the accuracy reached 100%, while at 40 LUX it ranged from 98-99%. A distance of 30-60 cm gave the best accuracy of 100%, while a distance of 90-150 cm showed a decrease in accuracy, and at 180 cm the accuracy decreased significantly. Hand tilt at an angle of 0° gives 100% accuracy for all fingers, while at angles of 30° and 60° there is a decrease in accuracy, especially at an angle of 60° for finger 5 with 64% accuracy. The average response time of the light-to-finger movement is 0.133 seconds.

REFERENCES

[1] L. Guo, Z. Lu, and L. Yao, "Human-Machine Interaction Sensing Technology Based on Hand Gesture Recognition: A Review," *IEEE Trans. Human-Machine Syst.*, vol. 51, no. 4, pp. 300–309, 2021.

[2] X. Wang and Z. Zhu, "Context understanding in computer vision: A survey," *Comput. Vis. Image Underst.*, vol. 229, p. 103646, Mar. 2023.

[3] E. Ertugrul, P. Li, and B. Sheng, "On Attaining User-friendly Hand Gesture Interfaces to Control Existing GUIs," *Virtual Real. Intell. Hardw.*, vol. 2, no. 2, pp. 153–161, 2020.

[4] H. Sharma, H. Kumar, and S. K. Mangla, "Enablers to computer vision technology for sustainable E-waste management," *J. Clean. Prod.*, vol. 412, p. 137396, Aug. 2023.

[5] F. I. Eyiokur *et al*., "A survey on computer vision based human analysis in the COVID-19 era," *Image Vis. Comput.*, vol. 130, p. 104610, Feb. 2023.

[6] V. Wiley and T. Lucas, "Computer Vision and Image Processing: A Paper Review," *Int. J. Artif. Intell. Res.*, vol. 2, no. 1, p. 22, 2018.

[7] Shreya M. Shelke, Indrayani S. Pathak, Aniket P. Sangai, Dipali V. Lunge, Kalyani A. Shahale, and Harsha R. Vyawahare, "A Review Paper on Computer Vision," *Int. J. Adv. Res. Sci. Commun. Technol.*, vol. 3, no. 2, pp. 673–677, 2023.

[8] Y. Weiss, V. Ferrari, C. Sminchisescu, and M. Hebert, "Special Issue: Advances in Architectures and Theories for Computer Vision," *Int. J. Comput. Vis.*, vol. 128, no. 3, pp. 573–574, 2020.

[9] H. Yu, Y. Wang, Y. Tian, H. Zhang, W. Zheng, and F. Y. Wang, "Social Vision for Intelligent Vehicles: From Computer Vision to Foundation Vision," *IEEE Trans. Intell. Veh.*, vol. 8, no. 11, pp. 4474–4476, Nov. 2023.

[10] A. Ardanza, A. Moreno, Á. Segura, M. de la Cruz, and D. Aguinaga, "Sustainable and flexible industrial human machine interfaces to support adaptable applications in the Industry 4.0 paradigm," *Int. J. Prod. Res.*, vol. 57, no. 12, pp. 4045–4059, 2019.

[11] A. Batch, Y. Ji, M. Fan, J. Zhao, and N. Elmqvist, "uxSense: Supporting User Experience Analysis with Visualization and Computer Vision," *IEEE Trans. Vis. Comput. Graph.*, 2023.

[12] M. Rafiei, J. Raitoharju, and A. Iosifidis, "Computer Vision on X-Ray Data in Industrial Production and Security Applications: A Comprehensive Survey," *IEEE Access*, vol. 11, pp. 2445–2477, 2023.

[13] M. Yasen and S. Jusoh, "A systematic review on hand gesture recognition techniques, challenges and applications," *PeerJ Comput. Sci.*, vol. 2019, no. 9, pp. 1–30, 2019.

[14] N. Bilal, V. Indradeep, S. Simran, and G. Mansi, "Hand Gesture Recognition," *IJRASET Int. J. Res. Appl. Sci. Eng. Technol.*, vol. 10, no. 5, pp. 5–24, 2020.

[15] A. Magdy, H. Hussein, R. F. Abdel-Kader, and K. A. El Salam, "Performance Enhancement of Skin Cancer

Classification Using Computer Vision," *IEEE Access*, vol. 11, pp. 72120–72133, 2023.

[16] M. Al-Hammadi *et al.*, "Deep learning-based approach for sign language gesture recognition with efficient hand gesture representation," *IEEE Access*, vol. 8, pp. 192527–192542, 2020.

[17] S. P, A. Jain, P. Jaiswal, R. Kumar, and D. Koolwal, "Hand Gesture Recognition System in Smart Environment," *Int. J. Recent Technol. Eng.*, vol. 9, no. 1, pp. 2194–2199, 2020.

[18] V. V. Dahale and D. V. T. Gaikwad, "Hand Gesture Based Touch-Free User Interface for Elevator/Lift," *Int. J. Adv. Res. Sci. Commun. Technol.*, vol. 7, no. 2, pp. 237–241, 2021.

ISSN 2355-3286

Air Quality Monitoring System Design Based on Wireless Sensor Network Integrated with the Internet of Things

Irvan Budiawan, Danu Febri Wigianto, Bagus Wicaksono, Arif Rohman Hakim
[1] Department of Electrical Engineering, Faculty of Engineering, Universitas Jenderal Achmad Yani, Cimahi, Indonesia
budiawan.irvan@gmail.com, danu.febri88@gmail.com, bagus.wicaks@gmail.com, rif.hakim1305@gmail.com

Accepted on 26 June 2024
Approved on 01 July 2024

***Abstract*— Government and officials set rules to keep the air clean and healthy. To accommodate this, an efficient air quality monitoring system is required. Real-time monitoring is crucial for observing air quality. This allows for immediate action if air quality declines. However, current systems often rely on just one measurement point, risking inaccurate results due to rapid pollutant dispersion. To overcome this problem, researchers propose designing an air quality monitoring system based on a wireless sensor network. Sensor nodes will be installed at various points within the area to be monitored, forming a connected sensor network using the ESP-Now protocol. The data obtained from each node will be sent to the base station, then the data will be transmitted via the Message Queuing Telemetry Transport (MQTT) protocol using the internet network. Thus, this design produces a wireless sensor network that is integrated with the internet of things (IoT). The advantages of the IoT system include ease of data storage and accessibility that can be accessed from anywhere as long as it is connected to the internet and has appropriate authorization.**

***Index Terms*— air quality sensor; ESP-Now; internet of things (IoT); wireless sensor network.**

I. INTRODUCTION

Regulations related to air quality in Indonesia have been issued through Government Regulations (PP) [1], [2], Minister of Environment and Forestry (LHK) Regulations [3], Minister of Energy and Mineral Resources (ESDM) Regulations [4]. In 2020, the MoEF has issued Minister of Environment and Forestry Regulation Number 14 of 2020 concerning the Air Pollutant Standard Index, which replaces Minister of Environment Decree Number 45 of 1997 concerning Calculation and Reporting and Information on the Air Pollutant Standard Index. In this replacement regulation, there are changes in the calculation of ISPU which now includes 7 (seven) parameters, namely particulates PM_{10} and $PM_{2.5}$, nitrogen dioxide NO_2, sulfur dioxide SO_2, carbon monoxide CO, ozone O_3, and hydrocarbons HC. Two additional parameters, HC and $PM_{2.5}$, have been included based on consideration of the great risks that HC and $PM_{2.5}$ pose to human health.

Many researchers have designed air quality monitoring systems [5], [6], [7], [8]. Air quality monitoring system research must be in line with policy regulations issued by the government. The policy is related to the Air Quality Standard Index (ISPU). ISPU is one of the parameters used to measure air quality at a location within a certain time span. ISPU provides information about the level of air pollution in an area, taking into account several air pollutant parameters that are commonly found. These parameters are particulates, pollutant gases, and ambient air quality. ISPU measurements and air quality monitoring in general are essential for understanding the impact of air pollution on human health, the environment, and the economy.

In general, checking air quality is still done manually by taking samples. Samples are analyzed by the laboratory to determine their content. As in the study of air quality analysis in underground parking spaces, sampling was carried out on weekdays and weekends at certain hours [9]. Some studies that are used as references regarding the impact of air quality are analyzed using questionnaire techniques to people who are in the area. As conducted by Westy conducted research on the description of the impact of industry on the surrounding community in Takalar Regency [10]. Furthermore, Aznaeni conducted research around the cement industry in the Bosowo area of Maros Regency [11]. Research on the impact of indoor air pollution and family health conditions was conducted by Indanazulfa [12].

An air monitoring system must have sensors that are distributed so that they can represent air quality over the area being monitored. Sensor network systems are well suited for this task. Previous researchers have only focused on how sensor readings can be transmitted through the internet network, which we know as the Internet of Thing (IoT) [13], [14], [15], [16]. IoT systems require an internet network for each sensor so that data can be sent. However, with a sensor network, not all sensor nodes must be connected to the internet,

just one sensor node that is used as a sensor station that is tasked with sending data out of the sensor network system. Sensor stations can be connected to the internet network or other communication systems for data storage.

The above-mentioned studies on air quality impacts were conducted on a questionnaire basis and did not look at air quality data directly. This is because air quality monitoring technology is still rarely installed for industrial purposes, public facilities and private rooms such as homes and offices. Nationally, the application of embedded system applications for air quality monitoring has been made by KLHK. KLHK built a portal for air quality monitoring in 50 major cities. The address of the air quality monitoring portal built by KLHK is https://ispu.menlhk.go.id. On the portal, realtime monitoring is carried out, the data is updated twice a day in the morning and evening. The parameters monitored on the KLHK website portal are PM_{10}, $PM_{2.5}$, NO_2, SO_2, CO, O_3. Some studies use data from KLHK applications such as those conducted by Putri [17]. Agusta conducted research based on air quality data taken from the Global Atmospheric Monitoring Station (SPAG) in Kotobang Hill, West Sumatra [18].

For the design of air quality monitoring applications, many have been proposed for urban areas [19], industrial areas [20], closed rooms [12], [14], [21], [22], [23], and hospital sanitation purposes [20]. These designs can be adopted for air quality monitoring applications in other fields such as indoors in homes and offices as well as in public places such as parks and highways. However, the proposed design is still a single sensor node integrated with the IoT system. The use of one sensor node in one area creates doubts because it does not represent the condition of the monitored area. In this journal, researchers will propose readings from more than one sensor in one area. The system is known as a sensor network system. Sensor networks make the readings more accurate because the sensor nodes are installed at several points in the area to be monitored. This represents the condition of the monitored area. An example of a CO gas monitoring application in a road area if one sensor is placed, it is less representative, it would be better if sensors are installed along the road area.

Sensor network applications mostly use wireless media. Some common protocols that are often used are zigbee, bluetooth low energy (BLE), LoRa, Narrowband IoT (NB-IoT). Air quality design using the LoRa protocol has been done [19], [25] as well as the zigbee protocol [26]. Both protocols are special communication devices that are separate from the main board in an embedded system. Currently there are ESP32 and ESP8266 devices that already have Wi-Fi capabilities. as a developer Espressif Systems has created the ESP-Now wireless protocol for ESP32 and ESP 8266 devices.

ESP-Now is a peer-to-peer (P2P) wireless communication protocol developed specifically for ESP8266 and ESP32 devices. It enables direct communication between two or more ESP devices without the need for access points or other Wi-Fi network infrastructure. The protocol supports AES-128 encryption to protect data transmitted between devices. The protocol is designed to have low latency and efficient power consumption, making it suitable for real-time applications of wireless sensor networks.

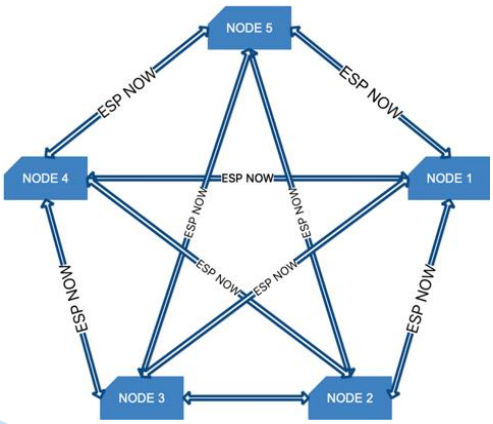

Fig. 1. ESP-Now Possible Topologies

Based on Figure 1 ESP-Now can build various types of topologies, namely P2P, mesh, star, tree or hybrid, a combination of two or more types of topologies mentioned. ESP-Now can also detect the presence of new sensor nodes as done by Arlingga [27].

The purpose of this research is to propose the design of a wireless sensor network-based air monitoring system using the ESP-Now protocol. With ESP8266 and ESP32 devices as microcontrollers that have peer-to-peer communication features to form a sensor network with the ESP-Now protocol. ESP devices can also be connected to various air quality sensors. ESP also has a wifi module so that data from the sensor network built can be sent via the internet network.

II. METHODS

A. System Design

In this design, a wireless sensor network system was built consisting of 5 sensor nodes, each node could read the temperature and humidity of the air using the DHT11 sensor, as well as the level of CO_2 in the air with the MQ136 sensor. Each node can communicate and exchange data using mesh topology. In the whole system, there is 1 sensor node that functions as a base station that serves to send data to the Message Queuing Telemetry Transport (MQTT) server on the internet network. Data sent to the MQTT server can later be read by the Node Red application. A dashboard is provided as an interface with the user to view the temperature, humidity and CO_2 values from each sensor node. The dashboard display can be accessed easily through the Node-RED application on computers and smartphones. Figure 2 is the design of the system integration that will be built.

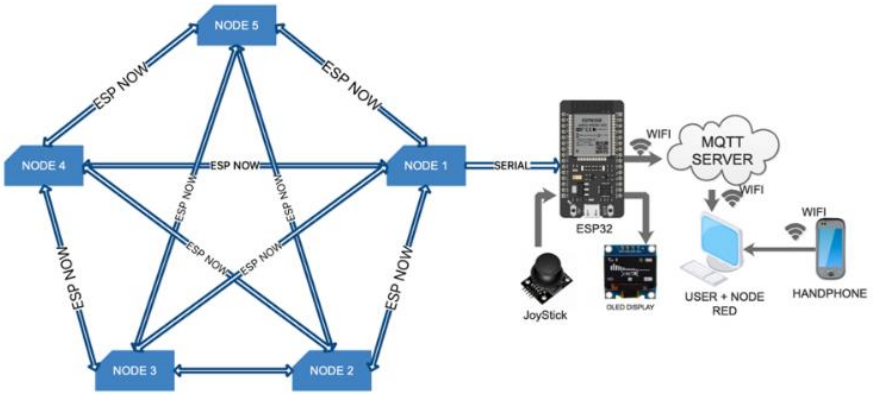

Fig. 2. Wireless Sensor Network with ESP-Now Protocol

The explanation of the design of Figure 2 is as follows:

- The communication protocol between sensor nodes uses ESP-Now with a mesh communication topology.
- In each sensor node there is an ESP8266 as the brain of the sensor node, an MQ135 sensor that functions to measure CO_2. There is a local display in the form of an Oled LCD to display the readings of the measured quantities.
- In sensor node 1, besides exchanging data with other sensor nodes through the ESP-Now protocol, this sensor node also sends data to an ESP32 using a serial communication line. The data sent is sensor reading data from the five sensor nodes that are interconnected via the ESP-Now protocol.
- The ESP32 will send data received from sensor nodes 1-5 via a serial line to the MQTT server.
- Data from the MQTT server will be read by Node-RED and will be displayed in the form of a dashboard of readings of each sensor node that can be accessed from a desktop or smartphone.

B. Sensor Node Design

The microcontroller used in sensor nodes 1-5 is the ESP8266 with a schematic design as shown in Figure 3 for sensor node 1 and Figure 4 for sensor nodes 2-5. In general, both schematics have the same design. Each sensor node is connected to DHT 11 and MQ 136 sensors for temperature, humidity and CO_2. There is an oled lcd display on each sensor node to display the sensor readings. The difference between the two schematics is that sensor node 1 is connected to an ESP32. This ESP32 will be the base station in the wireless sensor network in this design.

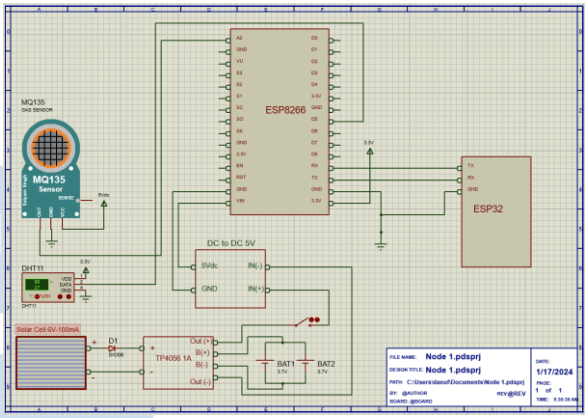

Fig. 3. Sensor Node 1 Circuit Schematic

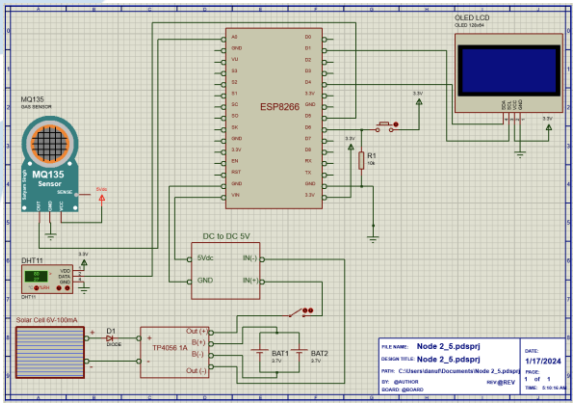

Fig. 4. Sensor Node Circuit Schematic 2-5

C. Sensor Node Design

The ESP32 microcontroller is used in the base station design. The components contained in the base station are an oled LCD and a joystick as an interface console. The base station is connected to sensor node 1 using serial communication between ESP microcontrollers. Where sensor node 1 is a sensor node that holds data from sensor nodes 1 to 5. The base station works to send data from sensor network readings through the MQTT Server protocol installed on cloud computing as shown in Figure 2.

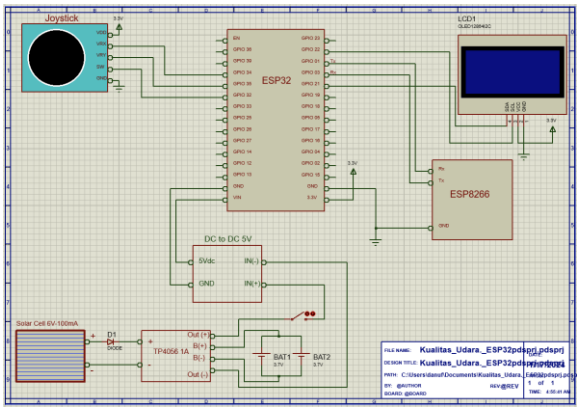

Fig. 5. Base Station Circuit Schematic

D. *Display and Data Center Design*

The display of the sensor network reading results is shown in Figure 7. The display is made with the Node-RED application. To be able to display the results of sensor network readings, Node-RED subcribes data to the MQTT server. The Node-RED program flow display built is shown in Figure 6. The workings of the Node-RED system are as follows:

- A palette of MQTT input nodes, used to receive data from the MQTT Server.
- A Remote Desktop Node, used to access the dashboard display from a computer or smartphone.
- A CSV Node, used for parsing data from the MQTT server.
- 15 switch nodes to direct the parsed data to the appropriate gauge.
- 15 gauge dashboards, used to display data from each sensor to the dashboard in the form of a gauge.

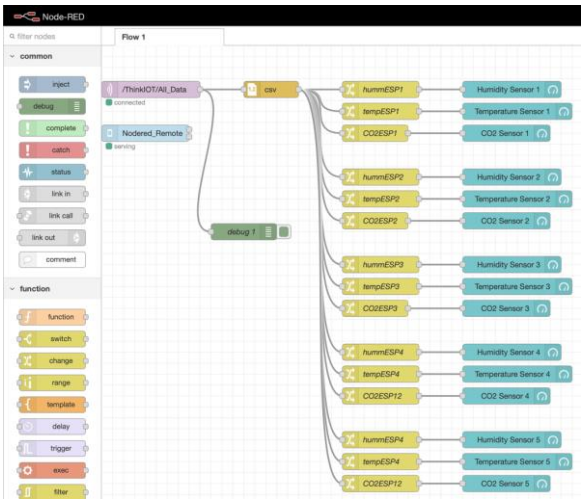

Fig. 6. Node-RED Programming Flow Diagram

Figure 7 shows the Node-RED dashboard when the system is running normally.

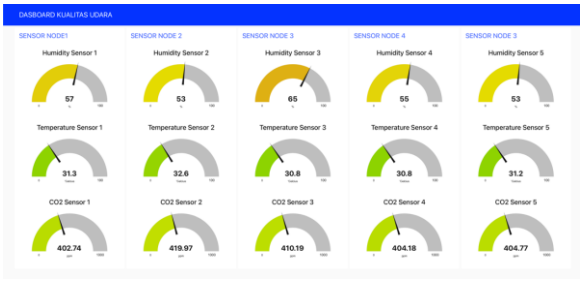

Fig. 7. Node-RED Dashboard View

Figure 7 shows the sensor readings from the five sensor nodes that have been made in the form of a gauge on the Node-RED dashboard.

III. Results and Discussion

A. *Wireless Sensor Network Testing*

Testing the sensor network is done by comparing the sensor readings at node 2 with the display at node 1. If the readings are the same then the data from node 2 can be successfully sent to node 1. The same is done for the other nodes.

Here are the test results on the sensor network (SN):

TABLE I. Network Testing Between Sensor Nodes

WSN Position	Displayed data sources				
	SN 1	SN 2	SN 3	SN 4	SN 5
SN 1	OK	OK	OK	OK	OK
SN 2	OK	OK	OK	OK	OK
SN 3	OK	OK	OK	OK	OK
SN 4	OK	OK	OK	OK	OK
SN 5	OK	OK	OK	OK	OK

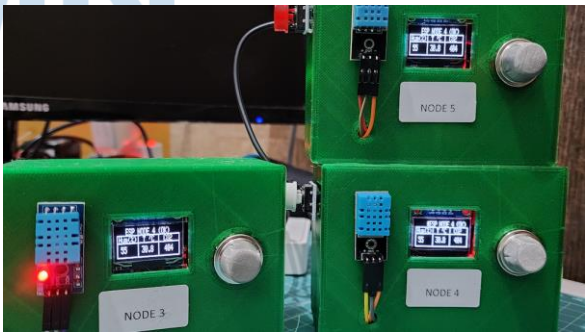

Fig. 8. Sending node 4 sensor values to nodes 3 and 5

From the test results, it was found that the sensor nodes could read and communicate well.

The next test is to turn off sensor node 3 as a sample of problem nodes and then read the status value of node 3 from other nodes. Here are the test results:

TABLE II. NETWORK TESTING BETWEEN SENSOR NODES

Sensor Nodes	SN 3 Off
1	BAD
2	BAD
3	OFF
4	BAD
5	BAD

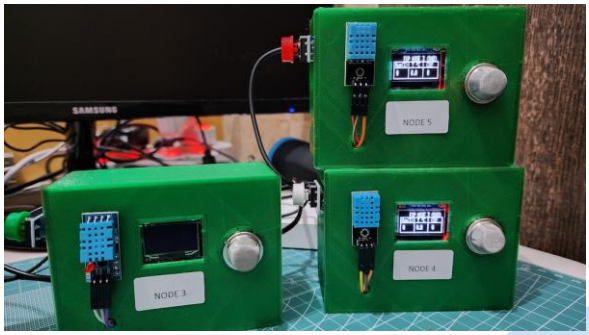

Fig. 9. Bad status display on nodes 4 and 5 when node 3 is OFF

From the test results, it is found that the bad status on one node can be read and detected by other sensor nodes. So it can be said that the network created has been running normally.

B. *IoT System Integration Testing*

Testing the integration of the IoT system with WSN is done by looking at the delivery results on the Node-Red dashboard. Figure 8 is the Node-Red dashboard test which is done by turning on the five sensor nodes and comparing the readings on the Node-Red dashboard with the readings on the display of each sensor node. If the readings are the same then the dashboard is appropriate.

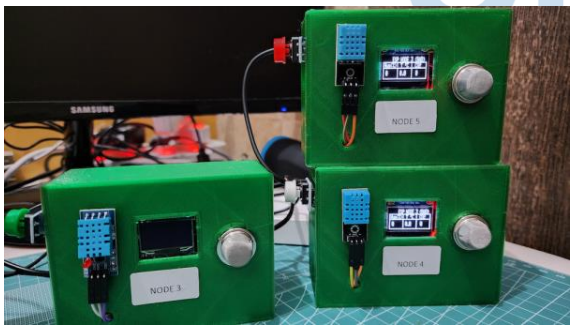

Fig. 10. Bad status display on nodes 4 and 5 when node 3 is OFF

C. *Sensor Node Range Testing*

The test was conducted by placing sensor node 2 in an outdoor location, then walking away from sensor node 2 with sensor node 5. Position the sensor node 5 display to sensor node 2. Continue walking away from sensor node 2 until the "BAD" status is detected on the display. Do this several times to determine the disconnection location of sensor node 2 from sensor node 5.

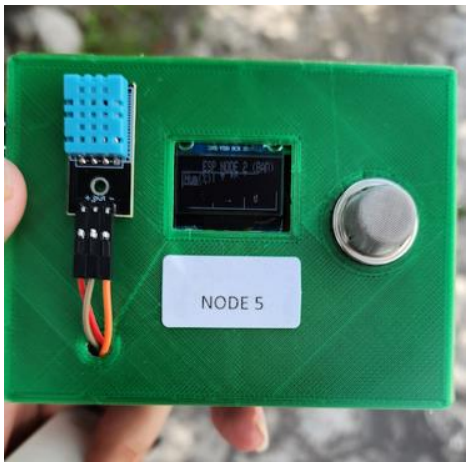

Fig. 11. Bad status on Node 5

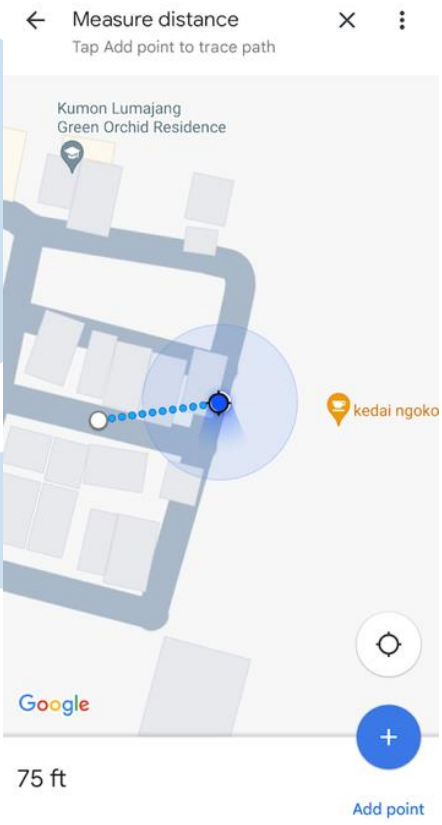

Fig. 12. Distance between Node 2 and Node 5 when the connection is lost

From the test results above, it is obtained that the farthest distance 2 sensor nodes can still communicate with each other is around 75 feet or 22 meters. This cannot be a reference only gives an idea of the communication distance of 2 nodes. Because the ability of 2 sensor nodes is influenced by the thickness and material of the barrier between the two sensor nodes. Barriers can be in the form of sensor container boxes, walls between 2 sensors, etc.

IV. CONCLUSION

The design of an air quality monitoring system based on a wireless sensor network makes the data more reliable for measuring the area being monitored. Because the nature of pollutants and polluting gases is unevenly distributed due to certain conditions. Because of this, the installation of air quality sensors is carried out at more than one point to guarantee the measurement. In this study, in addition to measurements using a sensor network, data collected by 5 sensor nodes can be sent to the internet network as an IoT system so that data can be stored in a data center and can be accessed anywhere. Further development of this research is to determine the standard value of air quality based on the installation site of the sensor network.

REFERENCES

[1] Presiden Republik Indonesia, Peraturan Pemerintah Republik Indonesia Nomor 74 Tahun 2001 Tentang Pengelolaan Bahan Berbahaya dan Beracun. 2001.

[2] Presiden Republik Indonesia, Peraturan Pemerintah Republik Indonesia Nomor 101 Tahun 2014 Tentang Pengelolaan Limbah Bahan Berbahaya dan Beracun. 2014.

[3] Kementrian Lingkungan Hidup dan Kehutanan, *Permen LHK Nomor 14 Tahun 2020*. 2020.

[4] Kementrian ESDM Republik Indonesia, Peraturan Menteri dan Sumber Daya Mineral Republik Indonesia Nomor 12 Tahun 2021 Tentang Klasifikasi, Kualifikasi, Akreditasi, dan Sertifikat Usaha Jasa Penunjang Tenaga Listrik. 2021.

[5] A. S. Handayani, R. A. Halimatussa'diyah, R. R. Aldi, dan N. L. Husni, "Perancangan Wireless Sensor Network Menggunakan Teknologi Multisensor Sebagai Sistem Monitoring Kualitas Udara," *Jurnal Qua Teknika*, vol. 10, no. 2, hlm. 1–13, 2020.

[6] A. Miranto dan E. Reynaldi, "Perancangan dan Implementasi Antarmuka Pengguna Sistem Pemantau Kualitas Udara Berbasis Aplikasi Android," *Cyberspace: Jurnal Pendidikan Teknologi Informasi*, vol. 7, no. 1, hlm. 1–14, 2023.

[7] A. D. Prakoso dan T. Wellem, "Perancangan dan Implementasi Sistem Pemantauan Kualitas Udara berbasis IoT menggunakan Wemos D1 Mini dan Android," *Building of Informatics, Technology and Science (BITS)*, vol. 4, no. 3, hlm. 1246–1254, Des 2022, doi: 10.47065/bits.v4i3.2498.

[8] M. A. Satryawan dan E. Susanti, "Perancangan Alat Pendeteksi Kualitas Udara dengan IoT (Internet of Things) Menggunakan Wemos ESP32 D1 R32," *Sigma Teknika*, vol. 6, no. 2, hlm. 410–419, 2023.

[9] G. A. Kristanto, J. Sumabrata, dan S. K. Astuti, "Analisis Kualitas Udara di Ruang Parkir Bawah Tanah dan Pengaruhnya Terhadap Pengguna," *Jurnal Sains dan Teknologi Lingkungan*, vol. 5, no. 2, hlm. 117–126, 2013.

[10] W. Tenriawi, "Gambaran Dampak Industri Terhadap Kualitas Lingkungan pada Masyarakat Sekitar di Wilayah Industri Daerah Kabupaten Takalar," *Media Informasi Sains dan Teknologi*, hlm. 408–413, 2022.

[11] A. Duppa, A. Daud, dan B. Bahar, "Kualitas Udara Ambien di Sekitar Industri Semen Bosowa Kabupaten Maros," *JKMM*, vol. 3, no. 3, hlm. 86–92, 2020.

[12] I. Q. A'yun dan R. Umaroh, "Polusi Udara dalam Ruangan dan Kondisi Kesehatan: Analisis Rumah Tangga Indonesia," *Jurnal Ekonomi dan Pembangunan Indonesia*, vol. 23, no. 1, hlm. 16–26, Jan 2023, doi: 10.21002/jepi.2022.02.

[13] T. N. Hakim dan M. F. Susanto, "Sistem Monitoring Kualitas Udara Berbasis Internet of Things," dalam *Prosiding The 11 th Industrial Research Workshop and National Seminar*, 2020, hlm. 496–502.

[14] L. Hanum dan E. Elfizon, "Rancang Bangun Pemantau Kualitas Udara Dalam Ruangan Berbasis Internet Of Things," *JTEIN: Jurnal Teknik Elektro Indonesia*, vol. 4, no. 2, hlm. 619–624, Agu 2023, doi: 10.24036/jtein.v4i2.473.

[15] D. Prasetyo, W. Nurrul Adzilla, dan Y. Saragih, "Implementasi Pemantauan Kualitas Udara dengan Menggunakan MQ-7 dan MQ-131 Berbasis Internet of Things," 2021.

[16] S. Sadi, S. Mulyati, dan P. B. Setiawan, "Internet of Things Pada Sistem Monitoring Kualitas Udara Menggunakan Web Server," *Formosa Journal of Multidisciplinary Research (FJMR)*, vol. 1, no. 4, hlm. 1085–1094, 2022, doi: 10.55927.

[17] P. Imas Agista, N. Gusdini, dan M. Dewi Dyah Maharani, "Analisis Kualitas Udara dengan Indeks Standar Pencemar Udara (ISPU) dan Sebaran Kadar Politannya di Provinsi DKI Jakarta," *Jurnal SEOI*, vol. 2, no. 2, hlm. 39–57, 2020.

[18] A. Kurniawan, "Pengukuran Parameter Kualitas Udara (CO, NO2, SO2, O3 dan PM10) di Bukit Kototabang Berbasis ISPU," *Jurnal Teknosains*, vol. 7, no. 1, hlm. 1, Jul 2018, doi: 10.22146/teknosains.34658.

[19] Y. Arafat dan E. Setyati, "Desain dan implementasi Wireless Sensor Network menggunakan LoRa untuk pemantauan tingkat pencemaran udara di Kota Surabaya," *Teknologi: Jurnal Ilmiah Sistem Informasi*, vol. 10, no. 2, hlm. 75–84, Jul 2020, doi: 10.26594/teknologi.v10i2.2070.

[20] B. Harpad, Salmon, dan R. M. Saputra, "Sistem Monitoring Kualitas Udara di Kawasan Industri dengan NodeMCU Berbasis IoT," *Jurnal Informatika Wicida*, vol. 12, no. 2, hlm. 39–47, Jul 2022, doi: 10.46984/inf-wcd.1955.

[21] R. N. Lesmana dan Y. Rahayu, "Membangun Sistem Pemantau Kualitas Udara Dalam Ruangan Dengan Mengaplikasikan Sensor CO, O3, PM10 Berbasis LabVIEW," 2016.

[22] R. Purbakawaca dan S. A. Fauzan, "Rancang Bangun Sistem Pemantauan Kualitas Udara Dalam Ruangan Berbiaya Rendah Berbasis IoT," *Jurnal Talenta Sipil*, vol. 5, no. 1, hlm. 118–125, Feb 2022, doi: 10.33087/talentasipil.v5i1.104.

[23] A. Sujarta, G. Putu, W. Wedashwara, dan A. Zubaidi, "Sistem Monitoring Kualitas Udara Di Ruangan Tertutup Berbasis IoT Menggunakan Sensor MQ-135 dan GP2Y1014AU0F," *J-COSINE (Journal of Computer Science and Informatics Engineering)*, vol. 7, no. 2, hlm. 93–102, 2023, [Daring]. Tersedia pada: http://jcosine.if.unram.ac.id/

[24] Y. A. Rozzi, J. Fredricka, dan E. P. Arimi, "Metode Real-Time Berbasis Android dalam Membangun Sistem Monitoring Kualitas Udara untuk Proses Sanitasi Rumah Sakit," *DECODE: Jurnal Pendidikan Teknologi Informasi*, vol. 3, no. 2, hlm. 420–428, 2023, doi: 10.51454/decode.v2i2.328.

[25] M. I. Munabbih, E. D. Widianto, Y. E. Windarto, dan E. Y. Indrasto, "Rancang Bangun Sistem Pemantau Kualitas Udara Menggunakan Arduino dan LoRa Berbasis Jaringan Sensor Nirkabel," *Transmisi*, vol. 22, no. 1, hlm. 6–14, Mar 2020, doi: 10.14710/transmisi.22.1.6-14.

[26] I. Muhammad, B. Sugiarto, dan I. Sakti, "Rancang Bangun Sistem Monitoring Kualitas Udara Menggunakan Teknologi Wireless Sensor Network (WSN)," *INKOM*, vol. III, no. 2, hlm. 90–96, 2009.

[27] A. Utama dan A. Setia Budi, "Sistem Pendeteksian Node Baru Otomatis pada WSN Topologi Mesh berbasis ESP-NOW," *Jurnal Pengembangan Teknologi Informasi dan Ilmu Komputer*, vol. 8, no. 1, hlm. 51–57, 2024, [Daring]. Tersedia pada: http://j-ptiik.ub.ac.id.

ISSN 2355-3286

Gross Error Detection and Data Correction in IIoT-Based Data Center Cooling System

Abdul Hamid[1], Eko Mursito Budi[2], Estiyanti Ekawati[2]
[1] Instrumentation and Control Engineering, Institut Teknologi Bandung, Bandung, Indonesia
[2] Engineering Physics, Institut Teknologi Bandung, Bandung, Indonesia
hamidabdul776@outlook.co.id

Accepted on 26 June 2024
Approved on 09 July 2024

***Abstract*— A data center always require a proper cooling system. This research study a data center with water based cooling system that consists of two chillers and two in-rack coolers. To control the system, an Industrial Internet of Things (IIoT) infrastructures has been deployed. It able to monitors real-time data from various sensors such as temperature (T), pressure (P), water flow (Q). The data were supposed to be used for optimization. However, early assessment showed that there were discrepancies between the sensors. Therefore, the data reconciliation method is very important to get valid data from the sensor by utilizing the least square optimization problem method. obtained the results of error detection on the temperature sensor reading +/- 2.5 degrees with an accuracy of 3 numbers behind the comma, then analyzed the Mean Square Error and Mean Average Error at the time before reconciliation the results were 7.21 and 2.68, and after the reconciliation process and gross error obtained the results of Mean Square Error of 0.33 and Mean Average Error of 0.5 from these results it can be concluded that the reconciliation and gross error detection method used with the least square method is better than the gross error detection method.**

***Index Terms*— Colleration matrix; Gross error detection; Industrial Internet of things; Least-square optimization method.**

I. INTRODUCTION

The advent of Industry 4.0 has ushered in a paradigm shift across diverse industrial sectors, necessitating the ubiquitous integration of data centers. Industry 4.0, a convergence of digital and physical technologies in industrial processes, has precipitated an escalating demand for High-Performance Computing (HPC). In this landscape, cloud technology services and the imperative for high computing loads constitute pivotal facets in industrial operations, facilitating real-time data processing, analysis, and responsiveness. Data centers, as linchpins in efficient data storage and management, furnish the computational prowess requisite for expanse data analytics [1].

Nevertheless, the challenges intrinsic to high computing loads in the industry 4.0 milieu exert formidable stress on data center performance. This necessitates the capacity to adeptly manage voluminous data and promptly respond to exigent demands [2]. Operational challenges further manifest in the inefficiencies of water-cooling systems, characterized by excessive energy consumption and necessitating disruptive downtimes for maintenance [3]. The utilization of data reconciliation methods becomes imperative to verify the accuracy of every sensor employed in process control [4] to archive goal creation an optimal control system and can reduce time of the cooling machine. other challenging in data center systems revolves around maintaining room temperatures below the dew point, crucial for optimal functionality of computer servers within the data center environment [5].

Therefore, we are developing an IIoT system for the water-based cooling machine in the data center, which will be constructed in Labtek 6, Building of Engineering Physics, Faculty of Industrial Technology, Institute Teknologi Bandung. One of the key aspects we need to focus on is ensuring that the measurement data are accurate to make the process effective and efficient [6]. Building an IIoT Integration system, measurement error can sometimes occur, and this error can be categorized into random errors and gross error [7]. These errors need to be minimized during the data acquisition process to make sure all those data for acquisition were accurate [8]. One or other method can be use is to minimize the objective function in linear state space equation over time and by detecting gross errors through a physical quantity approach in the control process has been used [9].

The approach involves employing the SciPy optimization method to minimize the objective function using a general equation for Least Square Optimization. The input for the SciPy function includes a correlation matrix, and the relationships between various processes in the data center cooling system are visualized using a heatmap method. Prior to analysis, the dataset undergoes preprocessing, which includes noise detection, training on 80% of the data, and validation using the remaining 20%. The primary goal of this process is to identify measurement errors in the sensors and subsequently adjust the measured values.

II. METHODS

A. Research Objective

The research focuses on a data center with water based cooling system located at Labtek 6, Engineering Physics, Faculty of Industrial Technology, Bandung Institute of Technology. An IIoT system for this system has been developed using the Node-RED platform. During the implementation of the IIoT integration system, it was observed that some sensors were less accurate, necessitating a gross error detection and correction method in the data acquisition process. This research involves several stages, as depicted in the overall research flow chart in Fig. 1.

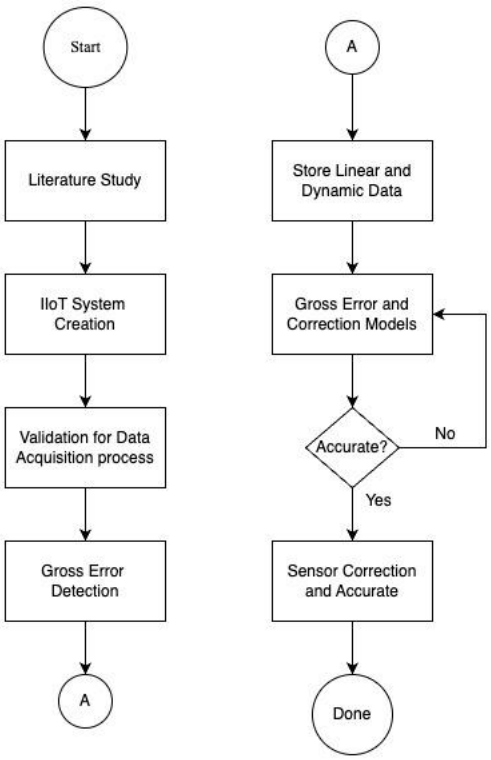

Fig. 1. Research Flow Diagram

B. Water Based Cooling System & Instrumentation

The schematic design of the Piping & Instrument Diagram in this study, as illustrated in Fig.2 reveals the representation of Chiller 1 and Chiller 2 as CH.1 and CH.2, both sharing the same water flow. A mixing pipe serves as a blending and redundancy system, enabling the alternating activation or deactivation of Chiller 1 and Chiller 2 every 12 hours. The sequence begins with Chiller 1 powered by Motor 1 (CHWP 1) followed by Chiller 2 powered by Motor 2 (CHWP 2). The controller employed in this study is a PLC of CP2E type, specifically designed for reading and controlling the data center cooling system effectively.

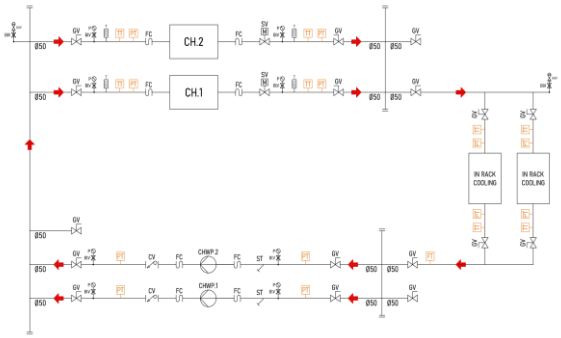

Fig. 2. Piping and Instrument Diagram

In the section illustrating the water inlet represented by red arrows from Chiller 1 and 2 before entering the Mixing Pipe, Solenoid Valves (SV) are strategically placed in each chiller section. This is to ensure that the water flow is directed only to the active chiller while the inactive one remains unaffected. After entering the mixing pipe, water flow is propelled by a pump towards the In-rack Cooling section through a branching pipe system, ensuring even distribution. Temperature (TT) and pressure (PT) sensors are strategically placed at the entry and exit points of the In-rack Cooling system. Each pipe in this process is equipped with temperature and pressure sensors to analyze the temperature and pressure differences between the incoming and outgoing water from Chiller 1 and Chiller 2. Additionally, a flow sensor (FT) is installed to detect any water leakage within the system. This P&ID system constructed fulfills the criteria for conducting data correction and detecting gross error values effectively. Multiple sensors installed in each relevant process enable the application of reconciliation principles for accurate data correction, ensuring high precision and suitability [18].

C. IIoT System

The architectural system for IoT integration in Data Center cooling machines utilizes the Node-RED platform. It serves as a communication bridge between physical devices (OT) and the IT system, allowing every process on the machine to be automatically recorded in a MySQL database and displayed on the HMI panel, as shown in Fig 3.

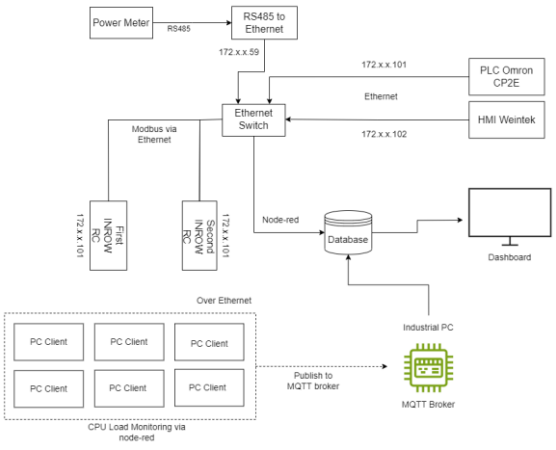

Fig. 3. IT Diagram for IT Process

Furthermore, Fig.4 illustrates the configuration of OT devices, which consist of sensors and actuators controlled by an Omron CP2E N-30DRA PLC. This PLC is connected via Analogue, Digital, or RS485 communication pin and the developed system must ensure that the data acquisition process and the implemented control system operate smoothly and without interruptions.

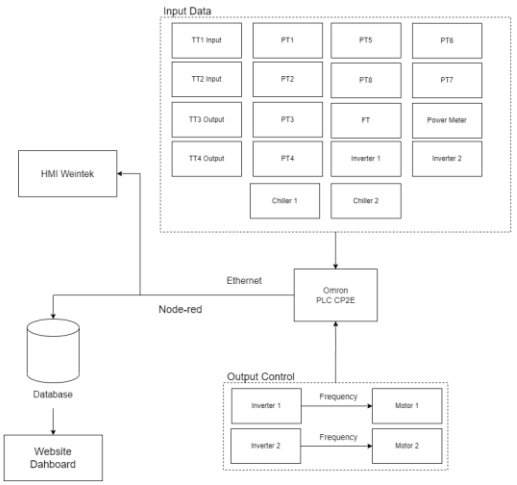

Fig. 4. OT Diagram for Field Device

D. Gross Error Detection & Correction Model

In state space analysis, a model is typically represented by first-order differential equations in a steady-state system [13]. The general state space equation is expressed as follows:

$$\dot{x}(t) = Ax(t) + Bu(t) \quad (1)$$

$$y(t) = Cx(t) + Du(t) \quad (2)$$

Equation (1) represents the state space equation, and equation (2) is the output equation of a linear system [14]. The author employs the Least Squares Optimization method to find the minimum value of the objective function in a linear system. This method is preferred over Weighted Least Squares because the dataset is predominantly linear, as described by the general function in Equation (3).

$$min \sum_{i=1}^{n} \omega_i \, (x_i - \hat{x}_i)^2 \quad (3)$$

And referring to Equation (1), we get Equation (4) matrix notation.

$$\min (x - \hat{x})^T \, W (x - \hat{x}) \quad (4)$$

To solve the optimization problem, the method of Lagrange multipliers, as shown in Equation (5), is used. This approach involves obtaining the value of the partial derivative of the Lagrangian function ($\mathcal{L}$) with respect to x dan λ by setting the equation equal to zero [15]. The optimal result of data reconciliation (X_r) and the offset/bias value, which are necessary for data correction, are then determined. These results represent the accuracy of a sensor under steady-state conditions.

$$\mathcal{L}_{(x,\lambda)} = (x - \hat{x})^T W (x - \hat{x}) + \lambda^T (A_x + b) \quad (5)$$

In a control process, an essential variable for data processing is converting time-based state space equations to discrete-based state space equations. This conversion requires selecting an appropriate sampling rate to accurately model a continuous system as a discrete one [16]. To minimize errors resulting from the discretization of the state space, suitable sampling intervals are necessary, these intervals are typically as small as possible relative to the system time constant, or the real-time sampling frequency of data obtained from the control process. The discrete state space equations are represented by Equation (6) and Equation (7) as follows:

$$X_k = FX_{k-1} + GU_{k-1} + W_k \quad (6)$$

$$Y_k = HX_k + V_k \quad (7)$$

Then, the data bias parameters represented by $W_k V_k$ and errors can be shown in Equation (8) as follows:

$$\begin{gathered} E[W_k] = E[V_k] = 0 \\ Cov[W_k] = Q \\ Cov[V_k] = R \\ Cov[W_k, W_i] = Cov[V_k, V_j] = 0 \\ Cov[W_k, V_j] = 0 \end{gathered} \quad (8)$$

The equation aims to ensure that the expected values of W_k and V_k are zero, with their covariances being Q and R respectively.

E. Gross Error Detection & Correction Calculation

The process of gross error detection and data correction in a system involves collecting real-time sensor data and comparing readings from potentially erroneous sensors with those from accurate sensors,

while adhering to relevant physical laws. Corrected sensors must maintain a constant physical mass and be within a relatively close range.

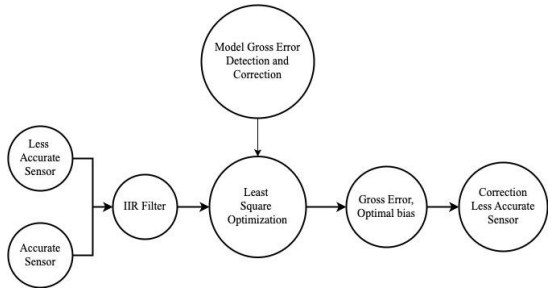

Fig. 5. Gross Error detection and Correction process

Figure 5 shows the data flow diagram of error detection and correction process. It begins by reading the data from the accurate sensors as well as the less accurate ones. To reduce the noise, the data then filtered with an IIR filter [10]. This is followed by sampling the steady state of the data center cooling process, indicated by water temperature measurements that match the setpoint. If the system is functioning normally but missing data is detected, the random forest method is used to predict and fill in the missing values [11]. Then, to analyze the processes and their correlations, resulting in a correlation matrix. Heatmap analysis is used to identify and visualize the relationships between each process within the system [12]. The resulting correlation matrix will be used as an input data for gross error detection.

In employing the least square optimization method, the dataset used must be in a stable state. This requirement arises because the least square optimization method necessitates stable data to accurately minimize objective functions. One critical factor affecting the accuracy of the least square optimization model is ensuring that both the training and validation data are free from noise. Therefore, it is essential to preprocess the data to eliminate any noise and enhance the reliability of the optimization results digital filter need to be applying on training and validation data. On this research specifically use an IIR filter, to the obtained dataset to eliminate noise in the sensor reading system. This results in a noise-free set of sensor data, aiming to provide the most optimal correction results. Following this, a heatmap analysis is performed on the filtered dataset to determine the correlation between the various processes.

The resulting matrix is then used as input data to minimize the objective function using the least square optimization method. Once the objective function is derived, it yields the bias value (b), which is subsequently used to correct data from sensors exhibiting intolerable bias [17]. Then, to correct the sensor data using Equation (9) to achieve accurate data readings.

$$\Delta_{correction} = (Xr - b) - E_{data} \quad (9)$$

After obtaining the corrected data values from the validation process of the sensor readings, the Mean Square Error (MSE) and Mean Absolute Error (MAE) were evaluated. The errors were assessed for the corrected sensor data in comparison to the calibrated sensor data. If the MSE and MAE values for the corrected sensor data are within ±0.5% of the calibrated sensor data, it can be concluded that the applied method is successful. This indicates that the corrections have effectively improved the accuracy of the sensor readings.

III. Results and Discussion

A. IIoT data logging

The data logger used in this research samples data every 10 seconds for all processes occurring within the water-based data center cooling machine and some crucial sensors are read with a per-second sampling rate, including the temperature sensor in the pipe (TT), the pressure sensor in the pipe (PT), the water flow sensor at the chiller output (FT1), and the water flow sensor at the chiller return (FT2). Fig. 8 shows the temperature sensor data readings with a 10-second time sampling interval. The set point changes sequentially from 16 degrees to 18 degrees, and then to 20 degrees, resulting in the graph shown in Fig 6.

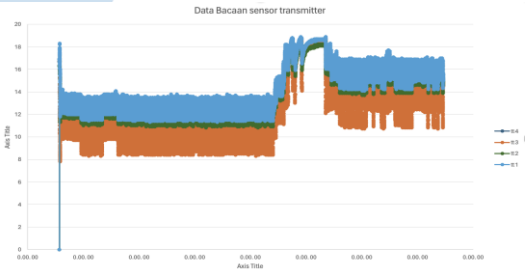

Fig. 6. Data Logger within 10 second sampling time

B. Error Detection & Correction Model

Based on the development of the IIoT system for data center cooling machines, sensors were positioned according to the P&ID design drawing. The system schematic is depicted in Fig. 7.

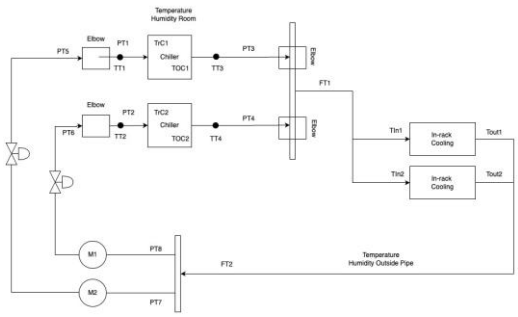

Fig. 7. Schematic of the IoT system of Water-based Data Center Cooling Machine

The sensor placement illustrated in Fig 7 adheres to the previously designed P&ID. Temperature (TT) and pressure (PT) sensors have been installed at the mixing pipe outlets (ToC) and returns (TrC) of the cooling machine. The water flow is monitored both before and after the in-rack cooling process to evaluate for potential leaks in the closed-loop system. This can be represented in the physical model as follows:

$$\begin{gathered} TrC1 - TT1 = 0 \text{ and } TrC2 - TT2 = 0 \\ ToC1 - TT3 = 0 \text{ and } ToC2 - TT4 = 0 \\ PT1 + \hat{x} = PT5 \text{ and } PT2 + \hat{x} = PT6 \\ PT1 + \hat{x} = PT3 \text{ and } PT2 + \hat{x} = PT4 \\ PT5 + \hat{x} = PT7 \text{ and } PT6 + \hat{x} = PT8 \\ Tin1 = TT3 - \hat{x} \text{ and } Tin2 = TT4 - \hat{x} \\ Tout2 = Tin1 - \hat{x} \text{ and } Tout1 = Tin1 - x \\ FT1 = FT2 = FT3 = FT4 \end{gathered} \tag{10}$$

In this model, it is assumed that the water flow rate remains constant and is independent of any processes occurring within the system. Therefore, it can be represented in matrix form as follows:

1. Current model condition $TrC1 - TT1 = 0$ and $TrC2 - TT2 = 0$.

$$\begin{bmatrix} TT_1 \\ TT_2 \\ TrC_1 \\ TrC_2 \end{bmatrix} = \begin{bmatrix} -1 & 0 & 1 & 0 \\ 0 & -1 & 0 & 1 \\ 1 & 0 & -1 & 0 \\ 0 & -1 & 0 & 1 \end{bmatrix} \begin{bmatrix} TT_1 \\ TT_2 \\ TrC_1 \\ TrC_2 \end{bmatrix} + b \tag{11}$$

2. Current model condition $ToC1 - TT3 = 0$ and $ToC2 - TT4 = 0$.

$$\begin{bmatrix} TT_3 \\ TT_4 \\ ToC_1 \\ ToC_2 \end{bmatrix} = \begin{bmatrix} -1 & 0 & 1 & 0 \\ 0 & -1 & 0 & 1 \\ -1 & 0 & 1 & 0 \\ 0 & -1 & 0 & 1 \end{bmatrix} \begin{bmatrix} TT_3 \\ TT_4 \\ ToC_1 \\ ToC_2 \end{bmatrix} + b \tag{12}$$

3. Current model condition $PT1 + \hat{x} = PT5$ and $PT2 + \hat{x} = PT6$.

$$\begin{bmatrix} PT_1 \\ PT_2 \\ PT_5 \\ PT_6 \end{bmatrix} = \begin{bmatrix} 1 & 0 & -1 & 0 \\ 0 & 1 & 0 & -1 \\ 1 & 0 & -1 & 0 \\ 0 & 1 & 0 & -1 \end{bmatrix} \begin{bmatrix} PT_1 \\ PT_2 \\ PT_5 \\ PT_6 \end{bmatrix} + b \tag{13}$$

4. Current model condition $PT1 + \hat{x} = PT3$ and $PT2 + \hat{x} = PT4$.

$$\begin{bmatrix} PT_1 \\ PT_2 \\ PT_5 \\ PT_6 \end{bmatrix} = \begin{bmatrix} 1 & 0 & -1 & 0 \\ 0 & 1 & 0 & -1 \\ 1 & 0 & -1 & 0 \\ 0 & 1 & 0 & -1 \end{bmatrix} \begin{bmatrix} PT_1 \\ PT_2 \\ PT_5 \\ PT_6 \end{bmatrix} + b \tag{14}$$

5. Current model condition $PT5 + \hat{x} = PT7$ and $PT6 + \hat{x} = PT8$.

$$\begin{bmatrix} PT_5 \\ PT_6 \\ PT_7 \\ PT_8 \end{bmatrix} = \begin{bmatrix} 1 & 0 & -1 & 0 \\ 0 & 1 & 0 & -1 \\ -1 & 0 & 1 & 0 \\ 0 & -1 & 0 & 1 \end{bmatrix} \begin{bmatrix} PT_5 \\ PT_6 \\ PT_7 \\ PT_8 \end{bmatrix} + b \tag{15}$$

6. Current model condition $Tin1 = TT3 - \hat{x}$ and $Tin2 = TT4 - \hat{x}$.

$$\begin{bmatrix} TT_3 \\ TT_4 \\ Tin_1 \\ Tin_2 \end{bmatrix} = \begin{bmatrix} 1 & 1 & -1 & 0 \\ 1 & 1 & -1 & -1 \\ 1 & 1 & -1 & 0 \\ 1 & 1 & 0 & -1 \end{bmatrix} \begin{bmatrix} TT_3 \\ TT_4 \\ Tin_1 \\ Tin_2 \end{bmatrix} + b \tag{16}$$

7. Current model condition $Tout2 = Tin1 - \hat{x}$ and $Tout1 = Tin1 - x$.

$$\begin{bmatrix} Tin_1 \\ Tin_2 \\ Tout_1 \\ Tout_2 \end{bmatrix} = \begin{bmatrix} 1 & 0 & -1 & 0 \\ 0 & 1 & 0 & -1 \\ 1 & 0 & -1 & 0 \\ 0 & 1 & 0 & -1 \end{bmatrix} \begin{bmatrix} Tin_1 \\ Tin_2 \\ Tout_1 \\ Tout_2 \end{bmatrix} + b \tag{17}$$

8. Current model condition $FT1 = FT2 = FT3 = FT4$.

$$\begin{bmatrix} FT_1 \\ FT_2 \\ FT_3 \\ FT_4 \end{bmatrix} = \begin{bmatrix} 1 & 1 & 1 & 1 \\ 1 & 1 & 1 & 1 \\ 1 & 1 & 1 & 1 \\ 1 & 1 & 1 & 1 \end{bmatrix} \begin{bmatrix} FT_1 \\ FT_2 \\ FT_3 \\ FT_4 \end{bmatrix} + b \tag{18}$$

C. Data Processing

The initial step involved analyzing the system by distinguishing between transient and steady-state conditions. After separating the transient and steady-state data, noise was detected in the data. Therefore, a digital filter was required to remove the noise. An Infinite Impulse Response (IIR) filter was employed for this purpose. The IIR filter was chosen to mitigate overfitting and underfitting, ensuring clean data for machine learning applications, which results in high accuracy. Assuming a fourth-order IIR filter with a cutoff value of 10, the filtered data, as shown in Figure 10 was the reduces noise in the dataset.

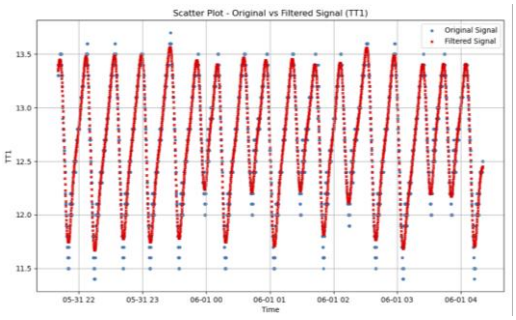

Fig. 8. Plot data from original data comparing with filtered data

The subsequent step involves constructing matrix A, which represents the correlation matrix derived from the least squares optimization problem to determine the objective function. This process utilizes a heat-map analysis approach based on the derived physical equations, as depicted in Fig. 11. Higher values in the heat-map, the 1 value in result that

indicate strong relationships between the conditions being analyzed.

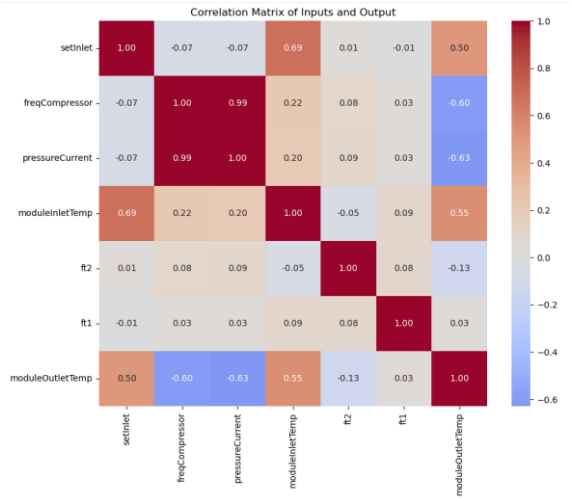

Fig. 9. Result of correlation matrix analysis using heat-map method

Subsequently, from these results, the author derived a 24x24 correlation matrix equation. Substituting this matrix equation into the least squares optimization method yielded X_r values, representing the accuracy of sensor readings, and optimal bias values (b) for each sensor. The optimal values of X_r and b obtained sequentially for the temperature sensor in the pipe (TT) and the water flow rate sensor (FT) readings are as follows:

1. Temperature sensor (TT)
   Optimal X_r= [12.69 12.36 11.52 12.48]
   Optimal b = [-2.5 -2.57 1.42 1.43]

This represents sensor condition TT1, TT2, TT3, TT4 that located on pipping area in return and outlet Chiller.

2. Water Flow Sensor (FT)
   Optimal X_r = [23.42 12.40 17.21 9.84]
   Optimal b = [-6.28 -6.28 -6.28 -6.28]

This represents sensor condition FT1, FT2, FT3, FT4 that located on return, outlet chiller, inside in rack-cooling, and feedback from in rack-cooling.

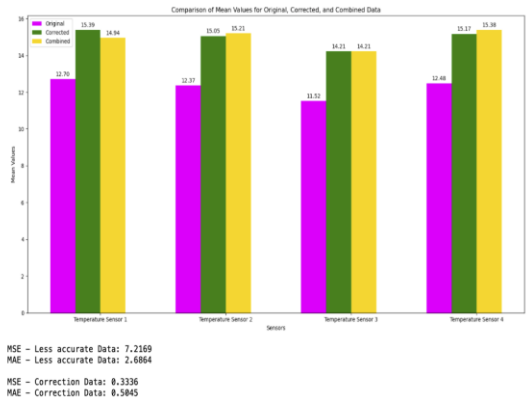

Fig. 10. Graphic plot result for temperature data correction

Then, after getting the results of the optimal $X_r$and optimal b values. Next, to make corrections, the sensor data is obtained using Equation (9). and the results obtained are as in Figure 10, namely a graphic plot of the results of the corrected temperature sensor data readings compared to the calibrated temperature sensor. The graph indicates a good adjustment with MAE results of 0.5045 and MSE 0.335.

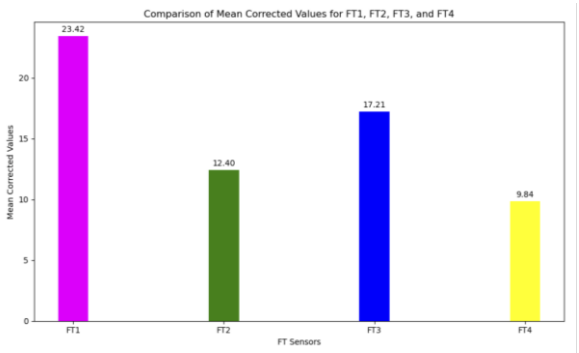

Fig. 11. Graph comparation on Water Flow sensor

The next analysis is the water flow sensor, the results obtained as in Figure 10 show a graph of the relationship between the water flow sensor before and after data correction and compared with the sensor that is considered accurate. On Pressure sensor there is no problem with that condition sensor. everything was accurate and no need adjustment variable.

IV. Conclusion

In the conducted research, it was determined that the number of sensors utilized in the data center cooling machine meets the criteria for detecting gross errors and correcting sensor inaccuracies. This enables thorough analysis and correction of inaccurate sensor readings to achieve high accuracy.

From the error correction process of sensor reading data compared to the original data, the results showed an MSE of 7.216 and an MAE of 2.6864. Furthermore, when comparing the error-corrected sensor reading data to the accurate sensor data from the water chiller machine, the results showed an MSE of 0.336 and an MAE of 0.5045.

Depending on those results of MAE and MSE obtained, it can be stated that by using the Least Square Optimization method by minimizing the objective function to obtain the gross error value and correcting the data has good performance so that this method can be applied to other data error correction case studies with a correction analysis approach on the sample dataset of steady state conditions.

Acknowledgment

This research has been part of the Laboratory Modernization Project in Engineering Physics, Faculty of Industrial Technology, ITB.

REFERENCES

[1] F. Ö. Koçoğlu and D. Demirkol, "Data in the Context of Industry 4.0," in *Who Runs the World: Data*, Istanbul University Press, 2020, pp. 71–92. doi: 10.26650/b/et06.2020.011.04.

[2] M. Panarotto, O. Isaksson, and V. Vial, "Cost-efficient digital twins for design space exploration: A modular platform approach," *Comput Ind*, vol. 145, Feb. 2023, doi: 10.1016/j.compind.2022.103813.

[3] R. He, G. Chen, C. Dong, S. Sun, and X. Shen, "Data-driven digital twin technology for optimized control in process systems," *ISA Trans*, vol. 95, pp. 221–234, Dec. 2019, doi: 10.1016/j.isatra.2019.05.011.

[4] E. M. Budi, E. Ekawati, and B. Efendy, "Comparison of structural analysis and principle component analysis for leakage prediction on superheater in boiler," *IAES International Journal of Artificial Intelligence (IJ-AI)*, vol. 11, no. 4, p. 1439, Dec. 2022, doi: 10.11591/ijai.v11.i4.pp1439-1447.

[5] C. F. Lazaga, A. K. S. Rodriguez, G. T. Salvador, and J.-A. V. Magsumbol, "Optimization of Dew Point, Humidity, and Temperature in Data Centers using Genetic Algorithm with Multiple Linear Regression," in *TENCON 2022 - 2022 IEEE Region 10 Conference (TENCON)*, IEEE, Nov. 2022, pp. 1–5. doi: 10.1109/TENCON55691.2022.9977710.

[6] H. Weytjens and J. De Weerdt, "Learning uncertainty with artificial neural networks for predictive process monitoring," *Appl Soft Comput*, vol. 125, p. 109134, Aug. 2022, doi: 10.1016/j.asoc.2022.109134.

[7] A. J. Sutrisno, P. Siregar Dan, and E. Ekawati, "Program Aplikasi Rekonsiliasi Data untuk Pendeteksian Gross Error pada Sistem Tangki Ganda yang Berinteraksi," *Ktrl.Inst (J.Auto.Ctrl.Inst)*, vol. 6, no. 1, p. 2014.

[8] S. Narasimhan and C. Jordache, "Data Reconciliation & Gross Error Detection: An Intelligent Use of Process Data," 2000.

[9] Y. Miao, H. Su, R. Gang, and J. Chu, "Industrial Processes: Data Reconciliation and Gross Error Detection," *Measurement and Control*, vol. 42, no. 7, pp. 209–215, Sep. 2009, doi: 10.1177/002029400904200704.

[10] S. R. Sutradhar, N. Sayadat, A. Rahman, S. Munira, A. K. M. F. Haque, and S. N. Sakib, "IIR based digital filter design and performance analysis," in *2017 2nd International Conference on Telecommunication and Networks (TEL-NET)*, IEEE, Aug. 2017, pp. 1–6. doi: 10.1109/TEL-NET.2017.8343596.

[11] D. Borup, B. J. Christensen, N. S. Mühlbach, and M. S. Nielsen, "Targeting predictors in random forest regression," *Int J Forecast*, vol. 39, no. 2, pp. 841–868, Apr. 2023, doi: 10.1016/j.ijforecast.2022.02.010.

[12] L. Aversano, M. L. Bernardi, M. Cimitile, M. Iammarino, D. Montano, and C. Verdone, "Using Machine Learning for early prediction of Heart Disease," in *2022 IEEE International Conference on Evolving and Adaptive Intelligent Systems (EAIS)*, IEEE, May 2022, pp. 1–8. doi: 10.1109/EAIS51927.2022.9787720.

[13] K. Ogata, *Modern Control Engineering*. New Jersey: Pearson Education, 2010.

[14] S. S. Rao, *Engineering Optimization: Theory and Practice*, 4 th Edition., vol. 13. John Wiley & Sons, 2009.

[15] G. Strang, *Linear Algebra and Its Applications (4th ed.)*. Brooks Cole, 2006.

[16] K. Ogata, *Discrete Time Control Engineering*. New Jersey: Pearson Education, 2010.

[17] W. Zhu, Z. Zhang, A. Armaou, G. Hu, S. Zhao, and S. Huang, "Dynamic data reconciliation to improve the result of controller performance assessment based on GMVC," *ISA Trans*, vol. 117, pp. 288–302, Nov. 2021, doi: 10.1016/j.isatra.2021.01.047.

[18] J. Prakash and P. Anbumalar, "An improved recursive non-linear dynamic data reconciliation for non-linear state estimation subject to bound constraints," *Int J Adv Eng Sci Appl Math*, vol. 15, no. 1, pp. 15–23, Mar. 2023, doi: 10.1007/s12572-023-00326-7.

AUTHOR GUIDELINES

1. Manuscript criteria

- The article has never been published or in the submission process on other publications.
- Submitted articles could be original research articles or technical notes.
- The similarity score from plagiarism checker software such as Turnitin is 20% maximum.
- For December 2021 publication onwards, Ultima Computing : Jurnal Sistem Komputer will be receiving and publishing manuscripts written in English only.

2. Manuscript format

- Article been type in Microsoft Word version 2007 or later.
- Article been typed with 1 line spacing on an A4 paper size (21 cm x 29,7 cm), top-left margin are 3 cm and bottom-right margin are 2 cm, and Times New Roman's font type.
- Article should be prepared according to the following author guidelines in this template. Article contain of minimum 3500 words.
- References contain of minimum 15 references (primary references) from reputable journals/conferences

3. Organization of submitted article

The organization of the submitted article consists of Title, Abstract, Index Terms, Introduction, Method, Result and Discussion, Conclusion, Appendix (if any), Acknowledgment (if any), and References.

- Title
  The maximum words count on the title is 12 words (including the subtitle if available)
- Abstract
  Abstract consists of 150-250 words. The abstract should contain logical argumentation of the research taken, problem-solving methodology, research results, and a brief conclusion.
- Index terms
  A list in alphabetical order in between 4 to 6 words or short phrases separated by a semicolon (;), excluding words used in the title and chosen carefully to reflect the precise content of the paper.
- Introduction
  Introduction commonly contains the background, purpose of the research, problem identification, research methodology, and state of the art conducted by the authors which describe implicitly.
- Method
  Include sufficient details for the work to be repeated. Where specific equipment and materials are named, the manufacturer's details (name, city and country) should be given so that readers can trace specifications by contacting the manufacturer. Where commercially available software has been used, details of the supplier should be given in brackets or the reference given in full in the reference list.
- Results and Discussion
  State the results of experimental or modeling work, drawing attention to important details in tables and figures, and discuss them intensively by comparing and/or citing other references.
- Conclusion
  Explicitly describes the research's results been taken. Future works or suggestion could be explained after it
- Appendix and acknowledgment, if available, could be placed after Conclusion.
- All citations in the article should be written on References consecutively based on its' appearance order in the article using Mendeley (recommendation). The typing format will be in the same format as the IEEE journals and transaction format.

4. Reviewing of Manuscripts

Every submitted paper is independently and blindly reviewed by at least two peer-reviewers. The decision for publication, amendment, or rejection is based upon their reports/recommendations. If two or more reviewers consider a manuscript unsuitable for publication in this journal, a statement explaining the basis for the decision will be sent to the authors within six months of the submission date.

5. Revision of Manuscripts

Manuscripts sent back to the authors for revision should be returned to the editor without delay (maximum of two weeks). Revised manuscripts can be sent to the editorial office through the same online system. Revised manuscripts returned later than one month will be considered as new submissions.

6. Editing References

- **Periodicals**
  J.K. Author, “Name of paper,” Abbrev. Title of Periodical, vol. x, no. x, pp. xxx-xxx, Sept. 2013.

- **Book**
  J.K. Author, “Title of chapter in the book,” in Title of His Published Book, xth ed. City of Publisher, Country or Nation: Abbrev. Of Publisher, year, ch. x, sec. x, pp xxx-xxx.

- **Report**
  J.K. Author, “Title of report,” Abbrev. Name of Co., City of Co., Abbrev. State, Rep. xxx, year.

- **Handbook**
  Name of Manual/ Handbook, x ed., Abbrev. Name of Co., City of Co., Abbrev. State, year, pp. xxx-xxx.

- **Published Conference Proceedings**
  J.K. Author, “Title of paper,” in Unabbreviated Name of Conf., City of Conf., Abbrev. State (if given), year, pp. xxx-xxx.

- **Papers Presented at Conferences**
  J.K. Author, “Title of paper,” presented at the Unabbrev. Name of Conf., City of Conf., Abbrev. State, year.

- **Patents**
  J.K. Author, “Title of patent,” US. Patent xxxxxxx, Abbrev. 01 January 2014.

- **Theses and Dissertations**
  J.K. Author, “Title of thesis,” M.Sc. thesis, Abbrev. Dept., Abbrev. Univ., City of Univ., Abbrev. State, year. J.K. Author, “Title of dissertation,” Ph.D. dissertation, Abbrev. Dept., Abbrev. Univ., City of Univ., Abbrev. State, year.

- **Unpublished**
  J.K. Author, “Title of paper,” unpublished. J.K. Author, “Title of paper,” Abbrev. Title of Journal, in press.

- **On-line Sources**
  J.K. Author. (year, month day). Title (edition) [Type of medium]. Available: http:// www.(URL) J.K. Author. (year, month). Title. Journal [Type of medium]. volume(issue), pp. if given. Available: http://www.(URL) Note: type of medium could be online media, CD-ROM, USB, etc.

7. Editorial Adress

Jl. Scientia Boulevard, Gading Serpong
Tangerang, Banten, 15811
Email: **ultimacomputing@umn.ac.id**

Paper Title

Subtitle (if needed)

Author 1 Name[1], Author 2 Name[2], Author 3 Name[2]
[1] Line 1 (of affiliation): dept. name of organization, organization name, City, Country
Line 2: e-mail address if desired
[2] Line 1 (of affiliation): dept. name of organization, organization name, City, Country
Line 2: e-mail address if desired

Accepted on mmmmm dd, yyyy
Approved on mmmmm dd, yyyy

***Abstract*—This electronic document is a "live" template which you can use on preparing your Ultima Computing paper. Use this document as a template if you are using Microsoft Word 2007 or later. Otherwise, use this document as an instruction set. Do not use symbol, special characters, or Math in Paper Title and Abstract. Do not cite references in the abstract.**

***Index Terms*—enter key words or phrases in alphabetical order, separated by semicolon (;)**

I. INTRODUCTION

This template, modified in MS Word 2007 and saved as a Word 97-2003 document, provides authors with most of the formatting specifications needed for preparing electronic versions of their papers. Margins, column widths, line spacing, and type styles are built-in here. The authors must make sure that their paper has fulfilled all the formatting stated here.

Introduction commonly contains the background, purpose of the research, problem identification, and research methodology conducted by the authors which been describe implicitly. Except for Introduction and Conclusion, other chapter's title must be explicitly represent the content of the chapter.

II. EASE OF USE

A. Selecting a Template

First, confirm that you have the correct template for your paper size. This template is for Ultima Computing. It has been tailored for output on the A4 paper size.

B. Maintaining the Integrity of the Specifications

The template is used to format your paper and style the text. All margins, column widths, line spaces, and text fonts are prescribed; please do not alter them.

III. PREPARE YOUR PAPER BEFORE STYLING

Before you begin to format your paper, first write and save the content as a separate text file. Keep your text and graphic files separate until after the text has been formatted and styled. Do not add any kind of pagination anywhere in the paper. Please take note of the following items when proofreading spelling and grammar.

A. Abbreviations and Acronyms

Define abbreviations and acronyms the first time they are used in the text, even after they have been defined in the abstract. Abbreviations such as IEEE, SI, MKS, CGS, sc, dc, and rms do not have to be defined. Abbreviations that incorporate periods should not have spaces: write "C.N.R.S.," not "C. N. R. S." Do not use abbreviations in the title or heads unless they are unavoidable.

B. Units

- Use either SI (MKS) or CGS as primary units (SI units are encouraged).
- Do not mix complete spellings and abbreviations of units: "Wb/m2" or "webers per square meter," not "webers/m2." Spell units when they appear in text: "...a few henries," not "...a few H."
- Use a zero before decimal points: "0.25," not ".25."

C. Equations

The equations are an exception to the prescribed specifications of this template. You will need to determine whether or not your equation should be typed using either the Times New Roman or the Symbol font (please no other font). To create multileveled equations, it may be necessary to treat the equation as a graphic and insert it into the text after your paper is styled.

Number the equations consecutively. Equation numbers, within parentheses, are to position flush right, as in (1), using a right tab stop.

$$\int_0^{r_2} F(r,\phi)\, dr\, d\phi = [\sigma r_2 / (2\mu_0)] \qquad (1)$$

Note that the equation is centered using a center tab stop. Be sure that the symbols in your equation have been defined before or immediately following the

equation. Use "(1)," not "Eq. (1)" or "equation (1)," except at the beginning of a sentence: "Equation (1) is ..."

D. Some Common Mistakes

- The word "data" is plural, not singular.
- The subscript for the permeability of vacuum μ_0, and other common scientific constants, is zero with subscript formatting, not a lowercase letter "o."
- In American English, commas, semi-/colons, periods, question and exclamation marks are located within quotation marks only when a complete thought or name is cited, such as a title or full quotation. When quotation marks are used, instead of a bold or italic typeface, to highlight a word or phrase, punctuation should appear outside of the quotation marks. A parenthetical phrase or statement at the end of a sentence is punctuated outside of the closing parenthesis (like this). (A parenthetical sentence is punctuated within the parentheses.)
- A graph within a graph is an "inset," not an "insert." The word alternatively is preferred to the word "alternately" (unless you really mean something that alternates).
- Do not use the word "essentially" to mean "approximately" or "effectively."
- In your paper title, if the words "that uses" can accurately replace the word using, capitalize the "u"; if not, keep using lower-cased.
- Be aware of the different meanings of the homophones "affect" and "effect," "complement" and "compliment," "discreet" and "discrete," "principal" and "principle."
- Do not confuse "imply" and "infer."
- The prefix "non" is not a word; it should be joined to the word it modifies, usually without a hyphen.
- There is no period after the "et" in the Latin abbreviation "et al."
- The abbreviation "i.e." means "that is," and the abbreviation "e.g." means "for example."

IV. Using the Template

After the text edit has been completed, the paper is ready for the template. Duplicate the template file by using the Save As command, and use the naming convention as below

ULTIMATICS_firstAuthorName_paperTitle.

In this newly created file, highlight all of the contents and import your prepared text file. You are now ready to style your paper. Please take note on the following items.

A. Authors and Affiliations

The template is designed so that author affiliations are not repeated each time for multiple authors of the same affiliation. Please keep your affiliations as succinct as possible (for example, do not differentiate among departments of the same organization).

B. Identify the Headings

Headings, or heads, are organizational devices that guide the reader through your paper. There are two types: component heads and text heads.

Component heads identify the different components of your paper and are not topically subordinate to each other. Examples include ACKNOWLEDGMENTS and REFERENCES, and for these, the correct style to use is "Heading 5."

Text heads organize the topics on a relational, hierarchical basis. For example, the paper title is the primary text head because all subsequent material relates and elaborates on this one topic. If there are two or more sub-topics, the next level head (uppercase Roman numerals) should be used and, conversely, if there are not at least two sub-topics, then no subheads should be introduced. Styles, named "Heading 1," "Heading 2," "Heading 3," and "Heading 4", are prescribed.

C. Figures and Tables

Place figures and tables at the top and bottom of columns. Avoid placing them in the middle of columns. Large figures and tables may span across both columns. Figure captions should be below the figures; table heads should appear above the tables. Insert figures and tables after they are cited in the text. Use the abbreviation "Fig. 1," even at the beginning of a sentence.

TABLE I. TABLE STYLES

Table Head	**Table Column Head**		
	Table column subhead	***Subhead***	***Subhead***
copy	More table copy		

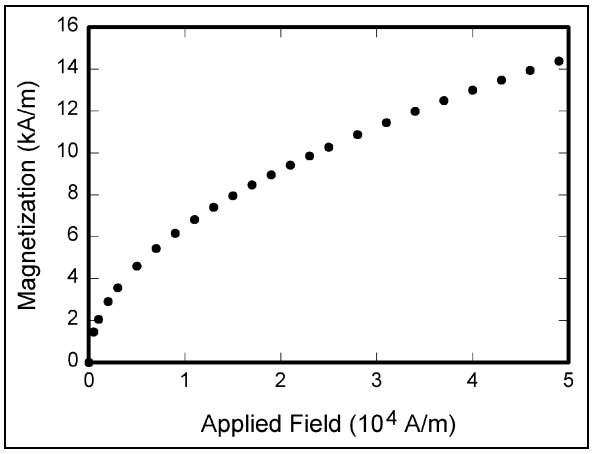

Fig. 1. Example of a figure caption

V. Conclusion

A conclusion section is not required. Although a conclusion may review the main points of the paper, do not replicate the abstract as the conclusion. A conclusion might elaborate on the importance of the work or suggest applications and extensions.

Appendix

Appendixes, if needed, appear before the acknowledgment.

ACKNOWLEDGMENT

The preferred spelling of the word "acknowledgment" in American English is without an "e" after the "g." Use the singular heading even if you have many acknowledgments. Avoid expressions such as "One of us (S.B.A.) would like to thank ... ." Instead, write "F. A. Author thanks ... ." You could also state the sponsor and financial support acknowledgments here.

References

The template will number citations consecutively within brackets [1]. The sentence punctuation follows the bracket [2]. Refer simply to the reference number, as in [3]—do not use "Ref. [3]" or "reference [3]" except at the beginning of a sentence: "Reference [3] was the first ..."

Number footnotes separately in superscripts. Place the actual footnote at the bottom of the column in which it was cited. Do not put footnotes in the reference list. Use letters for table footnotes.

Unless there are six authors or more give all authors' names; do not use "et al.". Papers that have not been published, even if they have been submitted for publication, should be cited as "unpublished" [4]. Papers that have been accepted for publication should be cited as "in press" [5]. Capitalize only the first word in a paper title, except for proper nouns and element symbols.

For papers published in translation journals, please give the English citation first, followed by the original foreign-language citation [6].

[1] G. Eason, B. Noble, and I.N. Sneddon, "On certain integrals of Lipschitz-Hankel type involving products of Bessel functions," Phil. Trans. Roy. Soc. London, vol. A247, pp. 529-551, April 1955. (*references*)

[2] J. Clerk Maxwell, A Treatise on Electricity and Magnetism, 3rd ed., vol. 2. Oxford: Clarendon, 1892, pp.68-73.

[3] I.S. Jacobs and C.P. Bean, "Fine particles, thin films and exchange anisotropy," in Magnetism, vol. III, G.T. Rado and H. Suhl, Eds. New York: Academic, 1963, pp. 271-350.

[4] K. Elissa, "Title of paper if known," unpublished.

[5] R. Nicole, "Title of paper with only first word capitalized," J. Name Stand. Abbrev., in press.

[6] Y. Yorozu, M. Hirano, K. Oka, and Y. Tagawa, "Electron spectroscopy studies on magneto-optical media and plastic substrate interface," IEEE Transl. J. Magn. Japan, vol. 2, pp. 740-741, August 1987 [Digests 9th Annual Conf. Magnetics Japan, p. 301, 1982].

[7] M. Young, The Technical Writer's Handbook. Mill Valley, CA: University Science, 1989.

UMN

UNIVERSITAS
MULTIMEDIA
NUSANTARA

ISSN 2355-3286

UMN
UNIVERSITAS
MULTIMEDIA
NUSANTARA

PRESS

Universitas Multimedia Nusantara
Scientia Garden Jl. Boulevard Gading Serpong, Tangerang
Telp. (021) 5422 0808 | Fax. (021) 5422 0800